CHALMERS UNIVERSITY OF TECHNOLOGY
Gothenburg, Sweden
www.chalmers.se

PHD THESIS

Future 5G and 6G systems need many small base stations, but connecting all of them with fiber is expensive, time consuming, and often impractical. This thesis explores Integrated Access and Backhaul (IAB), a solution where the same wireless equipment both serves users and carries data between base stations, making networks easier to deploy while keeping costs down. The research evaluates how IAB performs in real environments where buildings, trees, and rain weaken signals, and compares fully fibered networks with hybrid setups where only a fraction of the base stations rely on fiber and the remaining ones on IAB. The thesis also develops optimization methods using genetic algorithms and dynamic routing to decide how base stations should be arranged and connected so the network stays robust during temporary blockages. The results show that, with proper planning, IAB can offer strong coverage and flexibility. The work further examines deployment constraints, such as limits on inter-IAB distance and geographical barriers. By designing algorithms that account for these real-world limitations, the research shows that smart planning can significantly improve service coverage even in constrained areas. Finally, the thesis investigates new technologies such as reconfigurable intelligent surfaces (RIS) and free-space optical (FSO) links. When combined with IAB, these hybrid approaches can enhance coverage, energy efficiency, and cost-effectiveness, especially where laying fiber is difficult or costly.

CHALMERS
UNIVERSITY OF TECHNOLOGY

CHARITHA MADAPATHA • Integrated Access and Backhaul for 5G, 6G and Beyond • 2025

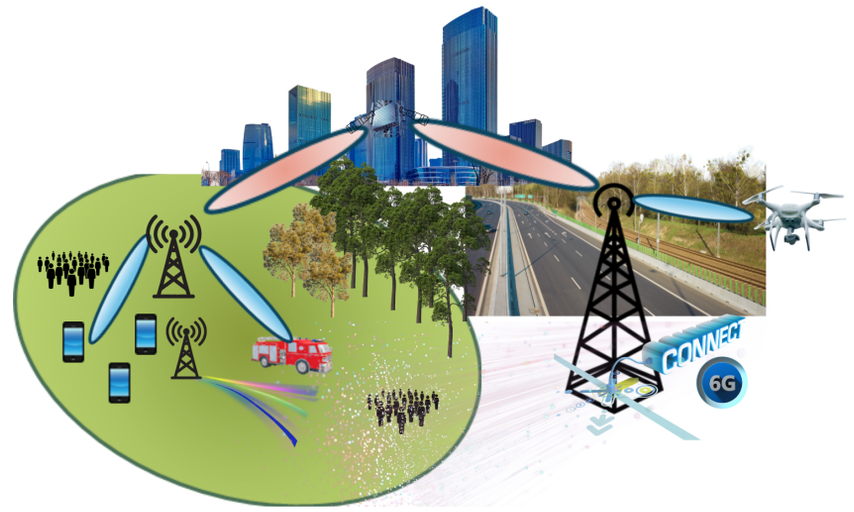

Integrated Access and Backhaul for 5G, 6G and Beyond

CHARITHA MADAPATHA

DEPARTMENT OF ELECTRICAL ENGINEERING
CHALMERS UNIVERSITY OF TECHNOLOGY
Gothenburg, Sweden 2025
www.chalmers.se

THESIS FOR THE DEGREE OF DOCTOR OF PHILOSOPHY

Integrated Access and Backhaul for 5G, 6G and Beyond

Charitha Madapatha

CHALMERS
UNIVERSITY OF TECHNOLOGY

Department of Electrical Engineering
Chalmers University of Technology
Gothenburg, Sweden, 2025

Integrated Access and Backhaul for 5G, 6G and Beyond

Charitha Madapatha
ISBN 978-91-8103-342-7

Acknowledgements, dedications, and similar personal statements in this thesis, reflect the author's own views.

Doktorsavhandlingar vid Chalmers tekniska högskola
Ny serie nr 5799
ISSN 0346-718X

Department of Electrical Engineering
Chalmers University of Technology
SE-412 96 Gothenburg, Sweden
Phone: +46 (0)31 772 1000

This work was supported in part by VINNOVA (Swedish Government Agency for Innovation Systems) within the VINN Excellence Center ChaseOn, in part by the Gigahertz-ChaseOn Bridge Center at Chalmers, in part by the European Commission through the H2020 Project Hexa-X under Grant 101015956, in part by the European Commission through the Horizon Europe/JU SNS project Hexa-X-II (Grant Agreement no. 101095759), and in part by the European Commission through the Horizon Europe/JU SNS project ECO-eNET (Grant Agreement no. 10113933). The simulations were performed in part on resources provided by the Swedish National Infrastructure for Computing (SNIC) at C3SE.

Cover:
Än illustration of an integrated access and backhaul (IAB) network demonstrating the applicability and importance.

Printed by Chalmers Digital Printing
Gothenburg, Sweden, December 2025

To my parents.

Integrated Access and Backhaul for 5G, 6G and Beyond

Charitha Madapatha
Department of Electrical Engineering
Chalmers University of Technology

Abstract

Enabling network densification to support coverage-limited millimeter-wave (mmWave) frequencies is a fundamental requirement for 5G, 6G and beyond. However, connecting a high density of base stations (BSs) to the core network remains a significant challenge. While fiber-based backhaul provides high-capacity, reliable links, its deployment may involve substantial costs and long installation times. Wireless backhaul offers a more flexible and rapidly deployable alternative but is often constrained by lower data rates and environmental vulnerabilities. To address these challenges, integrated access and backhaul (IAB) has emerged as a promising solution that repurposes part of the available spectrum for both access and backhaul, enhancing deployment flexibility and reducing time-to-market. Here, the same node/hardware is used to provide both backhaul and cellular services in a multi-hop architecture. This thesis investigates IAB as a scalable transport solution by analyzing and optimizing its performance under realistic conditions. Using analytical models and simulations, we study the effects of blockage, foliage, and rain attenuation on service coverage and compare IAB deployments with fully fibered and hybrid architectures. We develop methods for optimizing IAB topology design under practical constraints such as inter-node distance and geographical limitations, and evaluate routing strategies to mitigate temporary blockages. We also explore how complementary technologies including reconfigurable intelligent surfaces (RIS), network-controlled repeaters, and free-space optical (FSO) links can enhance IAB-based networks. Our results show that well-planned hybrid deployments can improve coverage and energy efficiency while reducing infrastructure costs.

Overall, the thesis offers an integrated assessment of IAB-based architectures and shows how careful planning and technology integration can enable cost-efficient and robust network densification. The findings suggest that, with appropriate design and optimization, IAB can serve as an effective and scalable backhaul solution for future wireless systems.

Keywords: Beyond 6G, 6G, 5G, Coverage probability, Densification, Free-Space Optical (FSO), Integrated access and backhaul (IAB), millimeter wave (mmWave), Poisson point process (PPP), Relay, Reconfigurable Intelligent Surface (RIS), Routing, Stochastic geometry, Topology optimization, Wireless backhaul, 3GPP

List of Publications

This thesis is based on the following publications:

[A] **C. Madapatha**, B. Makki, C. Fang, O. Teyeb, E. Dahlman, M-S. Alouni, and T. Svensson, "On integrated access and backhaul networks: current status and potentials". *IEEE Open Journal of the Communications Society*, vol. 1, pp. 1374-1389, Sept. 2020.

[B] **C. Madapatha**, B. Makki, A. Muhammad, E. Dahlman, M. -S. Alouini, and T. Svensson, "On topology optimization and routing in integrated access and backhaul networks: a genetic algorithm-based approach". *IEEE Open Journal of the Communications Society*, vol. 2, pp. 2273-2291, Sept. 2021.

[C] **C. Madapatha**, B. Makki, H. Guo, and T. Svensson, "Constrained Deployment Optimization in Integrated Access and Backhaul Networks". In Proc. *IEEE Wireless Communications and Networking Conference(WCNC)*' 2023, Glasgow, United Kingdom.

[D] **C. Madapatha**, B. Makki, H. Guo, and T. Svensson, "Reconfigurable Intelligent Surfaces-Assisted Integrated Access and Backhaul". In Proc. *IEEE International Black Sea Conference on Communications and Networking (BlackSeaCom)*' 2025, Chisinau, Moldova.

[E] **C. Madapatha**, P. Lechowicz, C. Natalino, P. Monti, and T. Svensson, "Joint Fiber and Free Space Optical Infrastructure Planning for Hybrid Integrated Access and Backhaul Networks". In Proc. *IEEE International Symposium on Personal, Indoor and Mobile Radio Communications (PIMRC)'* 2025, Istanbul, Turkey.

Other publications by the author, **not included** in this thesis, are:

[F] C. Fang, **C. Madapatha**, B. Makki, and T. Svensson, "Joint scheduling and throughput maximization in self-backhauled millimeter wave cellular networks". in *Proc. IEEE ISWCS*, Berlin, Germany, Sept. 2021, pp. 1-6.

[G] O. P. Adare, H. Babbili, **C. Madapatha**, B. Makki, and T. Svensson, "Uplink power control in integrated access and backhaul networks". in *Proc. IEEE DySPAN*, Los Angeles, CA, USA, Dec. 2021, pp. 163-168.

[H] A. V. Parambath, J. Flordelis, **C. Madapatha**, F. Rusek, E. Bengtsson, and T. Svensson, "Integrating Reconfigurable Intelligent Surfaces (RISs) into Indoor D-MIMO Networks for 6G". in *Proc. IEEE VTC-Fall*, 2024, pp. 1-6.

[I] O. Haliloglu, H. Yu, **C. Madapatha**, H. Guo, F. E. Kadan, A. Wolfgang, R. Puerta, P. Frenger, and T. Svensson, "Distributed MIMO systems for 6G". in *Proc. EuCNC/6G Summit*, Gothenburg, Sweden, 2023, pp. 156-161.

[J] S. Madhusudan, **C. Madapatha**, B. Makki, H. Guo, and T. Svensson, "Beamforming in wireless coded-caching systems". in *Proc. IEEE FNWF*, 2023, pp. 1-6.

[K] H. Guo, H. Wymeersch, B. Makki, H. Chen, Y. Wu, G. Durisi, M. F. Keskin, M. H. Moghaddam, **C. Madapatha**, H. Yu, et al., "Integrated communication, localization, and sensing in 6G D-MIMO networks". IEEE Wireless Communications, vol. 32, no. 2, pp. 214-221, Apr. 2025.

[L] H. Yu, B. Banerjee, B. Gouda, E. N. Tominaga, J. Flordelis, I. Atzeni, B. Xu, H. Farhadi, O. Haliloglu, C. Madapatha, A. Tölli, G. P. Fettweis, and T. Svensson, "Towards Resilient, Space, and Frequency Domain Cooperative Distributed-Large MIMO Systems". *IEEE Wireless Communications*, Jul. 2025.

Acknowledgments

Firstly, I would like to express my heartiest gratitude and thank my examiner and main supervisor, Prof. Tommy Svensson, for all the guidance given to me throughout this long fruitful journey since the summer internship in 2019, up until today and for many more great times to come. Tommy's role has influenced and shaped my way of thinking and character during this past time in a very progressive manner. The research work were always largely nourished by you. The way you kept calm, mindfulness and balanced the heavy work load was exemplary. It was great teaching time we had, and I learnt alot of skills from you during those times. I wholeheartedly value all those advice and support you have given to me both within academia and outside work related things. It helped me a lot, both during good and hard times. Thank you for all those and without those valued support things should be a lot different. There have always been alot to learn from you and undoubtedly is the best supervisor and mentor one can ever have.

Then foremost all, thank you very much Dr. Behrooz Makki for being my Ericsson co-supervisor, and for always being with me, guiding and nurturing me throughout this period. The frequent chats, talks, emails and communication we had, enriched me and pushed me further to explore and contribute more alleviating the harder times during this journey. You always had many great ideas to bring to the table and those nurtured my endeavours vastly. It is hard to imagine where things would have been positioned, without your immense guidance. I feel to be the luckiest and a lot privileged to have you on board.

The journey so far has been very nourishing and I hope for many great endeavours to come with the guidance from you two. Thanks alot Dr. Hao Guo, for always being there as the best collaborator and a best friend for all this time. Immensely grateful to Dr. Mikael Coldrey and Ericsson Lindholmen, for the reviews, technical advice and encouragement throughout which nourished our work alot. Thank you very much for those.

I would also like to highlight and thank the Optical Networks Group at Chalmers, especially Paolo Monti, Carlos Natalino, and Piotr Lechowicz for their fruitful and engaging collaboration within Eco-eNET, which resulted in the publication of several research papers and ongoing further explorations. Then my heartfelt thanks goes to Prof. M-S Alouini of KAUST, Saudi Arabia and Dr. Erik Dahlman of Ericsson, Kista for collaborating and giving your much valued input and advice. Many thanks to Dr. Oumer Teyeb, Dr. Ajmal Muhammad, Chao Fang from Ericsson Kista as well, for the valuable input given to enrich my work. It was great to collaborate with you and hope to be even more exciting in the future.

Thank you, Prof. Fredrik Brännström, Prof. Erik Ström for the great work at management level, which ensured smooth delivery of my work and also for the great advice. Also, many thanks go to Professors Giuseppe Durisi, Henk Wymeersch,

Alexandre Graell i Amat, Thomas Eriksson, Erik Agrell, Christian Häger, Ashraf Uz Zaman for providing very interesting discussions and enhancing the research atmosphere. The support of non-academic staff including Elizabeth, Daniela, Natasha, and Emma was great, and thank you for helping me with administrative and documentation related matter during the time.

I would also like to thank my dear wireless systems team comprising of our Akshay, Morteza, Amritha, Venkatesh and fellow PhD students Azadeh and Mehdi for all the support and kindness during this time. Azadeh, you have been a great friend all this time. The constant support from you really helped me a lot along the way. Thank you Mehdi for covering me up and supporting always when need along this journey. My heartiest thanks goes to my teaching work partner, Carl Kylin for always backing me up, Björn Gävert as my room mate and friend for life, Björn Langborn, Lise for always cheering up and been by side, Marvin, José, Nima, Yu Ge, Jiang, Priyanka and all others whose names could not be mentioned. Madhavi, Amitha, Adriana, Mehrangiz, Nazanin, thank you for all the great moments we have had during these times and a lot more to come. I have got to learn, it is these beautiful times that matter more than everything else. My thanks go also to Mustafa, Usman, Hoang, Furkan, Murali, Liqin, Raha, Yibo, Shen, Federico, and all in our corridor for bearing with me and helping me throughout.

There are people in my life who have never turned me down or said no to me, no matter what kind of help I've asked for. Thank you, Khun Ekkaphot, for the great times we've shared and continue to share, and for your guidance in helping me grow. To my closest ones, Nipun, and Haily from Sony; Vishvi, Viet from Microsoft; Samidhi, Pulasthi and Hasinie from Husqvarna; and Yodunika, Antony, the one and only Hetti ayya, Purnima akka, Sameera, Dr. Minidu-my life long friend, medical advisor and surgeon, dearest Randula, Dilesha from Alstom, Charuka, Udayanga, Tilani, Supun, Jananie, Baale, Nimanthie and Justin from Volvo, thank you very much. The list goes on, but I've tried to limit it mostly to those in Sweden, understandably.

Finally, I would like to express my sincere thanks to our ChaseOn and Hexa-X, Hexa-X-II projects, fellow collaborators including Jose Flordelis of Sony Research, Prof. Amir AghaKouchak of UCI, California, Communication systems group, my dear colleagues, my cousins, especially Thilini nangi who literary sacrifices her time and effort on anything I request expecting nothing in return, Maddu nangi (Dr.), Sanduni nangi and friends for their immense support and my beloved parents, brother who always try to give me the best and wish me all the success. Whatever I achieve in life, half the credit goes to my late father, my right hand then and forever, and to my mother, my left hand. Helps and time spent with all of you have been very encouraging and I hope for more of those times in the future.

Charitha Madapatha
Göteborg, December 2025

Acronyms

AP	Access Point
BAP	Backhaul Adaptation Protocol
BS	Base Station
CP	Coverage Probability
CSI	Channel State Information
CU	Centralized Unit
DU	Distributed Unit
D-MIMO	Distributed Multiple-Input Multiple-Output
FHPPP	Finite Homogeneous Poisson Point Process
FSO	Free-Space-Optics
FWA	Fixed Wireless Access
gNB	gNodeB
GA	Genetic Algorithm
HetNet	Heterogeneous Network
IAB	Integrated Access and Backhaul
IoT	Internet of Things
ISAC	Integrated Sensing and Communication
LoS	Line-of-sight
LTE	Long-Term Evolution
MBS	Macro Base Station
MAC	Medium Access Control
mmWave	Millimeter Wave
MT	Mobile Termination
mIAB	Mobile Integrated Access and Backhaul
MIMO	Multiple-Input-Multiple-Output
NLoS	Non-line-of-sight
PtP	Point-to-Point
QoS	Quality of Service
RAN	Random Access Network
RLC	Radio Link Control
RIS	Re-configurable Intelligent Surface
SBS	Small Base Station
SINR	Signal-to-Interference-plus-Noise Ratio
TDD	Time Division Duplex
UAV	Unmanned Aerial Vehicle
UMa	Urban Macro
UE	User Equipment
UMTS	The Universal Mobile Telecommunications System
3GPP	3rd Generation Partnership Project
5G NR	5G New Radio

Contents

Part I

Overview

CHAPTER 1

Introduction

1.1 Background

Wireless network traffic usage is predicted to skyrocket and thus, in order to tackle this massive increase in data traffic, the 5G and beyond networks have moved the transmissions into the until then non-traditional millimeter wave (mmWave) spectrum. Thus, network densification [1], [2] is a key enabler in the road map to 5G and beyond, driven by the high frequencies with limited coverage in mmWave. This is an important part in ensuring massive increment of user data throughput, and a large number of small base stations (SBSs) need to be connected to support the densification. Fiber offers reliable connections with high data rates, however, one main challenge which may hinder its deployment is the noteworthy initial investment required for trenching and installation of the fiber links [3]. Moreover, it can take long installation time and in some cases, may not be allowed, especially in historical sites and metropolitan areas.

Wireless backhauling is a feasible option compared to wired alternatives in ultra denss networks. The trend to use microwave backhaul links by the mobile operators world wide is likely to continue [4], [5], [6]. This is triggered by its scalability and the ability to meet increasing requirements in beyond 5G and 6G networks. Currently, microwave backhaul links mainly operate in the high-frequency wireless backhaul bands (e.g., 10-80 GHz), and lower microwave frequencies (e.g., 6 GHz) range in licensed point-to-point (PtP) spectrum [7], [8].

Regardless of having limited coverage, mmWaves are inherent with wide bandwidth, high transmission quality, strong detection ability, narrow beam, and thus

can significantly improve the rising wireless communication demands [9], [10]. Meanwhile, mmWave transmissions are highly directional and thus may render fairly noise-limited networks rather than being interference-limited in most cases [11], [12], [13], [14]. However, since these signals are easy to be blocked by the buildings/obstacles and have short coverage as noted earlier, it is important to have densified networks as well to compensate. Thus, due to the introduction of 5G with the access to wide bandwidth in mmWave spectrum, integrated access and backhaul (IAB) networks, where along with cellular access communications part of the radio resources can be utilized for backhauling in a more integrated manner, has received a significant attention [1], [15], [16], [17], [18], [19]. IAB is promising mainly thanks to its flexibility, ease of maintenance, and low time-to-market [20], [21], [22]. Figure. 1.1 illustrates an example of 5G expansion for dense networks using IAB.

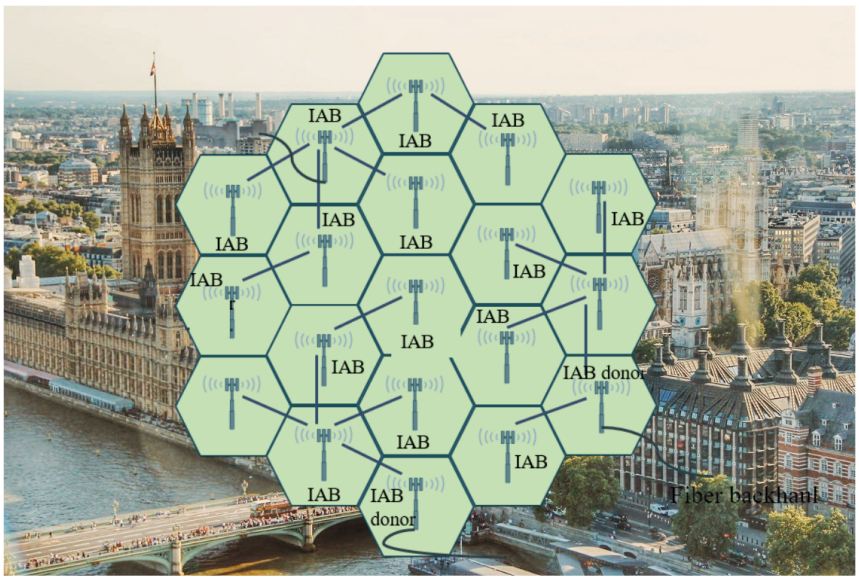

Figure 1.1: 5G NR coverage expansion with IAB.

Relayed backhaul links have been specified in long-term evolution (LTE) Release-10, as LTE-relaying [23], [24], [25], however, the commercial deployment cases were limited due to the unavailability of massive bandwidth and because the spectrum in sub-6 GHz band is expensive to be used for backhauling. The limitations of LTE relaying include, 1) the limitation on number of supported hops, i.e., designed to support only a single hop; 2) the inflexible static bandwidth allocation between access and backhaul; 3) static parent node to child node architecture [26], [27], [28]. However, in 5G and beyond networks IAB may be more successful because of the availability of massive bandwidth and the need for densified deployments due to

the short propagation range of mmWave. Also, in contrast to the LTE relaying, IAB allows greater flexibility due to its multi-hop architecture and dynamic resource sharing between access and backhaul. Moreover, new radio (NR) inherits highly directional beamforming capabilities and multiple-input-multiple-output (MIMO) which can help to mitigate the cross-link interference between the access and backhaul links.

Although it is not the focus of this thesis, IAB also permits deployment of mobile cells, called mobile IAB (mIAB) in par with the previously studied moving relay/mobile relay, which is supposed to be standardized beyond 3GPP Rel-18. In general, such IAB nodes could be placed in buses, trains and unmanned aerial vehicles (UAVs)[1] [28], [29], [30], [31]. An IAB node uses the same wireless channels for both providing service to users (access) and connecting back to the main network (backhaul). In such IAB networks, a parent node is either the IAB donor or an IAB node that provides backhaul connectivity to another IAB node. The parent node terminates and manages the backhaul link for its child node (as well as access for the UEs under its coverage) and forwards traffic toward the core network. Furthermore, a child node is an IAB node that receives its backhaul connection from a parent node instead of directly from fiber. The child node relies on the parent for connectivity while simultaneously serving UEs and/or further downstream IAB nodes.

Along with frequent handovers and interference management, one of the main challenges for mIAB is the fast-outdated channel state information (CSI) caused by mobility. One promising solution is to use predictor antenna [32], [33], [34], such that additional antennas are deployed in the front of the main antenna(s) and are used for CSI acquisition. Although mIAB has not yet been widely deployed, 3GPP Release 18 includes it as a fully specified feature under RAN3. Rel-18 introduces a dedicated network integration procedure for mIAB-nodes, as well as mobility procedures. Various system design and resource allocation methods for mIAB have been studied in, e.g., in [28], [32], [34], [35], [36], [37], [38], [39], [40], [41].

Topology Optimization and Related Work

Routing has been studied for multi-hop IAB networks in [42], [43], [44], [45], [46], [47], [48], [49]. Also, [50] designs cost-optimal node placement schemes while [51] evaluates joint resource allocation and node placement strategy to maximize the sum rate of downlink in IAB networks. Moreover, various network topology optimizations for non-IAB networks using machine-learning based solutions have been studied [52], [53], [54], [55], [56], [57], [58], [59], [60], [61], [62], [63], [64]. Still, in contrast to our work, these studies have not considered non-IAB backhaul distribution optimization nor joint optimization of non-IAB node placement and non-IAB backhaul link placement. Also, in our work, we study the effect of different deployment constraints on the performance of IAB networks.

[1]Note that 3GPP Rel-18 work-item does not support UAV-based mIAB.

Topology Optimization in IAB Networks

Well planned and optimized networks can achieve better performance while saving costs to the mobile network operators as well. This is resulted from the ability to avoid, e.g., static blockages like buildings and trees [65], [66]. For moving blockages, one way is to use routing to compensate for temporal blockages. Alternatively, context-information based dynamic blockage avoidance could be realized with cooperative base stations (BSs) [67]. Still, when the network size increases in urban dense areas, the derivation of closed-form solutions for network topology/routing/cooperative blockage avoidance becomes infeasible to achieve. It is worth noting that the network topology optimization can be performed offline and be recalculated whenever there are considerable changes in blocking conditions, addition of new BSs and different service coverage requirements. However, in all such cases, the optimization problem rapidly becomes very large, which motivates the efforts to go for a suboptimal machine learning-based approach, as searching over all possible options via exhaustive search is infeasible. In this way, machine learning techniques give effective (sub)optimal solutions with reasonable implementation complexity.

1.2 Scope of the Thesis

The main focus of this thesis is evaluating IAB networks and designing effective techniques to improve the network performance. Specifically, we evaluate the network performance in the cases with tree foliage, rain loss and blockages. Furthermore, we carry out analysis on the network performance when part of the network is non-IAB backhauled. Thereby, we optimize the network not only for IAB node placement but also for dedicated non-IAB/fiber/free-space optics (FSO) backhaul connection distribution. Moreover, we take into account spatial contraints when placing IAB nodes and develop efficient algorithms to optimize such constrained networks. We consider a dense urban area with a two-tier heterogeneous network (HetNet) [68], [69], i.e., a two-hop IAB network, where multiple MBSs (M: macro) and SBSs serve the user equipment (UE). In this way, following the 3GPP definitions (see Chapter 2), the MBSs and the SBSs represent the IAB donor and the child IABs, respectively. By adding fiber connectivity to a gNodeB (gNB) following the 3GPP requirements [14], an MBS can operate as an IAB donor and provide wireless backhaul connectivity to IAB child nodes [14]. Furthermore, we continue to investigate technologies such as reconfigurable intelligent surfaces (RISs) and network controlled repeaters (NCRs) aiding the IAB networks to overcome the tree foliage propagation losses. Later, focusing on cost and performance evaluation, we study joint fiber and free space optical infrastructure planning for hybrid integrated access and backhaul networks towards a confluent wireless/fiber access-transport design of 6G networks.

1.3 Organization of the Thesis

In Chapter 2, the HetNet model, 3GPP concepts and protocols are discussed. The details of the channel model are also presented. Thereby, in Chapter 3, different topology optimization and routing schemes are presented, specifically, GA-based methods to improve the network's service coverage probability (CP). Furthermore, discussion is carried out on optimization of node placement in spatially-constrained networks [70]. Later in Chapter 5, we investigate the enhancement of CP and cost in an IAB network with a joint fiber/FSO based infrastructure planning approach. Finally, Chapter 6 provides a brief overview of our contributions in the attached papers, and discusses possible future research directions.

CHAPTER 2

Network Model and 3GPP Concepts

2.1 Overview on Standardization

Since many years, wireless backhaul links have been around and 3GPP has already taken actions to standardize this matter in LTE Release 10 context [71], [72], [73]. The work on IAB within 3GPP started during the standardization of 5G NR. Particularly, IAB could operate in all spectrum in principle, however, 3GPP standardization work has been concentrated on mmWave spectrum. This has become the norm because the low spectrum is very expensive due to the limited bandwidth and given the fact that access to wider bandwidth is available in mmWave, in contrast to low bands.

The standardization process of IAB commenced in 2017 within 3GPP Rel-15 with IAB architectures, and radio protocols [74]. Later, Release 16 was endorsed in July 2020 with protocol layers and IAB architectures [75], [76]. Standardization continued in Rel-17 to enhance the performance of IAB networks. Due to this reason, IAB has a significant potential and also a lot of open areas to be researched. In particular, IAB specifies two different types of network nodes [77],

- The IAB-Donor node is the node consisting of Centralized Unit (CU) and Distributed Unit (DU) functionalities, and connects to the core network via non-IAB, e.g., fiber, microwave backhaul.

- The IAB node includes two modules, i.e., DU and mobile termination (MT). IAB-DU serves the UEs and, potentially, downstream IAB nodes in case of

multi-hop wireless backhauling. At its other side, an IAB-MT is the unit that connects an IAB node with the DU of the parent/upstream node.

When it comes to the connectivity with the parent node, the IAB-MT connects to the DU of its parent node essentially as a normal UE. On one hand, from the UE point-of-view, the DU of an IAB node appears as a normal DU. This is necessary to preserve backward compatibility so that legacy (pre Rel-16) NR UEs could also access the network via an IAB node. Figure 2.1 shows the types of connections in IAB networks.

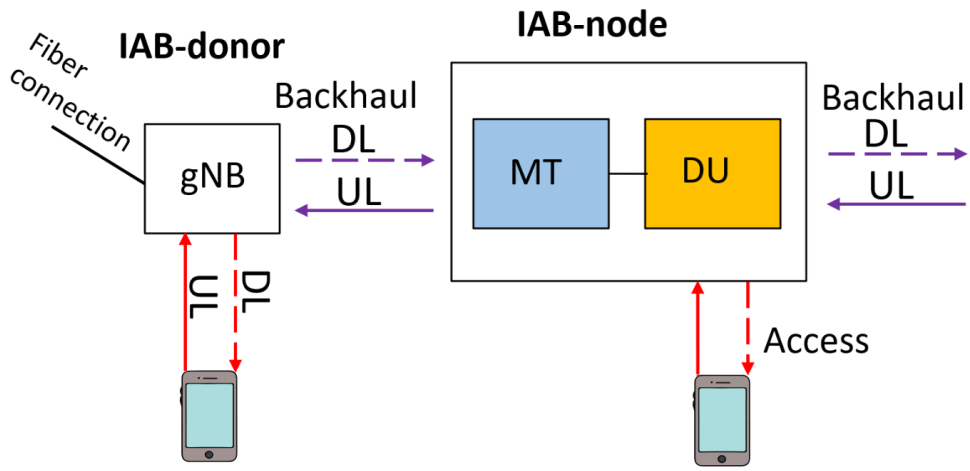

Figure 2.1: Types of connections in IAB networks.

IAB-DU classes

The requirements of the below specifications apply only to Wide Area IAB-DU, Medium Range IAB-DU and Local Area IAB-DU unless otherwise stated. The associated deployment scenarios for each class are exactly the same for IAB-DU with and without connectors.

For IAB type 1-O and 2-O, IAB-DU classes are defined as indicated below, following [78, Section 4.4.1], [79].

- Wide Area IAB-DU are characterised by requirements derived from Macro Cell scenarios with a BS to UE minimum distance along the ground equal to 35 m.
- Medium Range IAB-DU are characterised by requirements derived from Micro Cell scenarios with a BS to UE minimum distance along the ground equal to 5 m.
- Local Area IAB-DU are characterised by requirements derived from Pico Cell scenarios with a BS to UE minimum distance along the ground equal to 2 m.

Meanwhile, for IAB type 1-H, the IAB-DU classes are defined as indicated below, [78, Section 4.4.1],[79]:

- Wide Area IAB-DU are characterised by requirements derived from Macro Cell scenarios with a BS to UE minimum coupling loss equal to 70 dB.
- Medium Range IAB-DU are characterised by requirements derived from Micro Cell scenarios with a BS to UE minimum coupling loss equals to 53 dB.
- Local Area IAB-DU are characterised by requirements derived from Pico Cell scenarios with a BS to UE minimum coupling loss equal to 45 dB.

IAB-MT classes

The requirements in this specification apply to Wide Area IAB-MT and Local Area IAB-MT classes unless otherwise stated. For IAB type 1-H, 1-O, and 2-O, IAB-MT classes are defined as indicated below, [78, Section 4.4.2]:

- Wide Area IAB-MT are characterised by requirements derived from Macro Cell and/or Micro Cell scenarios.
- Local Area IAB-MT are characterised by requirements derived from Pico Cell and/or Micro Cell scenarios.

Backhaul Adaptation Protocol

A new IAB-specific protocol for routing and bearer mapping in data packets of IAB network is introduced by 3GPP as backhaul adaptation protocol (BAP). This BAP is taking care of packet forwarding in intermediate hops lying between IAB-donor-DU and access IAB node. In the downlink traffic, the BAP layer of IAB-Donor-DU adds a BAP header to the received packets from the upper layer. Similarly, BAP layer of access IAB-node appends an BAP header to the upper layer packets in the uplink traffic.

Although NR-IAB is expected to achieve greater commercial success than legacy LTE relaying, commercial deployments are yet to happen. A major factor is the complexity of the 3GPP IAB architecture and features, which increases implementation, interoperability, and operational challenges, thereby slowing commercial adoption at a viable cost of production. Since densification of sites also brings concerns on the mobile operators with higher site acquisition, power, and hardware costs, it also has contributed to the slower movement already happening due to high complexity of standardization[1].

[1] Some statements of the thesis are not necessarily aligned with the Ericsson's view on IAB, FWA, RIS, etc.

IAB in Fixed Wireless Access

In fixed wireless access (FWA) deployments, IAB may be attractive because it reduces the dependency on widespread fiber rollout while still enabling high-capacity access in suburban and urban neighborhoods. Instead of providing dedicated backhaul to every site, only a subset of access points are fiber-connected, while the remaining nodes obtain backhaul wirelessly through neighboring sites. This architecture allows operators to extend coverage rapidly, leverage wide mmWave spectrum, and incrementally densify the network as demand increases, without the upfront capital costs associated with full fiber build-outs [80], [81].

At the same time, applying IAB in FWA introduces architectural trade-offs that must be considered at a system level. Because access and backhaul share the same spectrum, network planning needs to account for traffic aggregation along relay chains, placement of fiber anchor nodes, and site locations that minimize blockage and path loss. When these aspects are jointly optimized, IAB provides an effective bridge between wireless access and transport, enabling scalable FWA deployments that can evolve toward denser or more fibered topologies over time. Although FWA is not within the scope of this thesis, given its importance as a main use case, it is important to highlight how IAB can support such deployments.

A practical way to mitigate the IAB bottlenecks observed in FWA deployments is to combine IAB agility with temporary, low-cost fiber anchoring. In particular, instead of attempting to operate long multi-hop backhaul chains, shorter, and portable fiber drops (for example, micro-trenched) can be deployed only at strategic points where traffic aggregates. Such fiber-connected anchor nodes can form a loose ring or mesh across the neighborhood, while intermediate nodes can continue to use IAB-type wireless backhaul toward the nearest anchor[2]. The IAB relays can auto-configure their routes, and backhaul scheduling is dynamically prioritized depending on load and traffic direction. As demand grows, temporary fiber segments can be upgraded to permanent infrastructure, allowing the operator to evolve gradually from a predominant IAB network towards a more fibered topology. Such hybrid approaches can retain much of the cost benefit of IAB while significantly improving robustness and throughput, particularly in scenarios where foliage, distance and aggregation effects would otherwise hinder backhaul performance. It also enables rapid deployment, since initial coverage can be provided using IAB, with targeted fiber reinforcement added only where it results in the highest network-wide gain.

[2]Note that meshed IAB is not supported by 5G NR.

CHAPTER 3

Topology Optimization with Constraints in IAB Deployments

3.1 System model

In this PhD thesis, we model the IAB network using finite homogeneous Poisson point processes (FHPPP), with implementation details described below (See Paper A for further reading).

Spatial Distribution

In general, we consider a two-tier heterogeneous (HetNet) IAB network with multiple IAB-donor nodes, i.e., MBSs and IAB-child nodes, i.e., SBSs, serving UEs, of which only the IAB-donors are fiber-connected while the IAB child nodes use wireless connections for both access and backhaul links. Please note that in this compilation, MBS, IAB donor, and SBS, IAB child are used interchangeably for generic understanding. The MBSs, SBSs and UEs are distributed using FHPPP distributions with respective densities, λ_{M}, λ_{S} and λ_{U} where, $\lambda_{\mathrm{M}} < \lambda_{\mathrm{S}} < \lambda_{\mathrm{U}}$.

We let the network area be a circular disk, where the FHPPPs are distributed on. For simplicity and without loss of generality, we let A be a circular disk with radius D. However, the approach is generic and can be applied on arbitrary regions A. The SBSs and the UEs are also located on the same area A in accordance with two other FHPPPs ϕ_{S} and ϕ_{U} having the densities λ_{S} and λ_{U}, respectively, which are all mutually independant.

The blockages are modeled using the well-known germ grain-model, [82], which performs well for environments with larger obstacles than the stochastic models,

under the assumption that the blocking is independant in different links. The distribution model is an FHPPP, distributed within the same circular disk area with a blockage density of λ_{B}. The blockages are given a length of l_{B} and orientation of θ. The blockages with these specified characteristics are distributed in random locations uniformly as of the FHPPP.

Channel Model

We consider an inband communication setup, where both the access and backhaul links operate in the same mmWave spectrum band. Following the state-of-the-art mmWave channel model, the received power at each node can be expressed as

$$P_{\mathrm{r}} = P_{\mathrm{t}} h_{\mathrm{t,r}} G_{\mathrm{t,r}} L_{(1\mathrm{m})} L_{\mathrm{t,r}}(||x_{\mathrm{t}} - x_{\mathrm{r}}||)^{-1} F_{\mathrm{t,r}} \gamma_{\mathrm{t,r}}. \tag{3.1}$$

Here, P_{t} denotes the transmit power in each link, and $h_{t,r}$ represents the independent small-scale fading of each link where $|h_{t,r}|$ is Rayleigh distributed. Then, $G_{t,r}$ represents the combined antenna gain of the transmitter and the receiver of the link, $L_{\mathrm{t,r}}(\cdot)$ denotes the path loss due to propagation, and $L_{(1m)}$ is the reference path loss at 1 meter distance. The tree foliage loss is denoted by $F_{\mathrm{t,r}}$, while $\gamma_{\mathrm{t,r}}$ represents the rain loss between the transmitter and the receiver of the link in linear scale. The total path loss, in dB, is characterized according to the 5GCM UMa close-in model described in [83].

In 5G, large antenna arrays with directional beamforming are used to mitigate the propagation losses. We model the beam pattern as a sectored-pattern antenna array, and thus the antenna gain between two nodes can be expressed by

$$G_{i,\varphi} = \begin{cases} G_0, & \frac{-\theta_{\mathrm{HPBW}}}{2} \leq \varphi \leq \frac{\theta_{\mathrm{HPBW}}}{2} \\ g(\varphi), & \text{otherwise.} \end{cases} \tag{3.2}$$

Here, i, j are the indices of the considered transmit and receive nodes, and φ is the angle between them in the considered link. Also, θ_{HPBW} is the half power beamwidth of the antenna, and G_0 is the directional antenna's maximum gain while $g(\varphi)$ is the side lobe gain.

The inter-UE interferences are neglected due to the low power of the devices and with the assumption of sufficient isolation. The interference model focuses on the aggregated interference on the access links due to the neighboring interferers, which for UE u is given by

$$I_u = \sum_{\mathbf{i,j} \in \phi_{i,j} \setminus \{\mathbf{x}_c\}} P_j h_{i,j} G_{i,j} L_{(1\mathrm{m})} L_{x_i,x_j}(\|\mathbf{x}_i - \mathbf{x}_j\|)^{-1}. \tag{3.3}$$

Here, i and j represent all BSs except for the associated cell x_{c}, which can either be an MBS or an SBS.

Cell Association and Resource Allocation

The UE can be served by only one cell, either from the MBS or from the SBS based on the maximum received power rule. That is the UE will connect to the serving node maximizing the received power. The backhaul link association of the SBSs is determined by the minimum pathloss rule, where the SBS will connect to the MBS with the minimum path loss. Furthemore, and without the loss of generality we consider a maximum of two hops.

For resource allocation, on the other hand, the mmWave spectrum available is partitioned into the access and backhaul links such that

$$\begin{cases} W_{\text{Backhaul}} = \mu W, \\ W_{\text{Access}} = (1-\mu)W. \end{cases} \tag{3.4}$$

with $\mu \in [0,1]$ being the percentage of bandwidth resources on backhauling. Also, W_{backhaul} and W_{access} denote the backhaul and the access bandwidths, respectively, while total bandwidth is W. The bandwidth allocated for each SBS, by the fiber-connected MBS is proportional to its load and the number of UEs in the access link. The resource allocation is determined based on the instantaneous load in which each SBS informs its current load to the associated MBS each time. Thus, the backhaul-related bandwidth for the j-th IAB node is given by

$$W_{\text{backhaul},j} = \frac{\mu W N}{\sum\limits_{\forall j} N_j}, \quad \forall j. \tag{3.5}$$

where N_j denotes the number of UEs connected to the j-th IAB node and the access spectrum is equally shared among the connected UEs according to

$$W_{\text{access},u} = \frac{(1-\mu)W}{\sum\limits_{\forall\ u} N_{j,u}}, \forall u, \tag{3.6}$$

where N is the number of UEs at the considered SBS and j represents each SBS connected to the MBS. Also, u represents the UEs, and $N_{j,u}$ denotes the load at the IAB node j of which UE u is connected. The signal-to-interference-plus-noise ratio (SINR) values are obtained in accordance with (3.3) by

$$\text{SINR} = P_{\text{r}}/(I_u + N_0), \tag{3.7}$$

where N_0 is the noise power. Then, considering sufficiently long codewords, which is an acceptable assumption in IAB networks, the rates experienced by the UEs in

access links can be expressed by

$$R_u = \begin{cases} \frac{(1-\mu)W}{N_m}\log(1+\mathrm{SINR}(x_u)), & \text{if } \mathbf{x}_\mathrm{c} \in \phi_\mathrm{m}, \\ \min\Bigg(\frac{(1-\mu)WN}{\sum\limits_{\forall\, u} N_{j,u}}\log(1+\mathrm{SINR}(x_u)), \\ \qquad \frac{\mu WN}{\sum\limits_{\forall\, j} N_j}\log(1+\mathrm{SINR}(x_\mathrm{b}))\Bigg), \text{if } \mathbf{x}_\mathrm{c} \in \phi_\mathrm{s} \end{cases} \tag{3.8}$$

and the backhaul rate is given by

$$R_\mathrm{b} = \frac{\mu WN}{\sum\limits_{\forall\, j} N_j}\log(1+\mathrm{SINR}(x_\mathrm{b})). \tag{3.9}$$

Here, m represents the associated MBS and s denotes the SBS. Based on the association cell, there are two cases for the rate of the UEs. First is the case in which the UEs are associated with the MBSs, as denoted by $x_\mathrm{c} \in \phi_\mathrm{m}$ in (3.8). Since the MBSs, *i.e.*, MBSs, have fiber backhaul connection, the rate will depend on the access bandwidth available at the UE.

In the second case, the UEs are connected to the SBSs, as denoted by $x_\mathrm{c} \in \phi_\mathrm{s}$ in (3.8). Here, the SBSs have shared backhaul bandwidth from the MBSs, *i.e.*, MBSs, and thus the UE's data rate depends on the backhaul rate of the connected SBS as well. Thus, in this case, the UE is bound to get the minimum between backhaul and access rate.

3.2 Topology Optimization

In general, it is preferred to have IAB-IAB backhaul links with strong line-of-sight (LoS) signal strength, although Rel-16 supports non-line-of-sight (NLoS) backhauling, since IAB network performance is considerably influenced by the quality of the backhaul links. Moreover, in most cases, a fraction of SBSs can be connected via dedicated non-IAB backhaul links. Thus, it has become important to identify the SBSs that are crucial to be backhauled using such links for optimum performance. However, since analytical solutions for the appropriate node location sets and non-IAB backhaul link placement schemes are not feasible in large network sizes, it is important to design feasible algorithms with low complexity, which can provide the (sub)optimal solutions for both of the cases. Figure 3.1 depicts the general system model of the IAB network with topology and constraint optimizations.

For example, in a use case with N_s SBSs and the possibility for a total of N_f non-IAB backhauled SBSs, we could have $\binom{N_\mathrm{s}}{N_\mathrm{f}}$ possible combinations of non-IAB

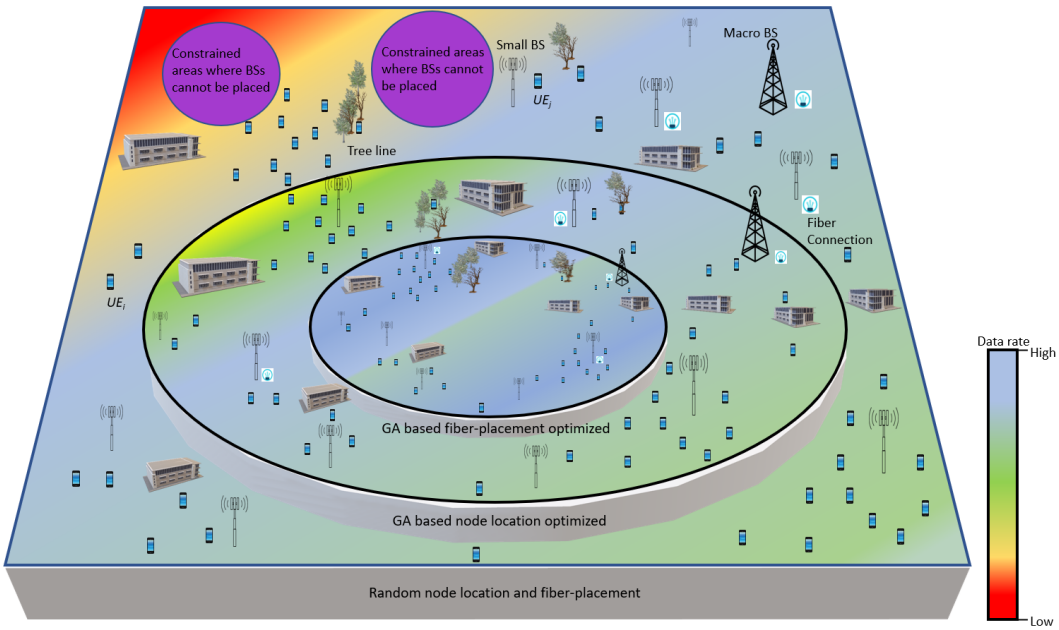

Figure 3.1: Schematic of system model.

backhauled SBS selections, which may need a lot of computational capacity if the solutions are obtained using exhaustive search, especially when the network size is large.

In Paper A, we study the potentials and challenges of IAB networks concentrating on mmWave-based communications on different use cases and deployment conditions, e.g, urban, suburban, blockage, tree foliage and rain. In particular, we use a finite stochastic geometry model, with random distributions of IAB nodes as well as UEs to study the CP defined as the probability of the event that the UEs' minimum rate requirements are satisfied. Furthermore, we summarize the recent Rel-16 as well as the upcoming Rel-17 3GPP discussions on IAB, and highlight the main IAB-specific agreements on different protocol layers.

With this background from Paper A and the need for topology optimization of IAB networks, in Paper B, we propose GA-based schemes [84] which outputs 1) the (sub) optimal locations of SBSs to be non-IAB backhauled and 2) (sub) optimal node locations within the network area, as described in Algorithms 1 and 2, respectively. Details are presented in the appended Paper B, i.e., [85]. The utility function that is supposed to be maximized is the CP, i.e., the fraction of UEs that have instantaneous data rates R_{U}) equal to or higher than that of a pre-defined threshold data rate η. Using these notations, the CP is given by

$$\mathrm{CP} = \Pr(R_{\mathrm{U}} \geq \eta). \tag{3.10}$$

As we show in [85], our proposed algorithms result in significantly lower complexity compared to the cases with exhaustive search, since they only evaluate KN_{it} number of potential solutions, where K is the possible selection strategies in each iteration and N_{it} is the maximum number of iterations pre-considered by the network designer. Moreover, as in each iteration we evaluate $K-J-1$ possible random solutions, where $J < K$, the algorithms can mimic the exhaustive search if $N_{\mathrm{it}} \to \infty$, i.e., they can achieve the global optimum selection if asymptotically large number of iterations are considered [84].

Algorithm 1 GA-based non-IAB Backhaul Link Placement

In each iteration with a budget for N_{f} non-IAB backhaul-connected SBSs, and $N_{\mathrm{s}} > N_{\mathrm{f}}$ SBSs, do the followings.

I. Consider K sets of N_{f} non-IAB backhaul-connected SBSs, where each of those sets is denoted by F_k. Then, for each set create the corresponding channel matrix H_k, $k = 1..., K$, according to the considered channel model.

II. For each selected possible solution set F_k, evaluate the objective function U_k, $k = 1, ..., K$. For instance, considering the CP as the objective function, U_k is given by (3.10).

III. Find the set of the SBSs among the considered solution sets $F_k, \forall k$, which results in the best value of the objective function, CP (defined as the *Queen*), e.g., F_i where $\mathrm{CP}(H_k) \leq \mathrm{CP}(H_i)$, $\forall k = 1, ..., K$.

IV. $F_1 \longleftarrow F_i$

V. Generate $J < K$, sets of SBSs F_j^{new}, $j = 1, ..., J$, around the Queen, i.e., F_i. These sets of SBSs are generated by making small changes to the Queen, for instance, by replacing few SBSs with other SBSs.

VI. $F_{j+1} \longleftarrow F_j^{\mathrm{new}}$, $j = 1, ..., J$.

VII. Use the same procedure as in Step I and regenerate the remaining sets $F_j, j = J + 2, ..., K$, randomly.

VIII. Proceed to Step II and continue the process for N_{it} iterations pre-considered by the network designer.

Return the Queen as the optimal SBS selection rule for non-IAB backhaul link placement.

In words, both algorithms are based on the same procedure described below.

Algorithm 2 GA-based SBS Location Selection

With N_{s} SBSs, from all possible locations in the space, do the followings.

I. Consider K sets of L_k locations, and for each set create the corresponding channel matrix H_k, $k = 1..., K$, according to the considered channel model.

II. Evaluate the objective function for each set, i.e., U_k, $k = 1, ..., K$. For instance, considering the CP as the objective function, U_k as given by (3.10).

III. Find the *Queen*, i.e., the set of locations which gives the best value of the objective function, i.e., CP, among the considered sets, e.g., L_i where $\rho(H_k) \leq \rho(H_i)$, $\forall k = 1, ..., K$,

IV. $L_1 \longleftarrow L_i$

V. Generate $J < K$, sets of locations L_j^{new}, $j = 1, ..., J$, around L_i. These sets of locations are generated by making small changes to the Queen, for instance, by replacing few locations with another sets of locations.

VI. $L_{j+1} \longleftarrow L_j^{\mathrm{new}}$, $j = 1, ..., J$.

VII. Use the same procedure as in Step I and regenerate the remaining sets $L_j, j = J + 2, ..., K$, randomly.

VIII. Proceed to Step II and continue the process for N_{it} iterations pre-considered by the network designer.

Return the Queen as the optimal SBS location selection rule.

Firstly, K possible selection strategies are considered and then, in each iteration we calculate the utility function and obtain the best strategy, i.e., selected solution, that maximizes the considered utility function. This best strategy is named as the Queen and thereby the Queen is considered as one of the possible solutions in the next iteration of the algorithm in order to guarantee the monotonic improvement of the algorithm performance in later successive iterations. Thereby, the Queen has become the regeneration operator in GA. Then, for each iteration, we create $J < K$ sets around the queen by applying slight changes to the Queen as a kind of mutation. Also, $K - J - 1$ sets of selection strategies are generated randomly in each iteration in order to avoid the scenario of the algorithm getting trapped in a local minimum. Thereby, this procedure will continue for N_{it} iterations determined by the network designer to output the best set solutions. Noteworthy is that, since in Step VII of the algorithms we check $K - J - 1$ random possible solutions in each iteration, the proposed algorithms can reach the globally optimal selection if asymptotically large number of iterations are considered.

3.3 Constraints of IAB Networks

In general, there are constraints on spatial deployment of IAB networks and thus, there are locations where the nodes cannot be deployed. On one hand, the mentioned constraints can be due to the regulatory restrictions from the authorities in protected areas [86]. These restrictions can be regional and country specific. Still, all provinces have their own enacted building and landscape protection laws, that could potentially create such constraints. Furthermore, national laws have to be followed when placing nodes, e.g., forest conservation, archaeological or listed buildings etc. On the other hand, these constraints can be imposed due to network planning especially to limit the interference.

As introduced in Sec. 2.1, the 3GPP RAN4 recognizes two types of IAB nodes categorically, i.e., wide-area and local-area IAB networks, where the differences mainly lie in the node capabilities and their level of network planning to accomadate them [87], [88]. Noteworthy, as specified in 3GPP RAN4, wide-area IABs are supposed to have a minimum inter-node distance to avoid extreme interference being created at the neighbouring nodes with LoS connections. However, local-area IAB networks can be comparatively unplanned as its main task is to give a boosting capacity to an already established service area served by an IAB node. However, the spatial constraints may still prevent installation of IAB nodes anywhere.

Network planning is crucial for IAB deployments due to the sensitivity of the backhaul links and the high rate demands. The paper C analyses and optimizes CP of IAB networks focusing on cases with either geographical or interference management constraints where IAB nodes may not be permitted/feasible to be deployed freely. To that end, we propose various mmWave blocking-aware constrained deploy-

ment optimization approaches. The results indicate that, even with limitations on deployment optimization, network planning boosts the coverage probability of IAB networks considerably.

With this background, Paper C analyses and optimizes the CP of IAB networks focusing on cases with either geographical or interference management constraints where IAB nodes may not be permitted/feasible to be deployed freely. As such, Algorithm 3 and Algorithm 4 in Paper C, [70] optimize the network performance for minimum inter-IAB distance requirement and the presence of constrained area use cases in, e.g., wide-area and local-area networks, respectively.

Algorithm 3 IAB placement with minimum inter-IAB distance requirement

With N_{d} IAB donors, N_{c} IAB child nodes inside the network area, do the followings:

I. Place the 1st node, $i = 1$, randomly in the considered network area.

II. Place the next node $i + 1$ where $i = 1, 2, 3, ..., (N_{\mathrm{c}} + N_{\mathrm{d}} - 1)$.

III. Find the minimum inter-node distances s_i between $(i + 1)$th node and each of other nodes.

IV. If any $s_i < r_{\mathrm{th}}$, redistribute the last node $(i + 1)$th by repeating Steps II-IV until $s_i > r_{\mathrm{th}}$.

V. For the obtained node locations, calculate the coverage. Then, proceed to Step I and continue the process for N_{it} iterations pre-considered by the network designer, saving the best set of node locations L_b among the considered solutions $L_j, \forall j, j = 1, 2, 3, ..., N_{\mathrm{it}}$, which gives the best value of the service coverage.

Return the set of the node locations in Step V as the optimal node location set.

In words, Algorithm 3, places the first IAB-node, $i = 1$, at a random location inside the network area. Then, it continues to place the $(i + 1)$th node from the set of IAB-donors N_{d} and IAB-child nodes N_{c}. Subsequently, the algorithm finds the minimum inter-node distances s_i between each of the other nodes and the $i + 1$th node. If any of the inter-node distances is less than a threshold r_{th}, then the $i + 1$th node is redistributed by repeating Steps II-IV given in the Algorithm 3, until all $s_i > r_{\mathrm{th}}$. Then, for the obtained set of node locations the CP is calculated, and the process is repeated until N_{it} iterations, pre-determined by the designer. The best set of node locations L_{b} giving the highest CP, is returned as the optimal node location set, which satisfies the inter-IAB distance requirement while maximizing the utility function.

Algorithm 4 firstly allocates a random set of node locations for the IAB-donors N_{d} and IAB-child nodes N_{c} within the network area without considering the constrained areas. Then, identifying the nodes falling inside the constrained areas, they are re-distributed inside the network area. We repeat this process until all nodes fall

Algorithm 4 IAB placement in the presence of constrained areas restricting IAB node placement

With N_{d} IAB donors, N_{c} IAB child nodes and a set of constrained areas inside the network area, do the followings:

I. Place the IAB donors/IAB nodes randomly in the considered network area.

II. Identify the IAB node(s) falling inside the constrained areas.

III. For each of the nodes identified in Step II, redistribute the nodes.

IV. Proceed to Step II and continue the process until all IAB nodes fall outside the constrained areas. Save the set of locations as L_i.

V. For the saved set of node locations L_i, compute the utility function, i.e., the service coverage given by (3.10). Proceed to Step I and continue the process for N_{it} iterations pre-considered by the network designer, saving the best set of node locations L_b among the considered solutions $L_i, \forall i, i = 1, ..., N_{\mathrm{it}}$ which gives the best value of the utility function, e.g., service coverage.

Return the set of the node locations in V as the optimal node location set.

outside the constrained areas. Then, the CP is calculated as our utility function which is averaged over multiple samples of UE PPP distributions and is saved as L_i, $i = 1, ..., N_{\mathrm{it}}$. This process is repeated over N_{it} iterations, where the best set of node locations resulting in the highest CP is saved as L_b. At the end of the N_{it} iterations, the L_b is returned as the optimal node locations set.

CHAPTER 4

Integration of Reconfigurable Intelligent Surfaces in Wide-Area IAB Networks for Enhanced Coverage

4.1 Introduction

Reconfigurable Intelligent Surfaces (RISs) have recently emerged as a promising technology for controlling the wireless propagation environment. An RIS is typically realized as a planar metasurface consisting of a large number of nearly passive reflective elements, whose phase responses can be electronically adjusted in a coordinated manner. By appropriately configuring these elements through a low-rate control link, RISs are capable of performing relative beamforming and shaping the radio channel. Unlike active repeaters, RISs do not require high power consumption, making it an energy-efficient alternative. Due to their passive nature, RIS panels can be manufactured at relatively low cost, consume only minimal energy, and can be mounted on existing infrastructure such as walls, building facades, lamp posts, or billboards. These characteristics make RISs attractive candidates for large-scale deployment, enabling new degrees of freedom in network design by transforming the propagation environment from a limiting factor into a configurable asset. From a system perspective, RISs are particularly appealing in scenarios where cost, energy efficiency, and deployment flexibility are critical. Their ability to redirect signals, create virtual line-of-sight paths, and mitigate shadowing makes them suitable for environments with severe blockage and heterogeneous channel conditions. Thus, the programmability of RIS provides an opportunity to support future wireless networks as an interesting enabler although some challenges remain such as interference management.

The introduction of RISs into IAB networks presents a unique opportunity to optimize service coverage probability, particularly in challenging environmental conditions such as foliage blockage and seasonal variations. In addition, RIS introduces new degrees of freedom for network design, enabling alternative signal paths when direct IAB donor–IAB child links experience deep fading or blockage. By intelligently steering reflected beams, RIS can strengthen backhaul connectivity, reduce outage probability, and support more reliable multi-hop communication. Recent studies also indicate that RIS-assisted systems can reduce interference and enhance spectrum utilization, particularly in dense deployments. Moreover, the ability to reconfigure RIS parameters in real time aligns well with the heterogeneity and adaptability of future 6G systems.

Note that RIS has no standardization support in 3GPP. Instead, in Rel-18 3GPP specified the methods for communication based on NCRs, as amplify-and-forward repeaters with beamforming and spectral filtering capabilities which are under the control of the network. In simple words, a (passive) RIS can be seen as an NCR with amplification gain smaller or equal to one, and with limited beamforming and spectral filtering capabilities as described earlier, performing only relative beamforming, compared to an NCR that can perform absolute beamforming given its possibility to use separate receive and transmit arrays (for detailed comparison between NCR and RIS, see [89], [90]). This chapter explores the role of RIS-assisted IAB networks in mitigating environmental factors such as tree foliage, rain intensity, and interference effects, with particular emphasis on the backhaul links. By dynamically adjusting RIS elements and optimizing backhaul connectivity, this approach provides a scalable and energy-efficient solution for robust network expansion in wide-area environments.

4.2 System model

Network Architecture

In a traditional wide-area IAB network, the IAB donor provides backhaul connectivity to multiple child IAB nodes, which, in turn, serve end-UEs. The backhaul links can either be direct connections or utilize RIS assistance when direct paths are obstructed or experiences deep performance drop. Unlike local-area IAB networks, which are constrained by shorter transmission ranges, wide-area IAB networks extend coverage across sub-urban and rural environments, making them suitable for large-scale deployments. Figure 4.1 shows how RIS-assisted IAB serves in the presence of seasonal tree foliage.

Impact of Tree Foliage on Backhaul Links

Tree foliage significantly impacts the reliability of backhaul links in IAB networks, particularly in regions with seasonal variations. The attenuation caused by foliage

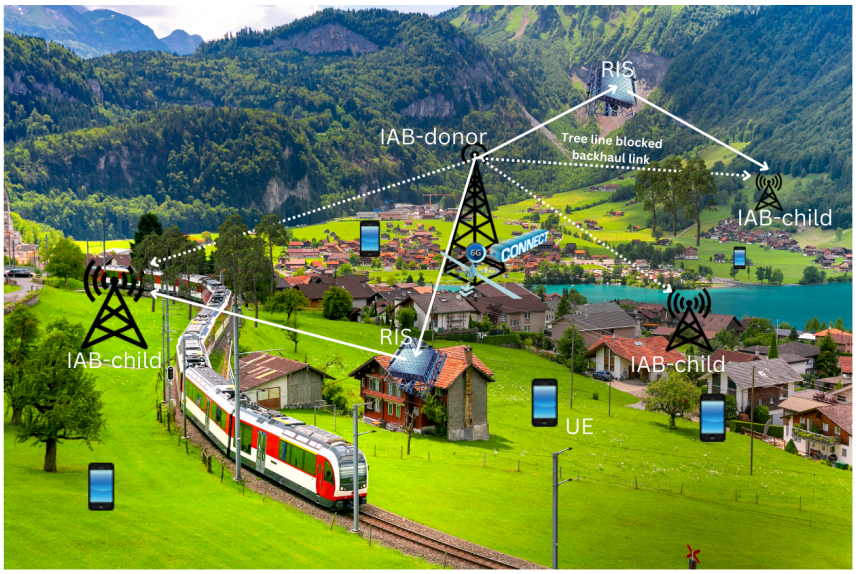

Figure 4.1: Wide-area IAB assisted with RIS for backhaul links amidst seasonal tree foliage changes.

can disrupt direct IAB donor to IAB child links, leading to increased service outages. By strategically placing RIS elements along the obstructed path, the system can dynamically redirect the signal, mitigating the degradation caused by foliage absorption.

Channel Model

The performance of backhaul links in an in-band wide-area IAB network is influenced by several factors, including transmission power, path loss, and environmental conditions such as tree foliage. Seasonal variations in foliage density can significantly impact signal propagation, necessitating alternative transmission strategies to maintain reliable connectivity.

The received power at a given node is expressed as:

$$P_{\text{rx}} = P_{\text{tx}} h_{\text{link}} G_{\text{ant}} \eta_{\text{path}} \phi_{\text{loss}}, \tag{4.1}$$

where P_{tx} represents the transmitted power, h_{link} is the channel fading coefficient, G_{ant} denotes the antenna gain, and η_{path} captures the path loss effect. The foliage-induced attenuation is modeled by ϕ_{loss}, which varies depending on the season and tree density.

In a conventional IAB network, the direct backhaul link is established between the

IAB donor and the IAB child node. However, foliage-induced loss can substantially degrade signal quality. The path loss follows the well-known 5GCM UMa close-in model, [83], given by:

$$\eta_{\text{path}} = 32.4 + 10\log_{10}(d)^{\alpha} + 20\log_{10}(f_c), \tag{4.2}$$

where d is the propagation distance between the nodes, f_c represents the carrier frequency, and α denotes the path loss exponent. The path loss characteristics vary based on the presence or absence of obstructions in the direct transmission path.

To mitigate path loss, modern wireless networks employ large antenna arrays with beamforming capabilities. The antenna gain model is defined as:

$$G_{\text{ant}}(\theta) = \begin{cases} G_{\text{main}}, & \frac{-\theta_{\text{HPBW}}}{2} \leq \theta \leq \frac{\theta_{\text{HPBW}}}{2} \\ g_{\text{side}}(\theta), & \text{otherwise.} \end{cases} \tag{4.3}$$

where G_{main} represents the main lobe gain, $g_{\text{side}}(\theta)$ denotes the side lobe gain, and θ_{HPBW} is the half power beamwidth of the antenna.

Interference in IAB Networks

Interference is a major factor influencing network performance. The aggregated interference on the access and backhaul links is modeled as:

$$I_u = \sum_{i,u \in \Lambda_{i,u} \setminus \{w_u\}} P_i h_{i,u} G_{i,u} \eta_{(1\text{m})} \eta_{x_i,x_u} \|\mathbf{x_i} - x_u\|^{-1}, \tag{4.4}$$

where P_i is the transmit power of the interfering node, $h_{i,u}$ represents the channel fading coefficient, and $\Lambda_{i,u}$ denotes the set of interferers. The interference on the backhaul links follows a similar expression.

Foliage-induced loss is accounted for using the Fitted International Telecommunication Union-Radio (FITU-R) model, [22]:

$$\phi_{\text{loss}} = \begin{cases} 0.39 f_{\text{c}}^{0.39} r^{0.25}, & \text{in-leaf} \\ 0.37 f_{\text{c}}^{0.18} r^{0.59}, & \text{out-of-leaf} \end{cases}. \tag{4.5}$$

where r represents vegetation depth.

Resource Allocation for Backhaul and Access Links

Efficient spectrum partitioning is crucial for network performance. The available bandwidth is split between backhaul and access links as follows:

$$B_{\text{backhaul}} = \psi B, \quad B_{\text{access}} = (1 - \psi)B, \tag{4.6}$$

where ψ is the fraction of total bandwidth allocated for backhaul transmissions. The bandwidth allocated to a specific IAB node depends on its load and the number of associated UEs:

$$B_{\text{backhaul},k} = \frac{\psi B N_k}{\sum_{\forall k} N_k}, \quad B_{\text{access},u} = \frac{(1-\psi)B}{\sum_{\forall u} N_{k,u}}. \tag{4.7}$$

The SINR at the UE is expressed as:

$$\text{SINR} = \frac{P_{\text{rx}}}{I_u + \sigma^2}, \tag{4.8}$$

where σ^2 represents the noise power.

Backhaul Link via RIS Assistance

To mitigate the impact of seasonal foliage, RISs can be introduced to assist the backhaul transmission. An RIS is composed of passive reflective elements that intelligently direct signals towards the intended destination. The received signal at the RIS-assisted IAB child node is expressed as:

$$y = \sqrt{P_{\text{tx}}}\mathbf{g}_c \mathbf{w}_c x + z, \tag{4.9}$$

where $\mathbf{w}_c$ is the beamforming vector and z represents additive Gaussian noise.

The equivalent channel gain with RIS assistance is given by:

$$\mathbf{g}_c = \mathbf{g}_{ru} \mathbf{\Omega} \mathbf{g}_{br}, \tag{4.10}$$

where $\mathbf{g}_{br}$ and $\mathbf{g}_{ru}$ are the channel coefficients for the donor-to-RIS and RIS to IAB-child links, respectively. The RIS reflection matrix is:

$$\mathbf{\Omega} = \text{diag}(e^{j\omega_1}, \ldots, e^{j\omega_M}). \tag{4.11}$$

The backhaul data rate with RIS assistance is given by:

$$R = \log\left(1 + \frac{P\left|\mathbf{g}_{ru}\mathbf{\Omega}\mathbf{g}_{br}\mathbf{w}_c\right|^2}{\sigma^2}\right). \tag{4.12}$$

By optimizing the RIS reflection phases, the effective channel gain can be maximized, improving signal propagation in dense foliage environments. This approach ensures seamless connectivity for IAB child nodes under challenging propagation conditions.

4.3 Service Coverage Probability under Different Environmental Effects

Simulation results in [91] illustrate the effectiveness of RIS-assisted IAB networks in maintaining CP despite challenging environmental conditions. The impact of tree foliage, user density, and carrier frequency on network performance is analyzed.

- **Tree Foliage Impact**: The results demonstrate that direct links suffer significant performance degradation with increasing tree foliage depth.
- **Carrier Frequency and User Density**: Lower frequencies (e.g., 28 GHz) perform better in dense foliage environments compared to higher frequencies (e.g., 38 GHz). Increasing user density reduces coverage probability due to increased competition for resources.

4.4 Role of Main Lobe Antenna Gain

Higher main lobe antenna gains contribute to improved coverage probability, especially in moderate foliage conditions. However, at deeper foliage depths, additional measures such as RIS placement or alternative backhaul solutions (e.g., NCRs) become necessary.

4.5 Practical Deployment Considerations

The deployment of RIS in wide-area IAB networks should consider:

- **Strategic RIS Placement**: Optimal positioning of RIS elements along known obstruction paths enhances performance.
- **Hybrid Network Solutions**: Combining RIS with IAB child nodes and NCRs improves coverage in high-density environments.
- **Frequency Band Selection**: Lower mmWave frequencies offer better coverage in foliage-heavy areas, while higher frequencies provide higher capacity but require additional signal optimization strategies.

The integration of RIS into wide-area IAB networks presents a viable solution for addressing environmental challenges such as tree foliage, rain intensity, and user density variations. Simulation results in paper [D] highlight the potential of RIS in improving CP while maintaining energy efficiency. By strategically deploying RIS elements, optimizing main lobe antenna gains, and selecting suitable frequency bands, network operators can enhance the reliability of IAB networks in sub-urban and rural deployments. Future research should focus on refining RIS beamforming algorithms

and exploring hybrid solutions combining RIS, SBS, and NCRs to further improve wireless connectivity in challenging environments.

CHAPTER 5

Hybrid Backhaul Architectures for IAB Networks with Joint Fiber and Free Space Optical Infrastructure Planning

As introduced in Section 1.1, a key bottleneck in realizing dense deployments is the backhaul, i.e., the link connecting the distributed APs to the core network. Traditional backhaul technologies such as fiber optics and microwave links present both benefits and drawbacks. Fiber offers high throughput and reliability but may come with high capital expenditure in some countries, extended installation times, and challenges in scaling to dense urban or remote rural environments. Conversely, microwave links are more flexible and easier to deploy but suffer from spectrum constraints, interference, and susceptibility to weather induced degradation, especially in mmWave bands.

IAB introduced in 3GPP Release 16, emerges as a promising solution to these challenges. IAB enables the use of the same radio access technology and spectrum for both access and backhaul, facilitating cost-efficient, wireless deployments without the need for extensive fiber infrastructure. IAB nodes act as relays, forming dynamic multi-hop networks that extend coverage.

To improve resilience and capacity, recent research has proposed hybrid backhaul architectures that integrate IAB with fiber/FSO communications. FSO utilizes tightly directed light beams typically in the infrared or visible range for high speed, wireless data transmission without requiring physical cabling. It offers several advantages including multi Gbps capacity, immunity to RF interference, strong security, and operation within license free spectrum. Moreover, FSO can help mitigate RF congestion and serve as an alternative or supplementary backhaul link to mmWave

IAB.

However, FSO systems are vulnerable to environmental factors such as fog, heavy rain, and dust, which can severely attenuate the signal. To counter these issues, adaptive link management strategies have been proposed, such as real time switching between FSO and RF links, dynamic load balancing, and context-aware dual mode transceivers. These strategies aim to improve reliability, enhance Quality of Service (QoS), and maintain robust network connectivity under varying conditions [92], [93], [94], [95]. In particular, a key advantage of incorporating FSO into IAB-based backhaul networks is that the two technologies exhibit complementary behavior under different weather conditions. The mmWave IAB links tend to degrade under heavy rain, whereas FSO links are comparatively resilient to rainfall but are more sensitive to fog, snow, and atmospheric scattering. Conversely, IAB is much less affected in such conditions. Furthermore, IAB, the access link can have the NLOS without bringing signficant degradations. In the backhaul link also 3GPP supports NLOS backhaul, and thus LOS is not a must. However, it is prefered to have LOS links. Therefore, combining IAB and FSO in a joint backhaul design provides built-in robustness, allowing the network to maintain reliable connectivity across a wide range of weather scenarios.

Despite the promise of both IAB and FSO, current research often treats them in isolation. IAB studies typically explore node placement, routing, and scheduling under idealized conditions, while FSO research focuses on beam alignment, channel modeling, and mitigation of atmospheric impairments, often neglecting their integration into broader network designs. This segmented approach creates a gap in the development of holistic hybrid backhaul solutions.

This chapter proposes an intelligent and unified backhaul framework that dynamically integrates fiber, IAB, and FSO technologies. By exploiting the scalability of IAB, the capacity of FSO, and the reliability of fiber, such a system can adapt to real time environmental conditions, traffic demands, and service requirements, thereby offering improved performance.

5.1 System Model

We consider a downlink transmission scenario in a two hop IAB network, where an IAB donor connected to the core network via a fiber link supports multiple child IAB nodes and UEs. An in-band operation is assumed for both access and backhaul links within the same mmWave band, providing resource flexibility at the cost of coordination complexity [96].

Each IAB node consists of a MT and a DU. The DU serves either UEs or the MT of downstream IAB nodes, while the MT establishes a backhaul connection to its upstream node. The DU is functionally similar to a gNB, while the MT acts similarly to a UE with some distinct capabilities.

Exponential blocking model is used to capture obstructions, and the mmWave channel is modeled using the 5GCM UMa close-in path loss model, [83], [97]:

$$P_{\mathrm{r}} = P_{\mathrm{t}} h_{\mathrm{t,r}} G_{\mathrm{t,r}} L_{\mathrm{t,r}} (\|x_{\mathrm{t}} - x_{\mathrm{r}}\|)^{-1}, \tag{5.1}$$

where P_{t} is the transmit power, $h_{\mathrm{t,r}}$ represents small-scale fading, $G_{\mathrm{t,r}}$ is the antenna gain, and $L_{\mathrm{t,r}}$ is the path loss depending on LoS or NLoS conditions.

The antenna gain follows a sectored model:

$$G_{\mathrm{t,r}}(\alpha) = \begin{cases} G_{\mathrm{m}} & \text{if } |\alpha| \leq \frac{\alpha_{\mathrm{HP}}}{2}, \\ G_{\mathrm{s}} & \text{otherwise,} \end{cases} \tag{5.2}$$

where G_{m} and G_{s} denote the main and side lobe gains respectively.

The interference at UE u is given by:

$$I_u = \sum_{i \in \chi_{i,u} \setminus \{w_u\}} P_i h_{i,u} G_{i,u} L_{i,u} (\|x_i - x_u\|)^{-1}, \tag{5.3}$$

and for a child IAB node c, the backhaul interference is:

$$I_c = \sum_{j \in \chi_{j,c} \setminus \{w_c\}} P_j h_{j,c} G_{j,c} L_{j,c} (\|x_j - x_c\|)^{-1}. \tag{5.4}$$

Bandwidth W is partitioned as follows:

$$\begin{cases} W_{\mathrm{Backhaul}} = \beta W, \\ W_{\mathrm{Access}} = (1-\beta) W, \end{cases} \tag{5.5}$$

where $\beta \in [0, 1]$ is the partitioning factor. The achievable data rate for UE u is:

$$R_u = \begin{cases} \frac{(1-\beta)W}{N_d} \log_2(1 + \mathrm{SINR}(x_u)), & \text{if } w_u \in \chi_d, \\ \min\left(\frac{(1-\beta)WN}{\sum N_{j,u}} \log_2(1 + \mathrm{SINR}(x_u)), \frac{\beta W N}{\sum N_j} \log_2(1 + \mathrm{SINR}(x_b)) \right), & \text{if } w_u \in \chi_c. \end{cases} \tag{5.6}$$

Here, χ_d, χ_c, and χ_u denote the sets of IAB donors, child nodes, and UEs respectively.

The network planning objective is to maximize service coverage, defined as the proportion of UEs whose data rates exceed a given threshold η:

$$\mathrm{CP} = \Pr(R_u \geq \eta). \tag{5.7}$$

Through optimization of deployment strategies under fiber distance and cost constraints, in Paper [E] we demonstrate that significant improvements in IAB network coverage can be achieved, particularly when FSO links are integrated.

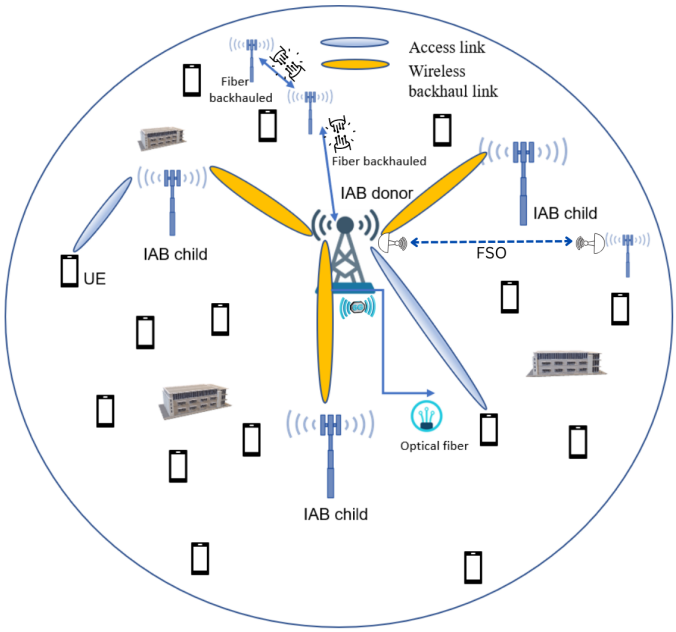

Figure 5.1: Schematic of the hybrid IAB system model.

5.2 Fiber Backhaul Connection Placement

Fiber Backhaul Connection Placement Algorithm

We model the fiber-backhaul planning of the network as a graph $\Gamma = (V, E)$, where V is the set of BSs and E the set of fiber links interconnecting them. BSs are categorized as IAB donors, i.e., MBSs, V_m and IAB-child nodes, i.e., SBSs, V_s. The IAB child nodes are further divided into two groups: those connected via fiber ($V_{Fib} \subset V_s$) and those connected via IAB wireless backhaul ($V_{IAB} \subset V_s$). The IAB donors V_m are assumed to be interconnected in a ring topology using fiber links $E_m \subset E$. Let $l(P)$ denote the total length of a path P, and $dist(v, u)$ be the Euclidean distance between two BSs v and u. Due to practical constraints in fiber rollouts, they require an incremental rollout to spread costs over time, which motivates a two-stage planning approach. Figure 5.1 depicts the schematic of such hybrid IAB network.

Algorithm 5: Planning Connected Fiber-Backhaul Topology

This algorithm generates a fully connected topology by iteratively connecting disconnected IAB child nodes to their nearest already-connected node. The process begins with the ring-connected IAB donors and ensures that all other nodes become reachable through minimum edge additions.

The algorithm maintains a working set V_0 of disconnected nodes (i.e., nodes with degree zero in the current graph). At each iteration, a random node $v \in V_0$ is selected and connected to the closest node $u \in V \setminus V_0$ already part of the graph. The edge (v, u) is then added to Γ, and v is removed from V_0. This continues until V_0 is empty and the graph is fully connected.

Algorithm 5 Plan connected fiber-backhaul topology

Require: $\Gamma = (V, E)$: Initial disconnected graph (e.g., only IAB donor node ring)
Ensure: Γ: Connected graph with all nodes reachable
$V_0 \leftarrow \{v \in V \mid \text{degree}(v) = 0\}$ {Nodes with no connections}
while $V_0 \neq \varnothing$ **do**
  Select random node $v \in V_0$
  $u \leftarrow \arg\min_{w \in V \setminus V_0} \text{dist}(v, w)$ {Closest connected node}
  Add edge (v, u) to Γ
  $V_0 \leftarrow V_0 \setminus \{v\}$
return Γ =0

This step provides a cost-efficient baseline structure where every IAB child node is reachable. However, the edge selection is purely distance-based and does not consider deployment costs such as trenching or transceivers. This motivates the second algorithm.

Algorithm 6: Fiber-Backhaul Connection Placement (FBCP)

While Algorithm 5 ensures connectivity, Algorithm 6 optimizes which N IAB child nodes to connect via dedicated fiber links. It uses a tunable weight parameter $\alpha \in [0, 1]$ to balance between minimizing deployment cost and maximizing spatial separation among fiber-connected IAB child nodes (for improved load balancing and coverage).

At each iteration, the algorithm evaluates all currently unconnected IAB child nodes in V_{IAB}. For each node v, it computes:

- The shortest path p^* to any IAB donor in V_m, using the connected topology from Algorithm 5.
- The cost of adding the required edges E' to reach v from the backbone, factoring in trenching (β_{dig}), fiber cost (β_{fiber}), and transceivers (β_{trx}).
- A separation metric, calculated as the inverse of distances from v to all already fiber-connected nodes in $V_{Fib} \cup V_m$.

These metrics are normalized, and a weighted objective is computed:

$$w_v = \alpha\, s_v + (1 - \alpha)\, c_v$$

where w_v is the weighted objective for IAB child node v, s_v is the normalized separation metric of v, and c_v is the normalized cost metric of v. The IAB child node v^* with the minimum score is selected for fiber connection. The graph is updated accordingly, and the process repeats until N IAB child nodes are fiber-connected.

Algorithm 6 Fiber-backhaul connection placement FBCP(α)

Require:
- $\Gamma = (V, E)$: Initial network with IAB donor nodes ring
- V_m: Set of IAB donors
- $V_{IAB} \subset V_s$: IAB child nodes with IAB backhaul
- $V_{Fib} \subset V$: Fiber-connected IAB child nodes
- N: Number of IAB child nodes to connect with fiber
- $\alpha \in [0, 1]$: Weight between separation and cost

Ensure: Updated graph Γ, V_{IAB}, V_{Fib}

$\Gamma_{design} \leftarrow$ Connected graph from Algorithm 5
for $i = 1$ to N **do**
  for all $v \in V_{IAB}$ **do**
    Find shortest path p^* from v to any $v_m \in V_m$ in Γ_{design}
    $E' \leftarrow$ Edges in p^* not already in Γ
    $\Gamma'[v] \leftarrow \Gamma + E'$
    $c_v \leftarrow \beta_{dig} \cdot l(E') + \beta_{fiber} \cdot l(p^*) + 2 \cdot \beta_{trx}$
    $s_v] \leftarrow \sum_{u \in V_{Fib} \cup V_m} \frac{1}{\text{dist}(v,u)}$
  Normalize c_v and s_v for all $v \in V_{IAB}$
  for all $v \in V_{IAB}$ **do**
    $w_v \leftarrow \alpha \cdot s_v + (1 - \alpha) \cdot c_v$
  $v^* \leftarrow \arg\min_{v \in V_{IAB}} w_v$
  $\Gamma \leftarrow \Gamma'[v^*]$
  $V_{IAB} \leftarrow V_{IAB} \setminus \{v^*\}$
  $V_{Fib} \leftarrow V_{Fib} \cup \{v^*\}$
return Γ, V_{IAB}, V_{Fib} =0

The FBCP algorithm is flexible and can support:

- Pure cost minimization by setting $\alpha = 0$
- Maximum separation-based planning with $\alpha = 1$
- Balanced trade-offs with $0 < \alpha < 1$

In practical deployment scenarios, α can be tuned based on available budget, expected UE spatial distribution, and desired QoS, performance targets.

CHAPTER 6

Summary of included papers and Future work

This chapter summarizes the contributions of each appended publication and lays out possible directions for future work based on the topics in this thesis.

6.1 Paper A

C. Madapatha, B. Makki, C. Fang, O. Teyeb, E. Dahlman, M. Alouini, T. Svensson, "On integrated access and backhaul networks: Current status and potentials," IEEE open j. Commun. Soc., vol. 1, pp. 1374–1389, Sep. 2020.

In this paper, we study the potential and challenges of IAB as a key enabler for 5G and beyond wireless networks. It provides a comprehensive evaluation of IAB from multiple perspectives, including a summary of relevant developments in 3GPP Release 16 and selected discussions from Release 17 available at the time of writing. The paper outlines key IAB-specific agreements across various protocol layers. Focusing on mmWave communications at 28 GHz, the study assesses IAB performance in both dense urban and suburban environments. A FHPPP-based stochastic geometry model is used to represent random distributions of IAB nodes and user equipment, enabling analysis of service coverage probability. Additionally, the network's resilience to environmental factors such as tree foliage, rainfall, and physical blockages is examined. The findings highlight IAB as a promising solution for providing flexible and cost-effective backhaul in future wireless networks.

Charitha contributed to formulating the research questions, conducted the analysis, and performed all the simulations and wrote the paper. Other co-authors contributed

to formulating the research, standardization insights in the paper, polishing of the result analysis, paper review and feedback.

6.2 Paper B

C. Madapatha, B. Makki, A. Muhammad, E. Dahlman, M.-S. Alouini, and T. Svensson, "On topology optimization and routing in integrated access and backhaul networks: A genetic algorithm-based approach," IEEE OJ-COMS, vol. 2, pp. 2273–2291, Sep. 2021.

In this paper, we investigate the topology optimization and routing strategies in IAB networks. It proposes efficient GA-based approaches for optimizing the placement of IAB nodes and the distribution of non-IAB backhaul links in mmWave frequency bands. The impact of temporal blockages on routing performance is also evaluated. In addition, the paper summarizes relevant 3GPP Release 16 and Release 17 discussions on IAB routing. It further analyzes the influence of key parameters such as blockage, tree foliage, and antenna gain on network performance.

Charitha contributed to formulating the research questions, conducted the analysis, and performed all the simulations and wrote the paper. Other co-authors contributed to formulating the research, standardization insights in the paper, polishing of the result analysis, paper review and feedback.

6.3 Paper C

C. Madapatha, B. Makki, H. Guo, and T. Svensson, "Constrained deployment optimization in integrated access and backhaul networks," in 2023 IEEE Wire-less Communications and Networking Conference (WCNC), 2023, pp. 1–6.

Network planning is crucial for IAB deployments due to the sensitivity of the backhaul links and the high rate demands. The paper analyses and optimizes service coverage probability of IAB networks focusing on cases with either geographical or interference management constraints where IAB nodes may not be permitted/feasible to be deployed freely. To that end, we propose various mmWave blocking-aware constrained deployment optimization approaches. The results indicate that, even with limitations on deployment optimization, network planning boosts the coverage probability of IAB networks considerably.

Charitha contributed to formulating the research questions, conducted the analysis, and performed all the simulations and wrote the paper. Other co-authors contributed to formulating the research, standardization insights in the paper, polishing of the result analysis, paper review and feedback.

6.4 Paper D

C. Madapatha, B. Makki, H. Guo, and T. Svensson, "Reconfigurable intelligent surfaces-assisted integrated access and backhaul," IEEE International Black Sea Conference on Communications and Networking (IEEE Blackseacom), Jun. 2025.

In this paper, we study the impact of RISs on the coverage extension of IAB networks. Particularly, using a finite stochastic geometry model, with random distributions of UEs in finite region, and planned hierachical architecture for IAB, we study the service coverage probability defined as the probability of the event that the UEs' minimum rate requirements are satisfied. We present comparisons between different cases including IAB-only, IAB assisted with RIS for backhaul as well as IAB assisted by NCRs.

Our investigations focus on wide-area IAB assisted with RIS through the lens of different design architectures and deployments, revealing both conflicts and synergies for minimizing the effect of tree foliage over seasonal changes. Our simulation results reveal both opportunities and challenges towards the implementation of RIS in IAB.

Charitha contributed to formulating the research questions, conducted the analysis, and performed all the simulations and wrote the paper. Other co-authors contributed to formulating the research, standardization insights in the paper, polishing of the result analysis, paper review and feedback.

6.5 Paper E

C. Madapatha, P. Lechowicz, C. Natalino, P. Monti, and T. Svensson, "Joint fiber and free space optical infrastructure planning for hybrid integrated access and backhaul networks," Accepted for IEEE International Symposium on Personal, Indoor and Mobile Radio Communications (PIMRC), Istanbul, Turkey, Sept. 2025.

Here, in this paper, we examine the role of infrastructure planning and optimization in enhancing the coverage performance of IAB networks, a key enabler for 5G and future 6G systems. IAB leverages the same hardware to deliver both backhaul and access services in a multi-hop architecture. Given the high rate and reliability demands of backhaul links, careful network design is essential. The study focuses on scenarios with limited fiber connectivity due to cost constraints and investigates the potential of integrating FSO communication links as an alternative. Results demonstrate that hybrid jointly optimized IAB/fiber/FSO deployments can significantly reduce costs while maintaining or improving service coverage probability. The analysis highlights that with strategic planning, IAB networks can achieve enhanced coverage, energy efficiency, and cost-effectiveness.

Charitha contributed to formulating the research questions, conducted the analysis, and Piotr performed simulations related to FSO/fiber infrastructure placement while

Charitha IAB/wireless network related simulations and wrote the paper. Other co-authors contributed to formulating the research questions in the paper, polishing of the result analysis, paper review and feedback.

6.6 Related other contributions

Contributions from related other publications by the author, but not included in the thesis are described below.

In Paper F, "Joint Scheduling and Throughput Maximization in Self-backhauled Millimeter Wave Cellular Networks"in *Proc. IEEE ISWCS*, Berlin, Germany, Sept. 2021, pp. 1-6, we discuss the joint scheduling and throughput maximization in IAB networks over mmWave cellular networks. In particular, IAB networks have the potential to provide high data rate in both access and backhaul networks by sharing the same spectrum. Due to the dense deployment of SBSs, IAB networks connect SBSs to the core network in a wireless manner without the deployment of high-cost optical fiber. As large spectrum is available in mmWave bands and high data rate is achieved by using directional beamforming, such IAB-type communication has become viable. The access and backhaul links can be integrated in the same frequency band while satisfying QoS constraints. This paper optimizes the scheduling of access and backhaul links such that the minimum throughput of the access links is maximized based on the revised simplex method. By considering a probability based LoS and NLoS path loss model and the antenna array gains, the paper compares the achievable minimum access throughput of the IAB network with the network having only macro base stations, and studies the effect of the network topology and antenna parameters on the achievable minimum throughput. Simulation results show that, for a broad range of parameter settings, the implementation of IAB networks improves the access minimum achievable throughput.

In Paper G, "Uplink Power Control in Integrated Access and Backhaul Networks" in *Proc. IEEE DySPAN*, Los Angeles, CA, USA, Dec. 2021, pp. 163-168, power control combined with resource allocation algorithms is used to develop efficient IAB networks with high service coverage. Particularly, the paper develops a genetic algorithm-based solution for the power control of both user equipments and IAB nodes such that the network uplink service coverage probability is maximized. Finally, considering mmWave channel models, the paper studies the effect of different parameters including minimum data rate requirement, coverage distance and transmit power on the network performance. As the results show, a power allocation scheme with well-tuned parameters can improve the uplink performance of IAB networks considerably. Moreover, with mmWave communications and a proper network deployment, the effect of interference on the service coverage probability is negligible.

In Paper H, "Integrating Reconfigurable Intelligent Surfaces (RISs) into Indoor D-MIMO Networks for 6G" in Proc. IEEE VTC2024-Fall, Washington, DC, USA,

2024, pp. 1–6, the integration of RISs into distributed MIMO (D-MIMO) systems is explored as a solution to enhance scalability, energy efficiency, and service coverage in future 5G and 6G indoor networks. The paper proposes dynamic user-centric AP clustering and optimized RIS placement techniques to address the challenges of high obstacle density in large indoor environments. An alternating optimization algorithm is used to configure RIS phase shifts with low computational complexity. The study evaluates key performance indicators including service coverage probability and energy consumption. As the results show, incorporating RISs into D-MIMO systems significantly improves energy efficiency and network scalability, making it a promising direction for future indoor wireless deployments.

In Paper I, "Distributed MIMO Systems for 6G" in Proc. 2023 Joint European Conference on Networks and Communications & 6G Summit (EuCNC/6G Summit), Gothenburg, Sweden, 2023, pp. 156–161, the role of D-MIMO systems in meeting the demanding requirements of 6G networks is explored. The paper highlights the advantages of D-MIMO, particularly its ability to provide macro diversity and enhance scalability in future wireless systems. Various deployment options are proposed, categorized by fronthaul/backhaul type (wireless or wired), signal format (analog or digital), processing architecture (distributed or centralized), and transmission method (coherent or non-coherent). The study aligns with 3GPP terminology to support ongoing standardization efforts and discusses essential enablers for large-scale D-MIMO implementation, including analog radio-over-fiber, channel estimation, and mobility support in dynamic environments. Simulation results demonstrate the potential of integrated access and backhaul, network-controlled repeaters, and reconfigurable intelligent surfaces as cost-efficient solutions for densifying D-MIMO networks at both low and high frequency bands.

In Paper J, "Beamforming in Wireless Coded-Caching Systems" in Proc. IEEE FNWF, 2023, pp. 1–6, a wireless transport network architecture is proposed that integrates beamforming and coded-caching techniques to address transport network capacity challenges caused by increased access network traffic. The system consists of a multi-antenna server broadcasting content to cache nodes that serve end users. Traditional caching approaches suffer from memory limitations and added overhead, which this design overcomes by leveraging coded caching and spatial multiplexing. A genetic algorithm-based method is developed to optimize beamforming in this setting, improving multicast efficiency, reducing interference, and lowering peak backhaul traffic. The paper compares the performance of this joint design with conventional uncoded caching schemes and analyzes the effects of various buffering and decoding strategies. Results show that proper beamforming significantly enhances the effectiveness of coded caching, leading to notable reductions in backhaul load.

In Paper K, "Integrated Communication, Localization, and Sensing in 6G D-MIMO Networks" in IEEE Wireless Communications, 2025, the potential of integrating sens-

ing and communication functionalities within 6G D-MIMO networks is investigated. The paper highlights the challenges of sensing, particularly limited coverage and infrastructure demands when compared to traditional communication services. By leveraging the dense deployment and coordinated control of D-MIMO nodes, the study explores distributed ISAC as a viable solution to improve service uniformity. Various architectural designs and deployment strategies for ISAC in D-MIMO are examined, identifying both conflicts and synergies. Through simulations and experimental demonstrations, the paper presents key insights into the performance trade-offs and practical challenges associated with implementing ISAC in future 6G networks.

In Paper L, "Towards Resilient, Space, and Frequency Domain Cooperative Distributed-Large MIMO Systems" accepted to IEEE Wireless Communications, 2025, the evolution of large MIMO architectures for 6G networks is explored, with a focus on resilient and adaptive deployment strategies. Building on key findings from the Hexa-X-II European 6G Flagship project, the paper examines a hybrid architecture combining co-located and D-MIMO systems, utilizing multiple carrier frequencies and coordinated transmissions under the assumption of ideal channel state information. The study evaluates energy efficiency and data rate performance across various user densities and proposes a framework for selecting the optimal MIMO configuration based on spatial user distribution. The paper underscores the importance of adaptive and scalable MIMO systems to meet the stringent performance demands of 6G and outlines future research directions for realizing resilient large MIMO deployments in practical networks.

6.7 Future Work

The thesis is contributing in evaluating IAB networks and design effective techniques to improve the performance for 5G NR and beyond, focusing on a two-hop (tier) multi-cellular system. In particular, the thesis analyzes IAB networks under environmental constraints, explored optimization of node placement and routing, and assessed RIS- and FSO-assisted architectures. While these results advance understanding, further work is needed on dynamic environments with mobility, heterogeneous traffic, and seasonal variations.

The thesis also focuses on IAB in various aspects including an overview of 3GPP discussion. In the literature, IAB remains mostly explored under simplified models, with limited prototypes and little attention to RIS control overhead, FSO optimality, or scalable interference management. Research on mIAB, while emerging, is still at an early stage and requires deeper study of handover, coverage continuity, and energy efficiency.

In 3GPP, IAB has been specified in Releases 16–17, with Releases 18–19 extending work on advanced routing, and IAB scenarios. Aligning future research with these

trends is essential.However, further investigation/research can be made in the future given that IAB has become an important and broad topic.

- Identify efficient algorithms for resource allocation.

  More advanced schemes can jointly optimize access and backhaul bandwidth, account for end-to-end bottlenecks and adapt to traffic and channel dynamics. This would extend current knowledge from the thesis to more intelligent, 3GPP-aligned scheduling approaches that improve fairness, efficiency, and robustness. Especially, the access bandwidth allocation among users can be done based on fairness or load.

- Conduct theoretical analysis of FHPPP in IAB node distributions.

  Tractable expressions on performance metrics such as service coverage probability, latency can be derived enabling better modelling and insights.

- Study interference cancellation in in-band IAB.

  Exploring schemes beyond simple avoidance, by focusing on beamforming, and cooperative transmission. An open direction is integrating cell-free/D-MIMO architectures, where distributed nodes jointly serve users, offering new degrees of freedom for interference cancellation and spectral efficiency in IAB networks.

- Derive the optimal value for access and backhaul bandwidth allocation.

  Derivation of optimal access–backhaul bandwidth splits is important not only in general deployments but also for specific scenarios such as emergency communications or temporary events. In such cases, dynamic optimization could ensure minimum QoS and speedy recovery, moving beyond static or heuristic allocations studied in current literature.

- Study joint beamforming for access and backhaul in IAB networks. In particular, unlike treating access and backhaul beamforming separately, joint optimization can balance coverage and backhaul quality, reduce interference, and enhance spatial multiplexing gains.

- Refine RIS beamforming algorithms and exploring hybrid solutions combining RIS, IAB-type SBSs, and network-controlled repeaters to further improve wireless connectivity using context information in challenging environments. This thesis is built upon a HetNet, however, the context information can be more actively used and beamforming algorithms can be refined, by incorporating into digital twin setups.

- Study IAB and optimal fronthaul/backhaul split in the context of cell-free/D-MIMO access using distributed antenna systems.

This thesis is built upon a HetNet with heirarchical cellular structure. Investigating the optimal fronthaul/backhaul on D-MIMO and similar networks will enhance the benefits, as such optimality derivations can balance the coordination overhead transmissions improving the scalability and spectral efficiency of distributed APs.

- Study the potential and challenges of mIAB.

  This thesis is built upon static IAB scenarios, however, given the applicability in various use cases including ubiquitous communication, analysis of a tractable framework in mIAB network is beneficial. Especially, mIAB can extend the coverage and support rapid deployment in emergency communication during natural disasters such as wild fires.

References

[1] C. Dehos, J. L. González, A. De Domenico, D. Ktenas, and L. Dussopt, "Millimeter wave access and backhauling: The solution to the exponential data traffic increase in 5G mobile communications systems?" *IEEE Commun. Mag.*, vol. 52, no. 9, pp. 88–95, 2014.

[2] S. Dang, O. Amin, B. Shihada, and M.-S. Alouini, "What should 6G be?" *Nature Electronics*, vol. 3, no. 1, pp. 20–29, 2020.

[3] C. Fang, C. Madapatha, B. Makki, and T. Svensson, "Joint scheduling and throughput maximization in self-backhauled millimeter wave cellular networks," in *Proc. IEEE ISWCS'2021*, Virtual, Sep. 2021, pp. 1–6.

[4] B. Tezergil and E. Onur, "Wireless backhaul in 5g and beyond: Issues, challenges and opportunities," *arXiv preprint arXiv:2103.08234*, 2021.

[5] S. Julião et al., "High performance microwave point-to-point link for 5G backhaul with flexible spectrum aggregation," in *Proc. IEEE MTT-S'2015*, Arizona, USA, May 2015, pp. 1–4.

[6] J. Edstam, J. Hansryd, S. Carpenter, T. Emanuelsson, Y. Li, and H. Zirath, "Microwave backhaul evolution—reaching beyond 100 Ghz," *Ericsson technology review*, no. 2, 2017.

[7] GSMA, "Spectrum for wireless backhaul," *GSMA*, 2021, Available: https://www.gsma.com/spectrum/wp-content/uploads/2021/02/wireless-backhaul-spectrum-positions.pdf (accessed July. 1, 2022).

[8] N. Rajatheva et al., "Scoring the terabit/s goal: Broadband connectivity in 6G," *arXiv preprint arXiv:2008.07220*, 2020.

[9] X. Wang et al., "Millimeter wave communication: A comprehensive survey," *IEEE Commun. Surv. Tutor.*, vol. 20, no. 3, pp. 1616–1653, Jun. 2018.

[10] A. Bhattacharjee, R. Bhattacharjee, and S. K. Bose, "Mitigation of beam blocking in mmwave indoor wpan using dynamic control delegation based approach," in *Proc. IEEE ANTS'2016*, IEEE, Bangalore, India, Nov. 2016, pp. 1–6.

[11] M. N. Kulkarni, S. Singh, and J. G. Andrews, "Coverage and rate trends in dense urban mmwave cellular networks," in *Proc. IEEE GLOBECOM'2014*, IEEE, Austin, USA, Dec. 2014, pp. 3809–3814.

[12] X. Zhang, Y. Liu, Y. Wang, and J. Bai, "Performance analysis and optimization for non-uniformly deployed mmwave cellular network," *EURASIP Journal on Wireless Communications and Networking*, vol. 2019, no. 1, pp. 1–15, 2019.

[13] J. G. Andrews, T. Bai, M. N. Kulkarni, A. Alkhateeb, A. K. Gupta, and R. W. Heath, "Modeling and analyzing millimeter wave cellular systems," *IEEE Trans. Commun.*, vol. 65, no. 1, pp. 403–430, Oct. 2016.

[14] M. Cudak, A. Ghosh, A. Ghosh, and J. Andrews, "Integrated access and backhaul: A key enabler for 5G millimeter-wave deployments," *IEEE Communications Magazine*, vol. 59, no. 4, pp. 88–94, 2021.

[15] Y. Li, E. Pateromichelakis, N. Vucic, J. Luo, W. Xu, and G. Caire, "Radio resource management considerations for 5G millimeter wave backhaul and access networks," *IEEE Commun. Mag.*, vol. 55, no. 6, pp. 86–92, Jun. 2017.

[16] A. H. Jazi, S. M. Razavizadeh, and T. Svensson, "Integrated access and backhaul in cell-free massive mimo systems," *arXiv preprint arXiv:2210.12633*, 2022.

[17] B. Makki, M. Coldrey, and M. Hashemi, "An adaptive multiple access scheme in integrated access and backhaul networks," 2019 / 0253136 A1, Aug. 2019.

[18] V. F. Monteiro et al., "Paving the way toward mobile iab: Problems, solutions and challenges," *IEEE open j. Commun. Soc.*, vol. 3, pp. 2347–2379, 2022.

[19] G. C. M. Da Silva et al., "Cellular network densification: A system-level analysis with iab, ncr, and ris," *IEEE Access*, vol. 13, pp. 129 269–129 283, 2025.

[20] B. Yin, N. Wang, Y. Fan, X. Sun, D. He, and W. Liu, "Evaluation of TDM-based integrated access and backhaul schemes for 5G and beyond at mmWave band," in *Proc. IEEE CyberC'2020*, IEEE, Chongqing, China, Oct. 2020, pp. 348–353.

[21] W. Xie, N.-T. Mao, and K. Rundberget, "Cost comparisons of backhaul transport technologies for 5G fixed wireless access," in *in Proc. IEEE 5GWF'2018*, IEEE, California, USA, 2018, pp. 159–163.

[22] C. Madapatha et al., "On integrated access and backhaul networks: Current status and potentials," *IEEE open j. Commun. Soc.*, vol. 1, pp. 1374–1389, Sep. 2020.

[23] J. Gamboa and I. Demirkol, "Softwarized lTE self-backhauling solution and its evaluation," in *Proc. IEEE WCNC'2018*, Barcelona, Spain, Apr. 2018, pp. 1–6.

[24] R. Favraud and N. Nikaein, "Analysis of lTE relay interface for self-backhauling in lTE mesh networks," in *Proc. IEEE VTC-Fall'2017*, Toronto, Canada, Sep. 2017, pp. 1–7.

[25] G. Liebl, T. M. de Moraes, A. Gonzalez Rodriguez, and M. D. Nisar, "Centralized interference coordination in relay-enhanced networks," in *Proc. IEEE WCNCW'2012*, Toronto, Canada, Apr. 2012, pp. 306–311.

[26] M. Polese et al., "Integrated access and backhaul in 5G mmWave networks: Potential and challenges," *IEEE Commun. Mag.*, vol. 58, no. 3, pp. 62–68, 2020.

[27] 3GPP TR 36.806, "Evolved Universal Terrestrial Radio Access (E-UTRA); Relay architectures for E-UTRA (LTE-Advanced)," 3rd Generation Partnership Project (3GPP), Technical Specification (TS), Apr. 2010.

[28] V. F. Monteiro et al., "Paving the way towards mobile IAB: Problems, solutions and challenges," *arXiv preprint arXiv:2206.14946*, 2022.

[29] B. Ai, A. F. Molisch, M. Rupp, and Z.-D. Zhong, "5G key technologies for smart railways," *Proceedings of the IEEE*, vol. 108, no. 6, pp. 856–893, 2020.

[30] Y. Sui, A. Papadogiannis, W. Yang, and T. Svensson, "Performance comparison of fixed and moving relays under co-channel interference," in *Proc. IEEE Globecom'2012*, IEEE, California, USA, Dec. 2012, pp. 574–579.

[31] M. Gapeyenko, V. Petrov, D. Moltchanov, S. Andreev, N. Himayat, and Y. Koucheryavy, "Flexible and reliable uav-assisted backhaul operation in 5G mmWave cellular networks," *IEEE J. Sel. Areas Commun.*, vol. 36, no. 11, pp. 2486–2496, 2018.

[32] H. Guo, B. Makki, D.-T. Phan-Huy, E. Dahlman, M.-S. Alouini, and T. Svensson, "Predictor antenna: A technique to boost the performance of moving relays," *IEEE Commun. Mag.*, vol. 59, no. 7, pp. 80–86, 2021.

[33] H. Guo, B. Makki, M.-S. Alouini, and T. Svensson, "A semi-linear approximation of the first-order marcum q-function with application to predictor antenna systems," *IEEE Open Journal of the Communications Society*, vol. 2, pp. 273–286, 2021.

[34] H. Guo, B. Makki, M.-S. Alouini, and T. Svensson, "On delay-limited average rate of HARQ-based predictor antenna systems," *IEEE Wireless Commun. Lett.*, vol. 10, no. 8, pp. 1628–1632, 2021.

[35] H. Guo, B. Makki, M.-S. Alouini, and T. Svensson, "Power allocation in HARQ-based predictor antenna systems," *IEEE Wireless Commun. Lett.*, vol. 9, no. 12, pp. 2025–2029, 2020.

[36] H. Guo, "Towards context information-based high-performing connectivity in internet of vehicle communications," Ph.D. dissertation, Chalmers Tekniska Hogskola (Sweden), 2022.

[37] Y. Sui, J. Vihriala, A. Papadogiannis, M. Sternad, W. Yang, and T. Svensson, "Moving cells: A promising solution to boost performance for vehicular users," *IEEE Commun. Mag.*, vol. 51, no. 6, pp. 62–68, 2013.

[38] M. Sternad, M. Grieger, R. Apelfröjd, T. Svensson, D. Aronsson, and A. B. Martinez, "Using "predictor antennas" for long-range prediction of fast fading for moving relays," in *Proc. IEEE WCNCW'2012*, IEEE, 2012, pp. 253–257.

[39] D.-T. Phan-Huy, S. Wesemann, J. Björsell, and M. Sternad, "Adaptive massive MIMO for fast moving connected vehicles: It will work with predictor antennas!" In *Proc. ITG WSA'2018*, 2018, pp. 1–8.

[40] J. Bjorsell, M. Sternad, and D.-T. Phan-Huy, "Enabling multi-user m-MIMO for high-mobility users with predictor antennas: A deep analysis based on experimental nlos measurements," *IEEE Trans. Veh. Technol.*, 2022.

[41] V. F. Monteiro et al., "TDD frame design for interference handling in mobile iab networks," *arXiv preprint arXiv:2204.13198*, 2022.

[42] M. N. Islam, S. Subramanian, and A. Sampath, "Integrated Access Backhaul in Millimeter Wave Networks," in *Proc. IEEE WCNC'2017*, CA, USA, Mar. 2017, pp. 1–6.

[43] M. N. Islam, N. Abedini, G. Hampel, S. Subramanian, and J. Li, "Investigation of performance in integrated access and backhaul networks," in *Proc. IEEE INFOCOM WKSHPS'2018*, HI, USA, Apr. 2018, pp. 597–602.

[44] Y. Li, J. Luo, R. A. Stirling-Gallacher, and G. Caire, "Integrated access and backhaul optimization for millimeter wave heterogeneous networks," *arXiv*, 2019.

[45] Y. Liu, A. Tang, and X. Wang, "Joint incentive and resource allocation design for user provided network under 5G integrated access and backhaul networks," *IEEE Trans. Netw. Sci. Eng.*, vol. 7, no. 2, pp. 673–685, Apr. 2020.

[46] N. Tafintsev et al., "Reinforcement learning for improved uav-based integrated access and backhaul operation," in *Proc. IEEE ICC Workshops'2017*, Paris, France, May 2020, pp. 1–7.

[47] A. HasanzadeZonuzy, I. Hou, and S. Shakkottai, "Broadcasting real-time flows in integrated backhaul and access 5G Networks," in *Proc. IEEE WiOPT'2019*, Avignon, France, Jun. 2019, pp. 1–8.

[48] M. Polese, M. Giordani, A. Roy, D. Castor, and M. Zorzi, "Distributed Path Selection Strategies for Integrated Access and Backhaul at mmWaves," in *Proc. IEEE GLOBECOM'2018*, Abu Dhabi, United Arab Emirates, Dec. 2018, pp. 1–7.

[49] B. Zhai, M. Yu, A. Tang, and X. Wang, "Mesh architecture for efficient integrated access and backhaul networking," in *Proc. IEEE WCNC'2020*, Seoul, Korea (South), May 2020, pp. 1–6.

[50] O. Teyeb, A. Muhammad, G. Mildh, E. Dahlman, F. Barac, and B. Makki, "Integrated Access Backhauled Networks," in *Proc. VTC-Fall'2019*, Honolulu, HI, USA, Sep. 2019, pp. 1–5.

[51] J. Y. Lai, W. Wu, and Y. T. Su, "Resource allocation and node placement in multi-hop heterogeneous integrated-access-and-backhaul networks," *IEEE Access*, vol. 8, pp. 122 937–122 958, Jul. 2020.

[52] N. Chen, T. Qiu, X. Zhou, K. Li, and M. Atiquzzaman, "An intelligent robust networking mechanism for the internet of things," *IEEE Commun. Mag.*, vol. 57, no. 11, pp. 91–95, Nov. 2019.

[53] X. Meng, H. Inaltekin, and B. Krongold, "Deep reinforcement learning-based topology optimization for self-organized wireless sensor networks," in *Proc. IEEE GLOBECOM'2019*, IEEE, HI, USA, 2019, pp. 1–6.

[54] X. Fu, F. R. Yu, J. Wang, Q. Qi, and J. Liao, "Dynamic service function chain embedding for NFV-enabled iot: A deep reinforcement learning approach," *IEEE Trans. Wirel. Commun.*, vol. 19, no. 1, pp. 507–519, Oct. 2019.

[55] P. Sun, Y. Hu, J. Lan, L. Tian, and M. Chen, "Tide: Time-relevant deep reinforcement learning for routing optimization," *Future Generation Computer Systems*, vol. 99, pp. 401–409, Oct. 2019.

[56] M. Wang et al., "Neural network meets DCN: Traffic-driven topology adaptation with deep learning," *Proceedings of the ACM on Measurement and Analysis of Computing Systems*, vol. 2, no. 2, pp. 1–25, Jun. 2018.

[57] S. Zhang, B. Yin, and Y. Cheng, "Topology aware deep learning for wireless network optimization," *arXiv preprint arXiv:1912.08336*, 2019.

[58] P. V. Klaine, M. A. Imran, O. Onireti, and R. D. Souza, "A survey of machine learning techniques applied to self-organizing cellular networks," *Commun. Surv. Tutor.*, vol. 19, no. 4, pp. 2392–2431, Jul. 2017.

[59] Q. Mao, F. Hu, and Q. Hao, "Deep learning for intelligent wireless networks: A comprehensive survey," *Commun. Surv. Tutor.*, vol. 20, no. 4, pp. 2595–2621, Jun. 2018.

[60] S. Troia, R. Alvizu, and G. Maier, "Reinforcement learning for service function chain reconfiguration in NFV-SDN metro-core optical networks," *IEEE Access*, vol. 7, pp. 167 944–167 957, Nov. 2019.

[61] S. Wang and T. Lv, "Deep reinforcement learning for demand-aware joint vnf placement-and-routing," in *Proc. IEEE GC Wkshps'2019*, HI, USA, 2019, pp. 1–6.

[62] H. Lu and W. Fang, "Joint transmit/receive antenna selection in MIMO systems based on the priority-based genetic algorithm," *IEEE Antennas Wirel. Propag. Lett.*, vol. 6, pp. 588–591, Dec. 2007.

[63] S. Yan, X. Zhang, H. Xiang, and W. Wu, "Joint access mode selection and spectrum allocation for fog computing based vehicular networks," *IEEE Access*, vol. 7, pp. 17 725–17 735, Jan. 2019.

[64] Y. Chang, X. Yuan, B. Li, D. Niyato, and N. Al-Dhahir, "Machine-learning-based parallel genetic algorithms for multi-objective optimization in ultra-reliable low-latency wsns," *IEEE Access*, vol. 7, pp. 4913–4926, Dec. 2018.

[65] K. N. R. S. V. Prasad, H. K. Rath, and A. Simha, "Wireless mobile network planning and optimization," in *Proc. IEEE COMSNETS'2014*, Bangalore, India, 2014, pp. 1–4.

[66] A. Al-Dulaimi, S. Al-Rubaye, J. Cosmas, and A. Anpalagan, "Planning of ultra-dense wireless networks," *IEEE Network*, vol. 31, no. 2, pp. 90–96, Mar. 2017.

[67] H. Guo, B. Makki, M.-S. Alouini, and T. Svensson, "High-rate uninterrupted internet-of-vehicle communications in highways: Dynamic blockage avoidance and csit acquisition," *IEEE Commun. Mag.*, 2022.

[68] S. Sun, K. Adachi, P. H. Tan, Y. Zhou, J. Joung, and C. K. Ho, "Heterogeneous network: An evolutionary path to 5G," in *Proc. IEEE APCC'2015*, Kyoto, Japan, Oct. 2015, pp. 174–178.

[69] E. Meesa-ard, S. Pattaramalai, and M. D. C. Madapatha, "Outage probability of mobility incorporated alpha-mu fading distribution with co-channel interference in heterogeneous networks," in *Proc. IEEE SmartIoT'2018*, IEEE Computer Society, Xian, China, Aug. 2018, pp. 76–80.

[70] C. Madapatha, B. Makki, H. Guo, M.-S. Alouini, and T. Svensson, "Constrained deployment optimization in iab networks," vol. 1, 2022.

[71] 3GPP, "Overview of 3GPP Release 10," 3rd Generation Partnership Project (3GPP), Technical Specification (TS), Jun. 2016, V0.2.1.

[72] T. Hu, J. Pang, and H.-J. Su, "LTE-advanced heterogeneous networks: Release 10 and beyond," in *Proc. IEEE ICC'2012*, Ottawa, Canada, Jun. 2012, pp. 6999–7003.

[73] M. Abdullah and A. Yonis, "Performance of lTE release 8 and release 10 in wireless communications," in *Proc. IEEE CyberSec'2012*, 2012, pp. 236–241.

[74] 3GPP, "NR; study on integrated access and backhaul (release 16), 3rd Generation Partnership Project (3GPP)," 3GPP TR 38.874, Technical Specification (TS), Dec. 2018, V0.2.1.

[75] 3GPP, "NG-RAN; F1 general aspects and principles (Release 16)," 3GPP TS 38.300, Technical Specification (TS), Sep. 2020, V16.4.0.

[76] 3GPP RP-201756, "Revised WID: Integrated Access and Backhaul for NR," 3rd Generation Partnership Project (3GPP), Tech. Rep. Meeting RAN#89e, Electronic Meeting, Jun. 2020.

[77] O. P. Adare, H. Babbili, C. Madapatha, B. Makki, and T. Svensson, "Uplink power control in integrated access and backhaul networks," in *Proc. IEEE DySPAN'2021*, IEEE, Virtual, Dec. 2021, pp. 163–168.

[78] 3GPP TS 38.174, "5G; NR; Integrated Access and Backhaul (IAB) radio transmission and reception," 3rd Generation Partnership Project (3GPP), Tech. Rep., Nov. 2020.

[79] 3GPP TS 138 175, "5G; NR; Integrated Access and Backhaul (IAB) Electromagnetic Compatibility (EMC)," 3rd Generation Partnership Project (3GPP), Tech. Rep., Nov. 2020.

[80] M. Hashemi, M. Coldrey, M. Johansson, and S. Petersson, "Integrated Access and Backhaul in Fixed Wireless Access Systems," in *Proc. VTC-Fall'2017*, Toronto, Canada, Sep. 2017, pp. 1–5.

[81] B. Skubic, M. Fiorani, S. Tombaz, A. Furuskär, J. Mårtensson, and P. Monti, "Optical transport solutions for 5g fixed wireless access," *Journal of Optical Communications and Networking*, vol. 9, pp. D10–D18, 2017.

[82] B. Błaszczyszyn, "Lecture Notes on Random Geometric Models—Random Graphs, Point Processes and Stochastic Geometry," 2017.

[83] T. S. Rappaport, Y. Xing, G. R. MacCartney, A. F. Molisch, E. Mellios, and J. Zhang, "Overview of Millimeter Wave Communications for Fifth-Generation (5G) Wireless Networks—With a Focus on Propagation Models," *IEEE Trans. Antennas Propag.*, vol. 65, no. 12, pp. 6213–6230, Dec. 2017.

[84] B. Makki, A. Ide, T. Svensson, T. Eriksson, and M. Alouini, "A genetic algorithm-based antenna selection approach for large-but-finite MIMO networks," *IEEE Trans. Veh. Technol.*, vol. 66, no. 7, pp. 6591–6595, Dec. 2017.

[85] C. Madapatha, B. Makki, A. Muhammad, E. Dahlman, M.-S. Alouini, and T. Svensson, "On topology optimization and routing in integrated access and backhaul networks: A genetic algorithm-based approach," *IEEE Open j. Commun. Soc.*, vol. 2, pp. 2273–2291, 2021.

[86] M. S. Elbasheir, R. A. Saeed, and S. Edam, "5G base station deployment review for rf radiation," in *Proc. IEEE ISNCC'2021*, 2021, pp. 1–5.

[87] 3. T. 38.174, "Integrated access and backhaul (iab) radio transmission and reception," 3rd Generation Partnership Project (3GPP), Tech. Rep. Meeting RAN#94-e, Electronic Meeting, Dec. 2021.

[88] H. Ronkainen, J. Edstam, C. Östberg, and A. Ericsson, "Integrated access and backhaul: A new type of wireless backhaul in 5g," *Frontiers in Communications and Networks*, vol. 2, p. 4, 2021.

[89] M. Åström, P. Gentner, O. Haliloglu, B. Makki, and O. Tageman, "Ris in cellular networks–challenges and issues," *arXiv preprint arXiv:2404.04753*, 2024.

[90] H. Guo et al., "A comparison between network-controlled repeaters and reconfigurable intelligent surfaces," *arXiv preprint arXiv:2211.06974*, 2022.

[91] C. Madapatha, B. Makki, H. Guo, and T. Svensson, "Reconfigurable intelligent surfaces-assisted integrated access and backhaul," IEEE International Black Sea Conference on Communications and Networking (IEEE Blackseacom), Jun. 2025.

[92] B. Makki, T. Svensson, K. Buisman, J. Perez, and M.-S. Alouini, "Wireless energy and information transmission in FSO and RF-FSO links," *IEEE Wireless Communications Letters*, vol. 7, no. 1, pp. 90–93, Feb. 2018.

[93] B. Makki, T. Svensson, M. Brandt-Pearce, and M.-S. Alouini, "On the performance of millimeter wave-based RF-FSO multi-hop and mesh networks," *IEEE Transactions on Wireless Communications*, vol. 16, no. 12, pp. 7746–7759, Dec. 2017.

[94] P. K. Singya, B. Makki, A. D'Errico, and M.-S. Alouini, "Hybrid FSO/THz-based backhaul network for mmWave terrestrial communication," *IEEE Transactions on Wireless Communications*, vol. 22, no. 7, pp. 4342–4359, Jul. 2023.

[95] P. K. Singya, B. Makki, A. D'Errico, and M.-S. Alouini, "High-rate reliable communication using multi-hop and mesh THz/FSO networks," *IEEE Open Journal of the Communications Society*, vol. 5, pp. 3804–3823, 2024.

[96] C. Madapatha, P. Lechowicz, C. Natalino, P. Monti, and T. Svensson, "Joint fiber and free space optical infrastructure planning for hybrid integrated access and backhaul networks," Accepted for IEEE International Symposium on Personal, Indoor and Mobile Radio Communications (PIMRC), Istanbul, Turkey, Jun. 2025.

[97] 3rd Generation Partnership Project (3GPP), "Study on channel model for frequencies from 0.5 to 100 GHz," 3rd Generation Partnership Project (3GPP), Technical Report TR 38.901 V14.1.1, Aug. 2017, Release 14.

Part II

Papers

PAPER A

On Integrated Access and Backhaul Networks: Current Status and Potentials

C. Madapatha, B. Makki, C. Fang, O. Teyeb, E. Dahlman, M-S. Alouni, and T. Svensson

IEEE Open Journal of Communication Society,
vol. 1, pp. 1374-1389, Sept. 2020.

The layout has been revised.

Abstract

—In this paper, we introduce and study the potentials and challenges of integrated access and backhaul (IAB) as one of the promising techniques for evolving 5G networks. We study IAB networks from different perspectives. We summarize the recent Rel-16 as well as the upcoming Rel-17 3GPP discussions on IAB, and highlight the main IAB-specific agreements on different protocol layers. Also, concentrating on millimeter wave-based communications, we evaluate the performance of IAB networks in both dense and suburban areas. Using a finite stochastic geometry model, with random distributions of IAB nodes as well as user equipments (UEs) in a finite region, we study the service coverage rate defined as the probability of the event that the UEs' minimum rate requirements are satisfied. We present comparisons between IAB and hybrid IAB/fiber-backhauled networks where a part or all of the small base stations are fiber-connected. Finally, we study the robustness of IAB networks to weather and various deployment conditions and verify their effects, such as blockage, tree foliage, rain as well as antenna height/gain on the coverage rate of IAB setups, as the key differences between the fiber-connected and IAB networks. As we show, IAB is an attractive approach to enable the network densification required by 5G and beyond.

Index terms— Integrated access and backhaul, IAB, densification, millimeter wave (mmWave) communications, 3GPP, Stochastic geometry, Poisson point process, Coverage probability, Germ-grain model, ITU-R, FITU-R, Wireless backhaul, 5G NR, Rain, Tree foliage, Blockage, Relay

1 INTRODUCTION

Different reports, e.g., [1], predict a steep increase of Internet devices connected through wireless access as well as a massive increase in mobile traffic. To cope with such requirements, along with utilizing more spectrum, the fifth generation (5G) wireless networks and beyond propose different ways for spectral efficiency and capacity improvements. Network densification [2], [3] is one of the key enablers among the alternative approaches, e.g., various distributed antenna systems techniques, including cell-free massive multiple-input-multiple-output (MIMO) and can be achieved via the deployment of many access points of different types, so that there are more resource blocks per unit area.

The base stations (BSs) need to be connected to the operators' core network via a

transport network. A transport network may consist of wired or wireless connections. Typically, wireless connections are used for backhaul transport in the radio access network (RAN), closer to the BSs, while wired high-capacity fiber connections are used for transport closer to the core network and in the core network, where the network needs to handle aggregated traffic from many BSs.

The deployed backhaul technology today has large regional variations, but on a global scale, wireless microwave technology has historically been a dominating media for a long time. Over the last 10 years there has however been a large increase in fiber deployments attributed to, e.g., geopolitical decisions and major governmental investments. Over the same time, the use of copper as a media has reduced a lot due to increasing demands on capacity and lower maintenance. Going forward there are thus two dominating backhaul media – microwave and fiber. Historical and predicted global backhaul media distribution can be found in [4].

Fiber offers reliable high-capacity transport with demonstrated Tbps rates. However, the deployment of fiber requires a noteworthy initial investment for trenching and installation, which could take a considerable installation time, and even might not be possible/allowed in, certain areas where trenching is not an option.

Wireless backhauling using microwave represents a competitive alternative to fiber since it today provides 10's of Gbps in commercial deployments and even 100 Gbps has recently been demonstrated [5]. Microwave is a backhaul technology used by most mobile operators worldwide, and this trend is likely to continue. This is because microwave is a scalable and economical backhaul option that can meet the increasing requirements of 5G systems. A key advantage over fiber is that wireless backhauling comes with significantly lower cost and flexible/timely deployment (e.g., no digging, no intrusion or disruption of infrastructure, and possible to deploy in principle everywhere) [4], [6]. Today microwave backhauling operates in licensed point-to-point (PtP) spectrum, typically in the 4–70/80 GHz range. However, with the introduction of 5G in millimeter wave (mmWave) spectrum and with the foreseen need for even wider bandwidths for backhaul, microwave is currently being extended to even higher frequencies, above 100 GHz.

For the same reasons, and driven by network densification and access to wide bandwidth in mmWave spectrum, integrated access and backhaul (IAB) networks, where the operator can utilize part of the radio resources for wireless backhauling, has recently received considerable attention [7], [8]. The purpose of IAB is to provide flexible wireless backhauling using 3GPP new radio (NR) technology in international mobile telecommunications (IMT) bands, *providing not only backhaul but also the existing cellular services in the same node.* Thus, IAB serves as a complement to microwave PtP backhauling in dense urban and suburban deployments, while it comes at the expense of using IMT bands not only for access but also for backhaul traffic.

Wireless backhauling has been studied earlier in 3GPP in the scope of LTE Rel-10, also known as LTE relaying [9]. However, there have been only a handful of

commercial LTE relay deployments, mainly because the existing LTE spectrum is very expensive to be used for backhauling, and also small-cell deployments did not reach the anticipated potential in the 4G timeline.

For 5G NR, IAB has been standardized in 3GPP Rel-16 and, as we detail later in the paper, standardization will continue in Rel-17. The main reason why NR IAB is expected to be more commercially successful than LTE relaying is that:

- The limited coverage of mmWave access creates a high demand for denser deployments, which, in turn, increases the need for backhauling.
- Also, the larger bandwidth available in mmWave spectrum provides more economically viable opportunity for wireless backhauling.
- Finally, MIMO, multi-beam systems, and multiple access, which are inherent features of NR, enable efficient backhauling of multiple radio BSs using the same equipment.

There have been several studies on the performance of IAB networks. For instance, cost-optimal node placement [10], resource allocation [11], [12], [13], [14] and routing [11], [12], [13], [14], [15], [16], [17] are studied in the cases with different numbers of hops. Particularly, [10] provides an overview of multi-hop IAB techniques supported in the 3GPP rel-16 standard and discusses its design strategies. A joint node placement and resource allocation scheme maximizing the downlink sum rate is developed in [18]. Also, [19] uses simulated annealing algorithms for joint scheduling and power allocation. The maximum extended coverage area of a single fiber site using multi-hop relaying is investigated in [20], and [21], [22] perform end-to-end simulations to check the feasibility/challenges of mmWave-based IAB networks. Also, [23] provides useful insights for IAB deployments, especially, related to network densification and multi-hop topology, as it simulates a multi-hop mmWave pico-cell network, and evaluates the user throughput. The potential of using IAB in a fixed wireless access use-case is evaluated in [24]. The impact of dynamic time division duplex (TDD)-based resource allocation on the throughput of IAB networks, how its performance compares with static TDD and FDD (F: frequency), is discussed in [25], [26]. Moreover, [27], [28], [29] characterize the coverage probability of IAB-enabled mmWave heterogeneous networks via infinite Poisson point processes (PPPs). Precoder design and power allocation, to maximize the network sum rate, is considered in [30]. Finally, [31] investigates the usefulness of IAB in unmanned aerial vehicle (UAV)-based communications, and [32] develops a reinforcement learning-based resource allocation scheme in such networks.

In this paper, we study the performance of IAB networks from different perspectives. We start by summarizing the most recent 3GPP discussions in Rel-16 as well as the upcoming ones in Rel-17, and highlight the main IAB-specific features on different protocol layers. Then, concentrating on mmWave-based communications, we

analyze the performance of IAB networks, and compare their performance with those achieved with hybrid IAB/fiber-connected networks. Here, the results are presented for the cases with an FHPPP (FH: finite homogeneous)-based stochastic geometry model, e.g., [27], [33], i.e., a PPP which depends on a constant density, with random distributions of the IAB nodes as well as the user equipments (UEs) in a finite region. Particularly, we study the network service coverage probability, defined as the probability of the event that the UEs' minimum data rate requirements are satisfied.

One of the key differences between fiber-connected and IAB networks is that, the backhaul link in IAB networks may, like any wireless link, be impacted by various weather effects and deployment conditions such as rain, blockage, antenna heights, and tree foliage. For this reason, we evaluate the impacts of these aspects. The results are presented for both suburban and urban areas, with the main focus on dense deployments, since that is the most interesting scenario for IAB.

In summary, the paper presents an easy-to-follow description of the most recent 3GPP agreements on IAB, gives cost/performance comparisons between the IAB and fiber-connected networks, and verifies the robustness of the network to different environmental effects, which makes the paper completely different from the related literature.

As we demonstrate, along with microwave backhauling, IAB is a cost-effective complement of fiber, especially in dense metropolitan areas. Moreover, independently of the cost, IAB is an appropriate tool in a number of use-cases of interest in 5G. Finally, as we show, while the coverage rate of the IAB network is slightly affected by heavy rainfall in suburban areas, for a broad range of parameter settings and different environments, the blockage and the rain are not problematic for IAB networks, in the sense that their impact on the coverage probability is negligible. High levels of tree foliage, however, may reduce the coverage probability of the network, especially in suburban areas.

The rest of the paper is organized as follows. Section 2 summarizes the key 3GPP discussions in Rel-16 and 17 on IAB. Section 3 describes the performance evaluation of IAB networks, compares their performance with those achieved in hybrid IAB/fiber-connected networks, and verifies the robustness of the IAB setup to different weather and deployment parameters. Finally, conclusions and a number of interesting open research problems that encourages researchers to contribute are provided in Section 4.

2 IAB in 3GPP

NR IAB was introduced in 3GPP Rel-16. It provides functionality that allows for the use of the NR radio-access technology not only for the link between BSs and devices, sometimes referred to as the access link, but also for wireless backhaul links, see Figure 1.

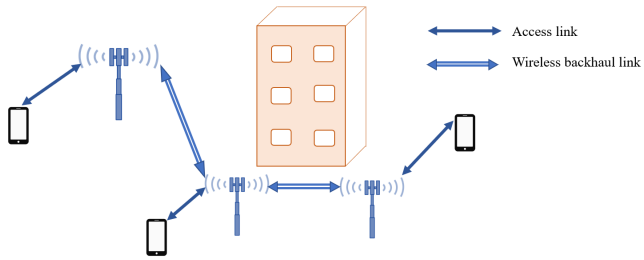

Figure 1: Integrated access and backhaul.

Wireless backhauling, that is, the use of wireless technology for backhaul links, has been used for many years. However, this has then been mainly based on radio technologies different from those used for the access links. Additionally, wireless backhaul has typically been based on proprietary, i.e., non-standardized[1], radio technology operating in mmWave spectrum above 10 GHz[2] and constrained to line-of-sight (LOS) propagation conditions.

However, along with massive amount of available spectrum due to the move to mmWave, there are at least two factors that now make it more relevant to consider an IAB solution, that is, reusing the standardized cellular technology, normally used by devices to access the network, also for wireless-backhaul links:

- With the emergence of 5G NR, the cellular technology is extending into the mmWave spectrum, a spectrum range that historically is used for wireless backhaul.
- With the emergence of small-cell deployments with BSs located, for example, on street level, there is a demand for a wireless-backhaul solution that allows for backhaul links to operate also under non-line-of-sight (NLOS) conditions, the kind of propagation scenarios for which the cellular radio-access technologies have been designed.

2.1 IAB Architecture

The IAB standard that is being specified in 3GPP Rel-16 [35] is based on the split architecture introduced in 3GPP Rel-15, where a base station (gNB) is split into a centralized unit (CU), which terminates the Packet Data Convergence Protocol (PDCP) and the Radio Resource Control (RRC) protocol, and a distributed unit

[1]Some aspects of microwave backhauling are standardized, but there is significant room for proprietary solutions.

[2]Traditional wireless backhaul operates also below 10 GHz, for example the longhaul links are typically at 6 GHz [34].

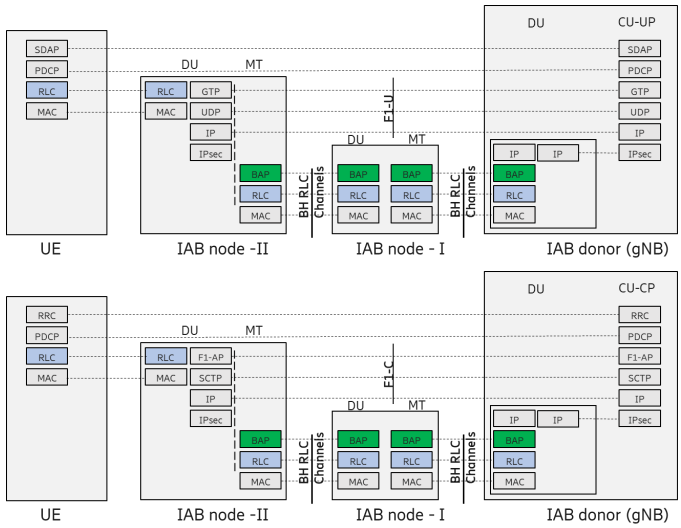

Figure 2: User plane and control plane protocol stack of a multi-hop IAB network according to 3GPP Rel-16.

(DU) that terminates the lower layer protocols, i.e., Radio Link Control (RLC), Medium Access Control (MAC) and the physical layer [36]. The motivation for the CU/DU functional split is that all time-critical functionalities, e.g., scheduling, fast retransmission, segmentation etc., can be realized in the DU, i.e., close to the radio and the antenna, while it is possible to centralize and resource-pool the less time-critical radio functionalities in the CU. A specified interface (F1 interface) is used to convey both the control-plane (F1-C) and user-plane (F1-U) messages between the CU and DU. The CU/DU split is transparent to the UE, i.e., it does not impact UE functionality or protocol stack.

Figure 2 shows the control and user plane protocol stack of a multi-hop IAB network according to 3GPP Rel-16. The IAB donor node is the node that is connected to the rest of the network in a conventional way (e.g., fiber or microwave) and serves the IAB nodes and other UEs that are directly connected to it. The IAB nodes have a mobile termination (MT) part and a DU part. The MT part is used to connect to a parent DU (which could be the donor DU or the DU part of another IAB node), while the DU part of an IAB node is used to serve UEs or the MT part of child IAB nodes.

In many respects, the MT part of an IAB node behaves like a UE in the sense that it communicates with the parent DU very much like a UE. On the other hand, from the UE point-of-view, the DU of an IAB node appears as a normal DU. This is necessary to preserve backwards compatibility so that legacy (pre Rel-16) NR UEs could also access the network via an IAB node.

As in legacy CU/DU split, for the user plane, the service data adaptation protocol (SDAP) and PDCP are terminated at the UE and the user plane part of the CU (CU-UP), and the corresponding packets are transported over an F1-U interface (basically, a set of GTP tunnels for each bearer) between the CU-UP and the DU part of the IAB node serving the UE (known as access IAB node). Similarly, for the control plane, the RRC and PDCP are terminated at the UE and the CU-CP, and the corresponding packets are transported over an F1-C interface, which is realized via a set of stream control transport protocol (SCTP) associations/streams between the CU-UP and the DU part of the access IAB node. The IAB-MTs can employ all the functionalities available to UEs such as carrier aggregation and dual connectivity to multiple parent nodes. The IAB nodes's protocol/architecture is transparent to the UE, i.e., UEs cannot differentiate between normal gNBs and IAB nodes.

In Rel-16, only a directed acyclic graph (DAG) multi-hop topology was supported, i.e., no mesh-based connectivity. Also, only decode-and-forward relaying was considered, where the signal is decoded in each hop and, with a successful decoding, it is re-encoded and transferred to the next hop. Compared to other relaying techniques, this gives the best E2E performance in the multi-hop setup and make it possible to scale the network to the cases with different numbers of hops, especially, due to its full processing capability. The IAB nodes are interconnected with each other at layer 2 level and a hop-by-hop RLC is employed. This provides a better performance than having an end-to-end (E2E) RLC between the donor and the UE because retransmissions, if any, are required only over the affected hop, rather than between the UE and the donor, leading to faster and most efficient recovery to transmission failures. Hop-by-hop RLC also leads to lower buffering requirements at the end points. With regard to security, no hop-by-hop security is needed between the IAB nodes since the PDCP at the UE and CU ensure E2E encryption and integrity protection (optional for user plane).

On Backhaul Adaptation Protocol

A new protocol known as backhaul adaptation protocol (BAP) is specified that is responsible for the forwarding of packets in the intermediate hops between the donor DU and the access IAB node [37]. Each IAB node is configured with a unique BAP ID by the donor node. For downlink (DL) packets, the donor DU inserts a BAP routing ID on the packets it is forwarding to the next hop, which is the BAP ID of the access IAB node serving the UE and a path identifier, in case there are several possible paths to reach the access IAB node. Similarly, for uplink (UL) packets, the access IAB node inserts the UL BAP routing ID, which is the BAP ID of the donor DU and a path identifier, in case there are several possible paths to reach the DU. Each IAB node is configured with UL and DL routing tables, which indicates to which child node (in the case of DL) or parent node (in the case of UL) the packet

should be forwarded. When an access IAB node receives a packet that is destined to it, the packet will be forwarded to higher layers and processed the same way a normal DU processes incoming F1-U or F1-C packets.

In addition to forwarding packets to a child or parent node, the BAP protocol also performs the mapping between ingress and egress backhaul RLC channels, to ensure that the packets are treated with the proper quality of service (QoS) requirements. Similar to RLC channels between a DU and a UE, the backhaul RLC channels can be configured with different QoS parameters such as priority and guaranteed bit rates. For bearers that have very strict QoS requirements, a 1:1 mapping could be used, where there is a dedicated backhaul RLC channel on each hop. Otherwise, an 1:N mapping can be employed where packets belonging to several bearers could be transported/multiplexed over a given backhaul RLC channel. Similar to the routing table, the IAB nodes are configured with a mapping configuration to determine which egress backhaul RLC channel a packet should be forwarded to once the next child/parent node has been identified via the routing table.

On Integration Procedure

Before becoming fully operational, the IAB node performs the IAB integration procedure, which is illustrated in Fig. 3 (interested reader is referred to [38] for the details). In the first step (startup), the IAB node performs an RRC connection establishment, like a normal UE, using its MT functionality. Once the connection is set up, it indicates to the network that it is an IAB node, which the network verifies/authenticates. Connectivity to the Operation and Maintenance (OAM) part of the network could also be performed at this phase to update configurations.

In the second step, the required/default backhaul RLC channel(s) are established, to enable the bootstrapping process where the DU part of the IAB node establishes the F1 connection with the donor as well as enable OAM connectivity (if not performed during the first step). A routing update is also made, which includes several sub-procedures such as IP address allocation for the IAB node and the (re)configuration of the BAP sub-layer at the IAB node and possibly all ancestor IAB nodes (BAP routing identifier(s) for downstream/upstream directions, routing table updates, etc.).

In the last step, the DU part of the IAB node can initiate an F1 connection request towards the donor CU, using its newly allocated IP address. After the F1 connection is set up, the IAB node can start serving UEs like a normal DU. Reconfigurations can be made anytime after this step, on a need basis, to update the backhaul RLC channels, routing tables, bearer mapping, etc.

2.2 Spectrum for IAB

As already mentioned, although IAB supports the full range of NR spectrum, for several reasons the mmWave spectrum is most relevant for IAB:

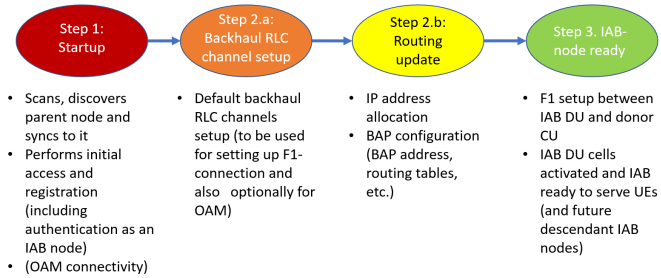

Figure 3: Schematic diagram of the IAB integration procedure in 3GPP Rel-16.

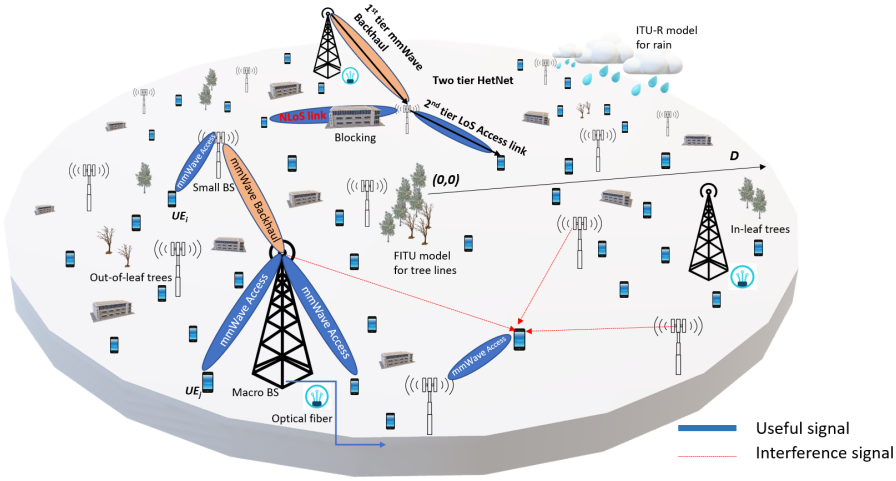

Figure 4: Schematic of the IAB system model.

- The potentially large amount of mmWave spectrum makes it more justifiable to use part of the spectrum resources for wireless backhaul.
- Massive beamforming enabled at higher frequencies is especially beneficial for the wireless-backhaul scenario with stationary nodes at both ends of the radio link.

Higher-frequency spectrum is mainly organized as unpaired spectrum. Thus, operation in unpaired spectrum has been the main focus for the 3GPP discussions on IAB. IAB supports both outband and inband backhauling:

- Outband backhauling: The wireless backhaul links operate in a different frequency band, compared to the access links.
- Inband backhauling: The wireless backhaul links operate in the same frequency

band, as the access links.

2.3 The IAB Radio Link

In most respects, the backhaul link, between a parent-node DU and a corresponding child IAB-node MT operates as a conventional network-to-device link. Consequently, the IAB-related extensions to the NR physical, MAC, and RLC layers are relatively limited and primarily deal with the need to coordinate the IAB-node MT and DUs for the case of inband operation when simultaneous DU and MT operation is not possible.

Similar to UEs, a time-domain resource of an IAB-node MT can be configured/indicated as:

- Downlink (DL): The resource will only be used by the parent node in the DL direction.
- Uplink (UL): The resource will only be used by the parent node in the UL direction.
- Flexible (F). The resource may be used in both the DL and UL directions with the instantaneous transmission direction determined by the parent-node scheduler.

Similarly, the time-domain resources of the DU part of an IAB node can be configured as:

- Downlink (DL): The DU can only use the resource in the DL direction.
- Uplink (UL): The DU can only use the resource in the UL direction.
- Flexible (F): The DU can use the resource in both the DL and UL directions.

In parallel to the DL/UL/F configuration, DU time-domain resources could be configured as hard or soft. In case of a hard configuration, the DU of a node can use the resource without having to consider the impact on its MTs ability to transmit/receive according to its configuration and scheduling. In practice this means that, if a certain DU time-domain resource is configured as hard, the parent node must assume that the IAB-node MT may not be able to receive/transmit. Consequently, the parent node should not schedule transmissions to/from the MT in this resource.

In contrast, in case of a DU time-domain resource configured as soft, the DU can use the resource if and only if this does not impact the MTs ability to transmit/receive according to its configuration and scheduling. This means that the parent node can schedule a DL transmission to the MT in the corresponding MT resource and assume that the MT is able to receive the transmission. Similarly, the parent node

can schedule MT UL transmission in the resource and assume that the MT can carry out the transmission.

The possibility to configure soft DU resources allows for more dynamic resource utilization. Take, as an example, a soft DU resource corresponding to an MT resource configured as UL. If the MT does not have a scheduling grant for that resource, the IAB node knows that the MT will not have to transmit within the resource. Consequently, the DU can dynamically use the resource, for example, for DL transmission, even if the IAB node is not capable of simultaneous DU and MT transmission.

The possibility to configure soft DU resources also gives an IAB node the chance to benefit from being able to perform simultaneous DU and MT operation. Whether or not a specific IAB node is capable of simultaneous DU and MT operation may depend on the IAB-node implementation and may also depend on the exact deployment scenario. Thus, an IAB node designed or deployed so that it can support simultaneous DU and MT operation can use a soft DU resource without the parent node even knowing about it.

These situations, when an IAB node, by itself, can conclude that it can use a soft DU resource has, in the 3GPP discussions, been referred to as implicit indication of availability of soft DU resources. The parent node can also provide an explicit indication of availability of a soft DU resource by means of layer-1 signaling.

Finally, it should be noted that, along with resource multiplexing which has been the main topic of discussions in RAN1, the over-the-air (OTA) timing alignment, the random access channel (RACH) as well as the extensions of SSBs for inter-IAB-node discovery and measurements have been discussed in 3GPP. However, due to space limits, we do not cover these topics, and the interested reader can find the final agreements in [39]. Moreover, while we concentrated mostly on RAN1 and RAN2 discussions, the main discussions/agreements in RAN3 and RAN4 can be found in [40]-[41] and [42], respectively (also see [10]).

2.4 IAB in Rel-17

The physical-layer part of the IAB Rel-16 specifications was finalized at the end of 2019 and the remaining parts (higher-layer protocols and architecture) are expected to be finalized in June 2020. Further enhancements to IAB will then be carried out within 3GPP Rel-17, with expected start in August 2020 [43]. The Rel-17 work aims to improve on various aspects such as robustness, degree of load-balancing, spectral efficiency, multi-hop latency and end-to-end performance. More specifically, the following is planned to be covered:

- Enhancements to the resource multiplexing between child and parent links of an IAB node, including:
  - Enhanced support of simultaneous operation (transmission and/or reception) of IAB-node's child and parent links, including enhancements such

Table 1: The Definition of the Parameters.

Parameter	Definition	Parameter	Definition
ϕ_{M}	FHPPP of the MBSs	ϕ_{U}	FHPPP of the UEs
ϕ_{S}	FHPPP of the SBSs	λ_{U}	UE density
ϕ_{B}	FHPPP of the blocking walls	θ	Orientation of blocking wall
ϕ_{T}	FHPPP of the tree lines	l_{hop}	Average hop length
λ_{M}	MBSs density	λ_{S}	SBSs density
H	Homogeneous Poisson Process	λ_{B}	Blocking wall density
l_{B}	Blocking wall length	ρ	Service coverage probability
A	Circular disk	D	Radius of the disk
P_{t}	Transmission power	P_{r}	Received power
h	Fading coeficient	G	Antenna gain
$L_{(1\mathrm{m})}$	Reference path loss at 1 meter distance	L	Propagation path loss
x	Location of the node	r	Propagation distance between the nodes
α	Path loss exponent	N	Number of UEs connected
f_{c}	Carrier frequency	φ	Angle between the BS and UE
θ_{HPBW}	Half power beamwidth of the antenna	G_0	Maximum gain of directional antenna
$g(\varphi)$	Side lobe gain	R_{th}	Minimum data rate threshold
x_{c}	Associated cell	R	Rain intensity
x_{u}	Connected UE at the location	i, j	Node index
F_{T}	Tree foliage	γ_{R}	Rainloss
d	Vegetation depth	W	Bandwidth of the DL
μ	Percentage of bandwidth resources on backhaul	l_{T}	Tree line length
λ_{T}	Tree blocking density	v	SBS antenna height

as new DU/MT timing relations, DL/UL power control and cross link interference mitigation.

  - Support for dual-connectivity scenarios for topology redundancy for improved robustness and load balancing.

- Enhancements in scheduling, flow and congestion control to improve end-to-end performance, fairness, and spectral efficiency.

- Introduction of efficient inter-donor IAB-node migration, increasing the robustness of IAB networks allowing for more refined load-balancing and topology management.

- Reduction of service interruption time caused by IAB-node migration and backhaul RLF recovery improves network performance, allows network deployments

to undergo more frequent topology changes, and provides stable backhaul performance.

Finally, it should be mentioned that in 3GPP RAN4 a number of simulations have been performed to evaluate the feasibility/efficiency of IAB networks, e.g., [44]. There, it has been mainly concentrated on defining RF requirements for both backhaul and access links of an IAB-node including requirements for their co-existence, and evaluate the performance in different possible scheduling scenarios of the the DU and MT. In Section 3, we mainly concentrate on the comparison between the performance of IAB and fiber networks as well as studying the robustness of IAB networks to different environmental effects using a novel stochastic geometry modeling for mmWave networks and 3D maps topology information. Such results provide insights about if the IAB performance expectations will be met in urban and suburban areas.

3 Performance Evaluation

This section studies the service coverage rate of IAB networks with various parameterizations, and compares the performance with those achieved by (partially) fiber-connected networks. First, we present the system model, including the channel model, the considered UE association rule as well as the rain, the blockage and the tree foliage models, which are followed by the simulation results.

3.1 System Model

As shown in Fig. 4., consider an outdoor two tier heterogeneous network (HetNet), i.e., a two-hop IAB network, with multiple MBSs (M: macro), SBSs (S: small) and UEs. This is motivated by different evaluations, e.g., [27], [28], [29], [30], where, although the standardization does not limit the number of hops, increasing the number of hops may lead to backhaul traffic aggregation. In an IAB deployment, both the MBSs and the SBSs use wireless connections for both access and backhaul. Also, only the MBSs are fiber-connected while the SBSs receive data from the MBSs wirelessly by using IAB. That is, following the 3GPP definitions (see Section 2), the MBSs and the SBSs can be considered as the donor and the child IABs, respectively. Therefore, throughout the section, we may use the terminologies MBS/SBS and donor IAB/IAB interchangeably. Considering an inband operation, the bandwidth is shared among access and backhaul links of the IAB nodes such that the network service coverage rate is maximized. For simplicity, the MBSs and the SBSs are assumed to have constant power over the spectrum of the system and are all active throughout the analysis[3].

[3]Developing adaptive power allocation schemes for IAB networks is an interesting open research topic.

Spatial Model

Table I summarizes the parameters used in the analysis. We model the IAB network by an FHPPP, e.g., [33], [45], which suits well to model a random number of nodes in a finite region. Particularly, FHPPPs ϕ_{M} and ϕ_{S} with densities λ_{M} and λ_{S}, respectively, are used to model the spatial distributions of the MBSs and the SBSs, respectively.

The MBSs' FHPPP is given by $\phi_{\mathrm{M}} = H \cap A$, where H with density λ_{M} is an HPPP (H: homogeneous) and $A \subset \mathbb{R}^2$ is a finite region. For simplicity and without loss of generality, we let A be a circular disk with radius D. However, the study is generic and can be applied on arbitrary regions A. The SBSs and the UEs are also located within the same A in accordance with two other FHPPPs ϕ_{S} and ϕ_{U} having densities λ_{S} and λ_{U}, respectively, which are all mutually independant.

We study the system performance for two blocking conditions. First, we use the well-known germ grain model [46, Chapter 14], which provides accurate results compared to stochastic models that assume the blocking in different links to be independant. Moreover, the germ grain model fits well for environments with large obstacles as it takes the obstacles induced blocking correlation into account. The model is an FHPPP, i.e., the blockages are distributed according to the FHPPP ϕ_{B} distributed in the same area A with density λ_{B}. This is a 2D model where all blockings are assumed to be walls of length l_{B} and orientation θ, which is an independantly and identically distributed (IID) uniform random variable in $[0,\ 2\pi]$. The walls are distributed in random locations uniformly as of the FHPPP.

With the 2D channel model, the elevation of the blocking and the BSs or the terrain information of the land are not taken into account. For this reason, in Subsection 3.3, we demonstrate the system performance for an example 3D use-case. Particularly, we distribute the same spatial arrangement of the MBSs, the SBSs and the UEs with their respective nodes heights on top of map data with real world blocking terrain using OpenStreetMap 3D environment. That is, while different MBS and SBS nodes are distributed randomly based on their corresponding FHPPPs, they are placed, on different heights, and the blockages are determined based on the map information. This enables us to evaluate the effect of the nodes and blocking heights on the service coverage probability.

Channel Model

We consider an inband communication setup, where both the access and backhaul links operate in the same mmWave spectrum band. Following the state-of-the-art mmWave channel model, e.g., [45], the received power at each node can be expressed as

$$P_{\mathrm{r}} = P_{\mathrm{t}} h_{\mathrm{t,r}} G_{\mathrm{t,r}} L_{(1\mathrm{m})} L_{\mathrm{t,r}} \left|\left|x_{\mathrm{t}} - x_{\mathrm{r}}\right|\right|^{-1} F_{\mathrm{t,r}} \gamma_{\mathrm{t,r}}. \tag{A.1}$$

Here, P_{t} denotes the transmit power in each link, and $h_{t,r}$ represents the independant small-scale fading for each link. The small-scale fading is modelled as a normalized Rayleigh random variable in our analysis. Then, $G_{t,r}$ represents the combined antenna gain of the transmitter and the receiver of the link, $L_{\mathrm{t,r}}$ which is a function of the distance between x_{t} and x_{r}, denotes the path loss due to propagation, and $L_{(1m)}$ is the reference path loss at 1 meter distance. The tree foliage loss is denoted by $F_{\mathrm{t,r}}$ while $\gamma_{\mathrm{t,r}}$ represents the rain loss between the transmitter and the receiver of the link in linear scale. The total path loss, in dB, is characterized according to the 5GCM UMa close-in model described in [47]. The path loss is given by

$$\kappa = 32.4 + 10\log_{10}(r)^{\alpha} + 20\log_{10}(f_{\mathrm{c}}), \tag{A.2}$$

where f_c is the carrier frequency, r is the propagation distance between the nodes, and α is the path loss exponent. Depending on the blockage, LOS and NLOS links are affected by different path loss exponents. The propagation loss of the path loss model is given by

$$L_{\mathrm{t,r}} = \begin{cases} r^{\alpha_{\mathrm{L}}}, & \text{if LoS,} \\ r^{\alpha_{\mathrm{N}}}, & \text{if NLoS,} \end{cases} \tag{A.3}$$

where α_{L} and α_{N} denote path loss exponents for the LOS and NLOS scenarios, respectively. In 5G, large antenna arrays with directional beamforming are used to mitigate the propagation losses. We model the beam pattern as a sectored-pattern antenna array and thus the antenna gain between two nodes can be expressed by

$$G_{i,j}(\varphi) = \begin{cases} G_0 & \frac{-\theta_{\mathrm{HPBW}}}{2} \leq \varphi \leq \frac{\theta_{\mathrm{HPBW}}}{2} \\ g(\varphi) & \text{otherwise.} \end{cases} \tag{A.4}$$

Here, i, j are the indices of the considered transmit and receive nodes, and φ is the angle between them in the considered link. Also, θ_{HPBW} is the half power beamwidth of the antenna, and G_0 is the directional antenna's maximum gain while $g(\varphi)$ is the side lobe gain. Also, we let the UE antenna gain to be 0 dB. This is in harmony with, e.g., [27], [29], [48], and because the UE has an omni-directional radiation pattern. For discussions on how the antenna gain is affected by the antenna array properties, see, e.g., [45].

We assume that we have high beamforming capability in the IAB-IAB backhaul links. Consequently, we ignore the interference in the backhaul links and assume them to be noise-limited. Also, the inter-UE interferences are neglected due to the low power of the devices and with the assumption of sufficient isolation [24]. On the other hand, as illustrated in Fig. 4, the interference model focuses on the aggregated interference on the access links, due to the neighbouring interferers, which for UE u

Table 2: Coefficients for ITU-R model. Here, β_h, k_h are the horizontal polarization coefficients and β_v, k_v denote the vertical polarization coefficients [49].

Frequency (GHz)	$\boldsymbol{\beta_h}$	$\boldsymbol{\beta_v}$	$\boldsymbol{k_h}$	$\boldsymbol{k_v}$
28	0.9679	0.9277	0.2051	0.1964

is given by

$$I_{\mathrm{u}} = \sum_{\mathbf{i,j}\in\phi_{i,j}\setminus\{\mathbf{x}_c\}} P_j h_{i,j} G_{i,j} L_{(1\mathrm{m})} L_{x_i,x_j} \|\mathbf{x}_i - \mathbf{x}_j\|^{-1}. \tag{A.5}$$

Here, i and j represents all BSs except for the associated cell x_{c} which can either be an MBS or an SBS.

Rain and Tree Foliage Model

With the need of understanding the performance of IAB networks in rainy conditions, we use the ITU-R Rec 8.38-3 rain model [49] to entail the rain effect on the links. This is an appropriate model used to methodically determine the amount of rain attenuation on radio links. The model is widely used in all regions of the world, for the frequency range from 1 GHz to 1000 GHz with no rain rate obligation. The model describes the rain loss as

$$\gamma_{\mathrm{R}} = kR^{\beta}, \tag{A.6}$$

where γ_{R} is the rain loss in dB/km, and R is the rain intensity in mm/hr. Moreover, k and β are coefficients that are precalculated depending on the carrier frequency. Table II shows the coefficients for horizontal and vertical losses at rainy conditions in 28 GHz on which we concentrate in the simulations.

Finally, FHPPP ϕ_{T} with density λ_{T} is used to spatially distribute the tree lines of length l_{T} [50]. We use the Fitted International Telecommunication Union-Radio (FITU-R) tree foliage model [51, Chapter 7] to model the effect of the trees on the received signal power. This is an appropriate model for the cases with frequency dependancy and with non-uniform vegetation. The model is suitable for the mmWave frequencies from 10 to 40 GHz and has been derived by further developing the ITU-R vegetation model. In this way, considering two, namely, *in-leaf* and *out-of-leaf*, vegetation states, the tree foliage in dB is obtained by

$$F_{\mathrm{T}} = \begin{cases} 0.39 f_{\mathrm{c}}^{0.39} d^{0.25}, & \text{in-leaf} \\ 0.37 f_{\mathrm{c}}^{0.18} d^{0.59}, & \text{out-of-leaf,} \end{cases} \tag{A.7}$$

where f_{c} is the carrier frequency expressed in MHz and d is the vegetation depth in meter.

3.2 Association and Allocation Strategy

In our setup, the UE can be served by either an MBS or an SBS following open access strategy and based on the maximum average received power rule. Also, in harmony with 3GPP, we do not take joint transmission into account, i.e., each UE can be connected to only one MBS or SBS. In this way, the association rule for UE u suffices

$$\sum_{\forall j} u_j = 1,\ \forall_u \in U, u_i \cdot u_j = 0, \forall j \neq i, \tag{A.8}$$

where $u_j \in \{0, 1\}$ is a binary variable indicating the association with 1 and 0 denoting the unassociated cell. For the access links of the UEs, we have

$$u_j = \begin{cases} 1 & \text{if } P_i G_{z,x} h_{z,x} L_{(1m)} L_{\mathrm{z,x}}(\|\mathbf{z}-\mathbf{x}\|)^{-1} \\ & \quad \geq P_j G_j h_{z,y} L_{(1m)} L_{\mathrm{z,y}}(\|\mathbf{z}-\mathbf{y}\|)^{-1}, \\ & \quad \forall\ \mathbf{y} \in \phi_j | \mathbf{x} \in \phi_i, i, j \in \{\mathrm{m}, \mathrm{s}\} \\ 0, & \text{otherwise.} \end{cases} \tag{A.9}$$

As in (A.9) for each UE u, the association binary variable u_j becomes 1 for the cell giving the maximum received power at the UE, while for all other cells it is 0 since the UE can only be connected to one IAB node.

Because the IAB nodes, i.e., both the MBSs and the SBSs, are equipped with large antenna arrays and can beamform towards the required direction, the antenna gain over the backhaul links can be assumed to be the same, and backhaul link association can be well determined based on the minimum path loss rule, i.e., by

$$x_{b,m} = \begin{cases} 1 & \text{if } L_{\mathrm{b_m}}(\|\mathbf{z}-\mathbf{x}\|)^{-1} \geq L_{\mathrm{b_m}}(\|\mathbf{z}-\mathbf{y}\|)^{-1}, \\ & \quad \forall\ \mathbf{y} \in \phi_{\mathrm{m}} | \mathbf{x} \in \phi_{\mathrm{m}}, \\ 0, & \text{otherwise} \end{cases} \tag{A.10}$$

(For the effect of interference in the backhaul links, see Fig. 6). For resource allocation, on the other hand, the mmWave spectrum available is partitioned into the access and backhaul links such that

$$\begin{cases} W_{\mathrm{Backhaul}} = \mu W, \\ W_{\mathrm{Access}} = (1-\mu) W, \end{cases} \tag{A.11}$$

with $\mu \in [0, 1]$ being the percentage of bandwidth resources on backhauling. Also, W_{backhaul} and W_{access} denote the backhaul and the access bandwidths, respectively, while total bandwidth is W. The bandwidth allocated for each SBS, i.e., child IAB, by the fiber-connected MBS, i.e., IAB donor, is proportional to its load and the number of UEs in the access link. The resource allocation is determined based on

the instantaneous load in which each SBS informs its current load to the associated MBS each time. Thus, the backhaul-related bandwidth for the j-th IAB node is given by

$$W_{\text{backhaul},j} = \frac{\mu W N_j}{\sum\limits_{\forall\, j} N_j}, \forall j, \tag{A.12}$$

where N_j denotes the number of UEs connected to the j-th IAB node. Therefore, the bandwidth allocated to the j-th IAB node is proportional to the ratio between its load, and the total load of its connected IAB donor. Meanwhile, the access spectrum is equally shared among the connected UEs at the IAB node according to

$$W_{\text{access},u} = \frac{(1-\mu)W}{\sum\limits_{\forall\, u} N_{j,u}}, \forall u, \tag{A.13}$$

where u represents the UEs, and j represents each IAB node. Also, $N_{j,u}$ denotes the users connected to the j-th IAB node of which UE u is connected. The signal-to-interference-plus-noise ratio (SINR) values are obtained in accordance with (A.5) by

$$\text{SINR} = P_{\text{r}}/(I_u + N_0), \tag{A.14}$$

where N_0 is the noise power. Then, considering sufficiently long codewords, which is an acceptable assumption in IAB networks, the rates experienced by the UEs in access links can be expressed by

$$R_u = \begin{cases} \frac{(1-\mu)W}{N_m} \log(1+\text{SINR}(x_u)), \quad \text{if } \mathbf{x}_{\text{c}} \in \phi_{\text{m}}, \\ \min\Bigg(\frac{(1-\mu)W}{\sum\limits_{\forall\, u} N_{j,u}} \log(1+\text{SINR}(x_u)), \\ \qquad \frac{\mu W N_j}{\sum\limits_{\forall\, j} N_j} \log(1+\text{SINR}(x_{\text{b}})) \Bigg), \text{if } \mathbf{x}_{\text{c}} \in \phi_{\text{s}} \end{cases} \tag{A.15}$$

and the backhaul rate is given by

$$R_{\text{b}} = \frac{\mu W N_j}{\sum\limits_{\forall\, j} N_j} \log(1+\text{SINR}(x_{\text{b}})). \tag{A.16}$$

Here, m represents the associated MBS and s denotes the SBS. Based on the association cell, there are two cases for the rate of the connected UEs, x_u at the location. First, is the case in which the UEs are associated to the MBSs, as denoted by $x_{\text{c}} \in \phi_{\text{m}}$

Table 3: Simulation Parameters.

Parameter	**Value**
Carrier frequency	28 GHz
Minimum data rate threshold	100 Mbps
Bandwidth	1 GHz
IAB node and UE density	(MBS, SBS, UE) = (8, 100, 500) /km^2
Blocking	(Density, Length) = (500 /km^2, 5 m)
Path loss exponents	(LoS, NLoS) = (2, 3)
Main lobe antenna gains	(MBS, SBS, UE) = (24, 24, 0) dBi
Side lobe antenna gains	(MBS, SBS, UE) = (-2, -2, 0) dBi
Half power beamwidth	(Azimuthal, Elevation) = (60°, 25°)
Noise power	5 dB
In-leaf percentage	20%
Tree depth	5 m
Antenna heights	(MBS, SBS, UE) = (25 m, 10 m, 1 m)

in (A.15). Since the MBSs, i.e., IAB donor nodes, have fiber backhaul connection, the rate will depend on the access bandwidth available at the UE. In the second case, the UEs are connected to the SBSs, as denoted by $x_c \in \phi_s$ in (A.15). Here, the SBSs have shared backhaul bandwidth from the IAB donor nodes i.e., MBSs, and thus the UEs data rates depend on the backhaul rate of the connected SBS as well. Thus, in this case the UE is bounded to get the minimum between backhaul and access rate.

3.3 Simulation Results and Discussions

The simulation results are divided into three parts in which 1) we compare IAB, hybrid IAB/fiber-connected, and fiber-connected networks, 2) verify the robustness of IAB networks, and 3) study the system performance in an example of 3D network deployment. Note that the 2D model is considered mainly to limit the simulation complexity. However, for different cases, the same qualitative conclusions as those presented in the 2D model hold in the 3D model as well. The general system parameters are summarized in Table 3 and, for each figure, the specific parameters are given in the figure caption. The network is deployed in a disk of radius of $D = 1$ km, where the rain occurrence, the blockage, and the vegetation distributions are also probable according to the statistical models described in Section 3.1. In all figures, except for Figs. 8 and 9 which study the system performance in both urban and suburban areas, we concentrate on dense areas as the most important point of interest in IAB networks. We assume that we have high beamforming capability in the IAB-IAB backhaul links. Consequently, in all figures except for Fig. 6, we

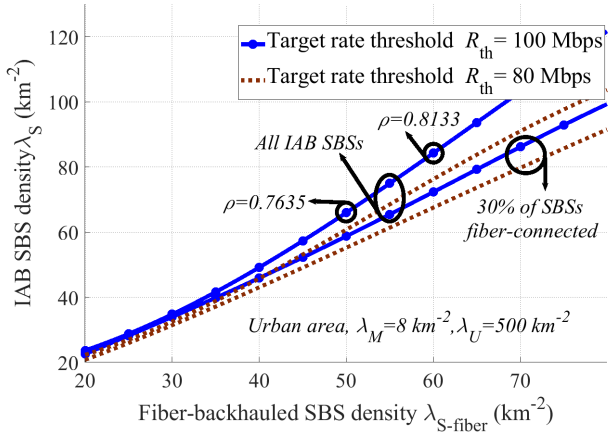

Figure 5: Density of the IAB nodes sufficing the performance of fiber-backhauled network, in terms of service coverage probability. The parameters are set to $\lambda_{\mathrm{B}} = 500$ km^{-2}, no rain, $R_{\mathrm{th}} = 100$ Mbps, and $P_{\mathrm{MBS}}, P_{\mathrm{SBS}}, P_{\mathrm{UE}} = (40, 24, 0)$ dBm.

ignore the interference in the backhaul links, in harmony with, e.g., [27], [28], [29]. In Fig. 6, however, we verify this assumption, and study the system performance in the cases where the interference is not ignored in the IAB-IAB links (More insights on mmWave interference in cellular networks are discussed in, e.g., [52], [53].)

Our metric of interest is the service coverage probability [54], defined as the fraction of the UEs which have instantaneous UE data rates higher than or equal to a threshold R_{th}. That is, using (A.15), the service coverage probability is given by

$$\rho = \Pr(R_{\mathrm{U}} \geq R_{\mathrm{th}}). \tag{A.17}$$

IAB versus Fiber

In Figs. 5-6, we compare the coverage probability of the IAB networks with those obtained by the cases having (a fraction of) fiber-connected SBSs, as well as the cases with no SBS. Also, Fig. 6 verifies the effect of the interference in the backhaul links on the system performance. In these figures, different parameters, e.g., bandwidth allocation between the access and backhaul, have been optimized to maximize the coverage probability in each case. Note that, in practice and depending on the network topology, a number of SBSs may also be fiber-connected. For this reason, in Figs. 5-6, we also consider the cases with a fraction of SBSs having fiber connections. In such cases, we assume the fiber-connected SBSs to be randomly distributed, and adapt the association and allocation rules as well as the achievable rates, correspondingly.

Figure 5 demonstrates the required number of IAB nodes to guarantee the same

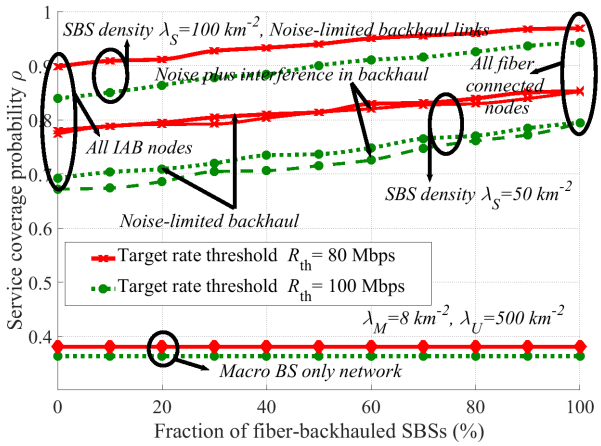

Figure 6: Service coverage probability as a function of the percentage of the fiber-backhauled SBSs for a dense network with $\lambda_{\mathrm{B}} = 500$ km^{-2}, no rain and $P_{\mathrm{MBS}}, P_{\mathrm{SBS}}, P_{\mathrm{UE}} = (40, 24, 0)$ dBm.

coverage probability as in the cases with hybrid IAB/fiber-connected SBSs. Then, Fig. 6 shows the network service coverage rate as a function of the fraction of fiber-connected SBSs, and compares the system performance with the cases having no SBS.

As demonstrated in Figs. 5-6, for a broad range of parameter settings, the same performance as in the fully fiber-connected networks can be achieved by the IAB network, with relatively small increment in the number of IAB nodes. As an example, consider the parameter settings of Fig. 5 and the UEs' target rate 100 Mbps. Then, a fully fiber-connected network with SBSs densities 50 and 60 km^{-2} corresponds, in terms of coverage probability, to an IAB network having densities $\lambda_{\mathrm{S}} = 65$ km^{-2} and 85 km^{-2}, respectively, leading to coverage probabilities 0.76 and 0.81. Interestingly, with a 30% of SBSs having fiber connections, which is practically reasonable, these numbers are reduced to $\lambda_{\mathrm{S}} = 70$ and 85 km^{-2}, i.e., only 16% and 21% increase in the required number of SBSs. Then, as the network density increases, the effect of the UEs target rate as well as the relative performance gap of the IAB and fiber-connected networks decrease (Fig. 6). Moreover, in harmony with intuitions and motivated by the high beamforming capability of the IAB nodes, the effect of the interference in the backhaul links is negligible, and the IAB-IAB links can be well assumed to be noise-limited (Fig. 6).

Here, it should be noted that our results, based on the FHPPP and random node drop, give a pessimistic performance of IAB networks. In practice, the network topology will be fairly well-planned, further reducing the gap between the performance of IAB and fiber-connected networks. Also, for simplicity and in order to mainly

concentrated on the effect of environmental parameters, we considered the minimum path loss rule in the backhaul links. A smart network operator may, however, use load balancing techniques to avoid congestion in the network, e.g., [55], [56]. Finally, while we considered a fixed bandwidth split between the access and backhaul which limits the resource allocation/coordination complexity, an adaptive split between access and backhaul of different nodes would improve the network performance.

On Some Practical Benefits of IAB

Using IAB with such a relatively small increment of the nodes reduces the network cost considerably[4]. This is because an SBS is much cheaper than fiber[5]. For example, and only to give an intuitive view, as reported in [57], Table 7], in an urban area the fiber cost is estimated to be in the range of 20000 GBP/km, while an SBS in 5G is estimated to cost around 2500 GBP per unit [58][6]. More importantly, internal evaluations at Ericsson indicates that, for dense urban/suburban areas, even in the presence of dark fiber, the deployment of IAB networks is an opportunity to reduce the total cost of ownership (TCO) as well as the time-to-market. Especially, the same hardware can be used both for access and backhaul such that no extra and seperate system is needed for backhaul.

Thus, although IAB may not support the same peak rate as fiber, IAB will be sufficient and a cost-effective solution for SBSs in dense networks, and with no digging[7], traffic jam and/or infrastructure displacement.

Along with the cost reduction, IAB increases the network flexibility remarkably. With optical fiber, the access points, of different types, can be installed only in the places with fiber connection. Such a constraint is, however, relaxed in IAB networks, and the nodes can be installed in different places as long as they have fairly good connection to their parent nodes. These are the reasons that different operators have shown interest to implement IAB in 5G networks [61], and it is expected that IAB would be ultimately used in up to 10-20% of 5G sites, e.g., [62].

It is interesting to note that, regardless of the cost, IAB is an attractive solution for a number of use-cases:

- Street trenching and digging not only are expensive but also may destroy historical areas or displace trees. For such reasons, some cities may consider a moratorium on fiber trenching [59], and instead rely on wireless backhaul

[4]It is reasonable to consider almost the same cost for an IAB node and a typical SBS.

[5]Indeed, the exact cost of the fiber varies vastly in different regions, due to many factors including labour cost, etc. However, for different areas, fiber laying accounts to a significant fraction of the total network cost.

[6]The price estimates are based on [57], and [58], and should not be considered as the cost estimations in Ericsson.

[7]According to different reports, e.g., [59], [60], for fiber connection in metropolitan areas, a large portion (about 85%) of the total cost figure is tied to trenching and installation.

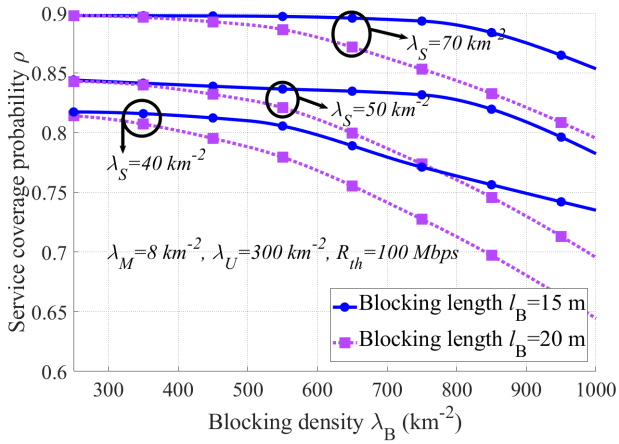

Figure 7: Service coverage probability of the IAB network as a function of the blocking density λ_{B}, with $P_{\mathrm{MBS}}, P_{\mathrm{SBS}}, P_{\mathrm{UE}} = (40, 24, 0)$ dBm, and no rain/tree foliage.

methods such as IAB and microwave backhaul.

- Fiber installation may take a long time, as it requires different permissions, labor work, etc. In such cases, IAB can establish new radio sites quickly. Thus, starting with IAB and, if/when needed, replacing it by fiber is expected to become a quite common setup.

- Low income zones of dense cities suffer from poor Internet connection. This is mainly because current fiber-based solutions are not economically viable, and the companies are not interested in fiber installation in such areas. Here, IAB is a low TCO solution to reduce the cost of Internet infrastructure.

- Public safety, and in general mission critical (MC), systems should be able to provide temporally on-demand coverage in all scenarios where the MC UEs are within terrestrial cellular network coverage or out of terrestrial cellular network coverage. In such cases, an IAB node, e.g., on a drone or a fire truck, can extend the coverage with high reliability and low latency[8].

Finally, as expected and also emphasized in Fig. 6, as the number of UEs increases, MBSs alone can not support the UEs' QoS requirements, and indeed we need to densify the network with, e.g., using (IAB) nodes of different types.

[8]It should be noted that, within Rel-16 and 17, mobile IAB is not supported. Thus, with an IAB on, e.g., a drone, the node position should remain fixed during the data transmission.

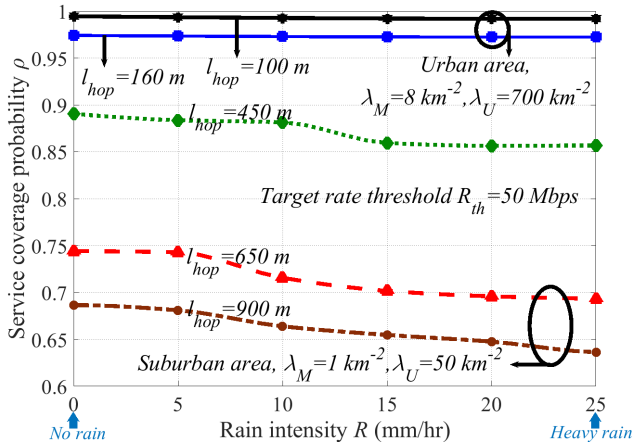

Figure 8: Service coverage probability of the IAB network as a function of the rain intensity in urban and suburban areas and for different average hop distances. The parameters are set to $P_{\text{MBS}}, P_{\text{SBS}}, P_{\text{UE}} = (45, 33, 0)$ dBm, $\lambda_{\text{B}} = 500$ km^{-2} for urban area and no blocking for the suburban area. Average hop distances $l_{\text{hop}} = 100, 160, 450, 650, 900$ m correspond to SBS densities λ_{S}= 100, 50, 8, 5, 3 km^{-2}, respectively.

Effect of Rain, Blocking and Tree Foliage

As opposed to fiber-connected setups, an IAB network may be affected by blockage, rain and tree foliage, the effects of which are analyzed in Figs. 7-9, respectively. Particularly, considering the 2D FHPPP blockage model, Fig. 7 investigates the coverage probability for different blockage densities λ_{B} and walls lengths l_{B} (also, see Fig. 11 for the effect of blockage in a 3D model).

Although IAB is of particular interest in dense urban areas, it has the potential to be used in suburban areas as well. For this reason, in Figs. 8 and 9 we demonstrate the coverage probability as a function of, respectively, the rain intensity, R in (6), and the tree line length l_{T} in both urban and suburban areas. Here, the results are presented for the average hop distances l_{hop}=100, 160, 450, 650 ,900 m which correspond to SBSs densities λ_{S}=100, 50, 8, 5 and 3 km^{-2}, respectively. For a suburban area, i.e., the cases with large average hop distance, we consider a single MBS, no blockage and UEs' density λ_{U} =50 km^{-2}. On the other hand, for the cases with urban areas, i.e., low average hop distance, the blockage and the UEs, densities are set to $\lambda_{\text{B}} = 500$ km^{-2} and $\lambda_{\text{U}} = 700$ km^{-2}, respectively. According to Figs. 7-9, the following points can be concluded:

- Unless for low network densities, the coverage probability is not much affected by the blockage density/length (Fig. 7. also, see Fig. 11 for the effect of

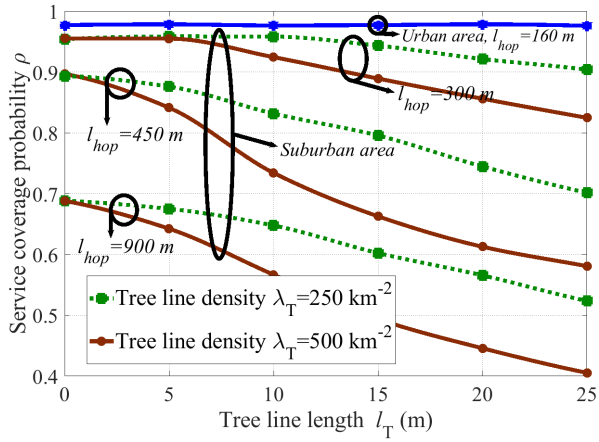

Figure 9: Service coverage probability of the IAB network, in both suburban and urban areas, as a function of the tree line length l_{T} with $R_{\mathrm{th}} = 50$ Mbps, $P_{\mathrm{MBS}}, P_{\mathrm{SBS}}, P_{\mathrm{UE}}$ = (45, 33, 0) dBm, $d = 5$ m, in (A.7), and no rain. In the suburban area, we set $\lambda_{\mathrm{M}} = 1$ km^{-2}, $\lambda_{\mathrm{U}} = 50$ km^{-2} with no blockage, while for the urban area we set $\lambda_{\mathrm{M}} = 8$ km^{-2}, $\lambda_{\mathrm{U}} = 700$ km^{-2} with blockage having density $\lambda_{\mathrm{B}} = 500$km^{-2} and length $l_{\mathrm{B}} = 5$ m. Average hop distances l_{hop}=160, 300, 450, 900 m correspond to SBS densities $\lambda_{\mathrm{S}} = 50, 20, 8, 3$ km^{-2}, respectively.

blockage in a 3D example use-case). This is intuitive because, as the network density increases, with high probability each UE can be connected to an SBS with strong LOS signal component.

- Considering 28 GHz, rain will not be a problem for IAB, unless for the cases with very heavy rainfall in suburban areas (Fig. 8). Particularly, the system performance is robust to different rain intensities in suburban/urban areas. Moreover, in suburban areas, even with high intensities the rain reduces the coverage probability slightly[9].

- As opposed to the rain and the blockage, depending on the network density, in the cases with low/moderate IABs' densities the coverage probability may be considerably affected by the tree foliage. For instance, consider the parameter settings of Fig. 9, in suburban area, with 1 MBS, $\lambda_{\mathrm{U}} = 50$ km^{-2} and an average hop distance of $l_{\mathrm{hop}} = 900$ m, corresponding to $\lambda_{\mathrm{S}} = 3$ km^{-2}. Then, the presence of trees with line length $l_{\mathrm{T}} = 15$ m and density $\lambda_{\mathrm{T}} = 250$ km^{-2} reduces the coverage probability from 70% for the cases with no trees to 60%, i.e., for 10% more of the UEs the rate requirement 50 Mbps can not be provided.

[9]It should be noted that, while Fig. 8 presents the results for 28 GHz which is the frequency of interest for IAB, the effect of the rain will be more visible at higher carrier frequencies.

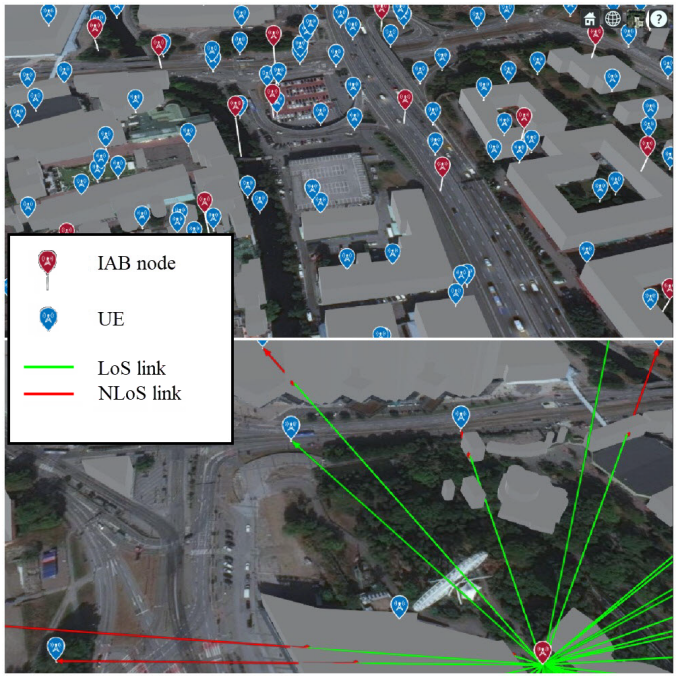

Figure 10: An example of the distribution of the IAB network in 3D space with OpenStreetMap.

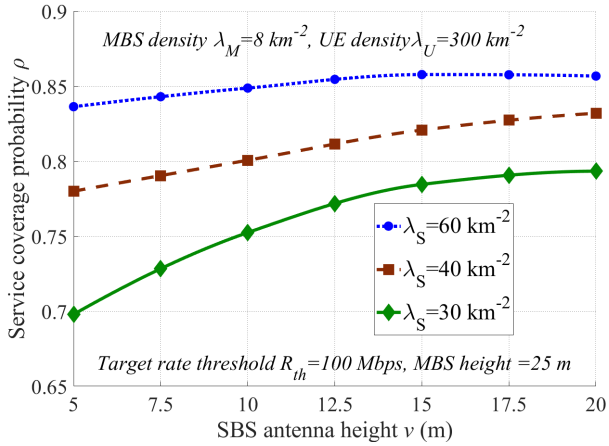

Figure 11: Service coverage probability as a function of the SBSs antenna height v for the cases with no rain and $P_{\text{MBS}}, P_{\text{SBS}}, P_{\text{UE}} = (40, 24, 0)$ dBm.

Thus, in the presence of tree foliage, more IAB nodes are required to satisfy the same QoS requirement. On the other hand, with high network density, the coverage probability is not affected by the tree foliage (Fig. 9). In general, predicting the link performance for IAB is difficult when accepting foliage. This is because, for instance, the backhaul link quality may change due to wet trees, snow on the trees, wind and varying percentage of leaves in different seasons. However, based on the presented results, we believe that, with appropriate nodes heights, mmWave IAB will work well for areas with low/moderate foliage level.

Finally, it should be mentioned that in Figs. 8-9 we considered the same parameter settings for the IAB nodes, independently of their area of implementation. However, in practice, different types of short-range and wide-area IAB nodes, with considerably higher capabilities for the wide-area IAB nodes, may be developed and used in urban and suburban areas, respectively [63]. This will help to reduce the effect of rain/foliage in suburban areas even more.

Performance Evaluation in an Example 3D Use-case

In Figs. 5-9, we investigate the system performance in the 2D FHPPP-based model. To evaluate the effect of the nodes and blockages heights, in this subsection we study the coverage probability in an example 3D setup. Particularly, as shown in Fig. 10, the UEs and the IAB nodes (both MBSs and SBSs) are still randomly distributed based on their corresponding FHPPPs, while they are positioned at different heights. Moreover, the blockages (as well as the distance between the nodes) are determined

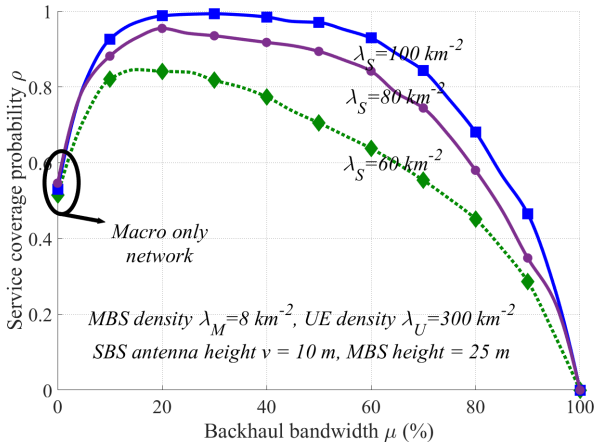

Figure 12: Service coverage probability as a function of the backhaul bandwidth allocation percentage μ in (A.11) for a dense network, no rain, $R_{\text{th}} = 100$ Mbps, and $P_{\text{MBS}}, P_{\text{SBS}}, P_{\text{UE}} = (40, 24, 0)$ dBm.

based on the map information, i.e., the real world blocking terrain is considered using OpenStreetMap 3D environment. The results have been tested on a disk of radius $D = 0.5$ km over the Chalmers University of Technology, Gothenburg, Sweden. Particularly, considering the MBSs and the UEs heights to be 25 and 1 m, respectively, Figs. 11 and 12 show the coverage probability as a function of the SBSs' heights and the backhaul bandwidth allocation percentage, μ in (A.11), respectively.

As demonstrated in Fig. 11, with a low SBS density, increasing the height of the SBSs helps to reduce the required number of IAB nodes considerably. For instance, with the parameter settings of Fig. 11, the same coverage probability as in the cases with density $\lambda_{\text{S}} = 40$ km^{-2} and height $v = 5$ m is achieved by a setup having $\lambda_{\text{S}} = 30$ km^{-2} and $v = 15$ m. However, as the network density increases, the effect of the SBSs height becomes negligible. This is intuitively because, with moderate/high densities, with high probability one can always find IAB donor-IAB, IAB-UE, and IAB donor-UE links with strong LOS signal components, even if the IAB nodes are located on the street level.

Finally, as shown in Fig. 12, with an optimal bandwidth allocation between the access and backhaul, IAB network increases the coverage probability, compared to the cases with only MBSs, significantly (Also, see Fig. 6). With $\mu = 0$, the system performance decreases to those achieved by only MBSs, as no bandwidth is allocated for backhauling. With $\mu = 100\%$, on the other hand, no resources are considered for access, and the coverage probability tends to zero. Thus, for different parameter settings, there is an optimal value for the portion of backhaul/access bandwidth allocation maximizing the coverage probability (Fig. 12). Deriving this optimal

value, which increases with the SBSs' density and decreases with the UEs' density, is an open research topic for which the results of [27] is supportive.

4 Conclusion

We studied IAB networks from both standardization and performance points of view. As we showed, depending on the QoS requirements, IAB can be considered as a cost-effective alternative to optical fiber that complements conventional microwave backhaul, in different use-cases and areas. Particularly, the same coverage probability as in fiber-connected networks is achieved by relatively small increment in the number of IAB nodes, leading to considerable network cost reduction/flexibility increment. Moreover, unless for the cases with moderate/high tree foliage in suburban areas, the system performance is not much affected by, e.g., the blockage, the rain, and the tree foliage, which introduces the IAB as a robust setup for dense networks.

While the industry has well proceeded in standardization of different aspects of the network, there are still many open research problems to be addressed by the academia. Among such research topics are topology optimization using, e.g., machine learning, studying the effect of hardware impairments on the system performance, developing efficient methods for simultaneous transmission/reception, improving the system performance using network coding, designing efficient (hybrid) beamforming methods for IAB networks, combination of IAB nodes and repeaters/intelligent surfaces, as well as mobile IAB. Also, load balancing and adaptive routing in a mesh-based network are interesting research topics for which the fundamental results of relay networks, e.g., [64], [65], [66], will be supportive. Although some of these topics are not supported in Rel-16 and 17, a deep analysis of such problems may pave the way for further enhancements of IAB in industry.

Reference

[1] Ericsson, "Mobile data traffic growth outlook," *Ericsson Mobility Report*, 2018.

[2] M. Agiwal, A. Roy, and N. Saxena, "Next Generation 5G Wireless Networks: A Comprehensive Survey," *Commun. Surv. Tutor.*, vol. 18, no. 3, pp. 1617–1655, Feb. 2016.

[3] S. Dang, O. Amin, B. Shihada, and M.-S. Alouini, "What should 6G be?" *Nature Electronics*, vol. 3, no. 1, pp. 20–29, Jan. 2020.

[4] P. Cerwall, "Mobile data traffic growth outlook," *Ericsson Mobility Report*, Jun. 2018.

[5] C. Czegledi et al., "Demonstrating 139 Gbps and 55.6 bps/Hz Spectrum Efficiency Using 8x8 MIMO over a 1.5 km Link at 73.5 GHz," accepted for presentation in IMS2020, CA, USA, Aug. 2020.

[6] H. Dahrouj, A. Douik, F. Rayal, T. Y. Al-Naffouri, and M. Alouini, "Cost-effective hybrid RF/FSO backhaul solution for next generation wireless systems," *IEEE Wireless Commun. Mag.*, vol. 22, no. 5, pp. 98–104, Oct. 2015.

[7] C. Dehos, J. L. González, A. D. Domenico, D. Kténas, and L. Dussopt, "Millimeter wave access and backhauling: the solution to the exponential data traffic increase in 5G mobile communications systems?" *IEEE Commun. Mag.*, vol. 52, no. 9, pp. 88–95, Sep. 2014.

[8] Y. Li, E. Pateromichelakis, N. Vucic, J. Luo, W. Xu, and G. Caire, "Radio Resource Management Considerations for 5G Millimeter Wave Backhaul and Access Networks," *IEEE Commun. Mag.*, vol. 55, no. 6, pp. 86–92, Jan. 2017.

[9] 3GPP, "Overview of 3GPP Release 10," 3rd Generation Partnership Project (3GPP), Technical Specification (TS), Jun. 2016, V0.2.1.

[10] O. Teyeb, A. Muhammad, G. Mildh, E. Dahlman, F. Barac, and B. Makki, "Integrated Access Backhauled Networks," in *Proc. VTC-Fall'2019*, Honolulu, HI, USA, Sep. 2019, pp. 1–5.

[11] M. N. Islam, S. Subramanian, and A. Sampath, "Integrated access backhaul in millimeter wave networks," in *Proc. IEEE WCNC'2017*, CA, USA, Mar. 2017, pp. 1–6.

[12] M. N. Islam, N. Abedini, G. Hampel, S. Subramanian, and J. Li, "Investigation of performance in integrated access and backhaul networks," in *Proc. IEEE INFOCOM WKSHPS'2018*, HI, USA, Apr. 2018, pp. 597–602.

[13] Y. Li, J. Luo, R. A. Stirling-Gallacher, and G. Caire, "Integrated access and backhaul optimization for millimeter wave heterogeneous networks," *arXiv*, 2019.

[14] Y. Liu, A. Tang, and X. Wang, "Joint incentive and resource allocation design for user provided network under 5G integrated access and backhaul networks," *IEEE Trans. Netw. Sci. Eng.*, vol. 7, no. 2, pp. 673–685, Apr. 2020.

[15] A. HasanzadeZonuzy, I. Hou, and S. Shakkottai, "Broadcasting real-time flows in integrated backhaul and access 5G Networks," in *Proc. IEEE WiOPT'2019*, Avignon, France, Jun. 2019, pp. 1–8.

[16] M. Polese, M. Giordani, A. Roy, D. Castor, and M. Zorzi, "Distributed Path Selection Strategies for Integrated Access and Backhaul at mmWaves," in *Proc. IEEE GLOBECOM'2018*, Abu Dhabi, United Arab Emirates, Dec. 2018, pp. 1–7.

[17] B. Zhai, M. Yu, A. Tang, and X. Wang, "Mesh architecture for efficient integrated access and backhaul networking," in *Proc. IEEE WCNC'2020*, Seoul, Korea (South), May 2020, pp. 1–6.

[18] J. Y. Lai, W. Wu, and Y. T. Su, "Resource allocation and node placement in multi-hop heterogeneous integrated-access-and-backhaul networks," *IEEE Access*, vol. 8, pp. 122 937–122 958, Jul. 2020.

[19] F. Gómez-Cuba and M. Zorzi, "Twice simulated annealing resource allocation for mmWave multi-hop networks with interference.," in *Proc. IEEE ICC'2020*, Dublin, Ireland, 2020, pp. 1–7.

[20] M. N. Kulkarni, A. Ghosh, and J. G. Andrews, "Max-min rates in self-backhauled millimeter wave cellular networks," *arXiv*, 2018.

[21] M. Polese, M. Giordani, A. Roy, S. Goyal, D. Castor, and M. Zorzi, "End-to-End Simulation of Integrated Access and Backhaul at mmWaves," in *Proc. IEEE CAMAD'2018*, Barcelona, Spain, Sep. 2018, pp. 1–7.

[22] M. Polese et al., "Integrated Access and Backhaul in 5G mmWave Networks: Potential and Challenges," *IEEE Commun. Mag.*, vol. 58, no. 3, pp. 62–68, Mar. 2020.

[23] F. Gomez-Cuba and M. Zorzi, "Optimal link scheduling in millimeter wave multi-hop networks with space division multiple access," in *Proc. IEEE ITA'2016*, La Jolla, CA, Feb. 2016, pp. 1–9.

[24] M. Hashemi, M. Coldrey, M. Johansson, and S. Petersson, "Integrated Access and Backhaul in Fixed Wireless Access Systems," in *Proc. VTC-Fall'2017*, Toronto, Canada, Sep. 2017, pp. 1–5.

[25] M. N. Kulkarni, J. G. Andrews, and A. Ghosh, "Performance of Dynamic and Static TDD in Self-Backhauled Millimeter Wave Cellular Networks," *IEEE Trans. Wireless Commun.*, vol. 16, no. 10, pp. 6460–6478, Oct. 2017.

[26] B. Makki, M. Hashemi, L. Bao, and M. Coldrey, "On the Performance of FDD and TDD Systems in Different Data Traffics: Finite Block-Length Analysis," in *Proc. VTC-Fall'2018*, IL, USA, Aug. 2018, pp. 1–5.

[27] C. Saha, M. Afshang, and H. S. Dhillon, "Integrated mmWave Access and Backhaul in 5G: Bandwidth Partitioning and Downlink Analysis," in *Proc. ICC'2018*, MO, USA, May 2018, pp. 1–6.

[28] S. Singh, M. N. Kulkarni, A. Ghosh, and J. G. Andrews, "Tractable Model for Rate in Self-Backhauled Millimeter Wave Cellular Networks," *IEEE J. Sel. Areas Commun.*, vol. 33, no. 10, pp. 2196–2211, Oct. 2015.

[29] C. Saha and H. S. Dhillon, "Millimeter Wave Integrated Access and Backhaul in 5G: Performance Analysis and Design Insights," *arXiv*, 2019.

[30] A. Fouda, A. S. Ibrahim, I. Guvenc, and M. Ghosh, "UAV-Based In-Band Integrated Access and Backhaul for 5G Communications," in *Proc. IEEE VTC-Fall'2018*, IL, USA, Aug. 2018, pp. 1–5.

[31] N. Tafintsev et al., "Aerial Access and Backhaul in mmWave B5G Systems: Performance Dynamics and Optimization," *IEEE Commun. Mag.*, vol. 58, no. 2, pp. 93–99, Feb. 2020.

[32] N. Tafintsev et al., "Reinforcement learning for improved uav-based integrated access and backhaul operation," in *Proc. IEEE ICC Workshops'2017*, Paris, France, May 2020, pp. 1–7.

[33] S. M. Azimi-Abarghouyi, B. Makki, M. Haenggi, M. Nasiri-Kenari, and T. Svensson, "Coverage analysis of finite cellular networks: A stochastic geometry approach," in *Proc. IEEE IWCIT'2018*, Tehran, Iran, Apr. 2018, pp. 1–5.

[34] Ericsson, "Long Haul,"

[35] 3GPP TR 38.874, "NR; Study on integrated access and backhaul," 3rd Generation Partnership Project (3GPP), Tech. Rep., Dec. 2018.

[36] 3GPP TS 38.401, "NG-RAN;Architecture description," 3rd Generation Partnership Project (3GPP), Tech. Rep., Mar. 2020.

[37] 3GPP TS 38.340, "NR; Backhaul Adaptation Protocol (BAP) specification," 3rd Generation Partnership Project (3GPP), Tech. Rep., Apr. 2020.

[38] 3GPP, "CR to 38.401 Support for IAB," 3rd Generation Partnership Project (3GPP),Ericsson, Tech. Rep., Mar. 2020.

[39] 3GPP R1-1913600, "RAN1 agreements for Rel-16 IAB," 3rd Generation Partnership Project (3GPP), Tech. Rep. Meeting #99, Reno, USA, Nov. 2019.

[40] 3GPP TS 38.473, "Technical Specification Group Radio Access Network; NG-RAN; F1 application protocol (F1AP)," 3rd Generation Partnership Project (3GPP), Tech. Rep., Mar. 2020.

[41] 3GPP TS 38.401, "Technical Specification Group Radio Access Network; NG-RAN; Architecture description," 3rd Generation Partnership Project (3GPP), Tech. Rep., Mar. 2020.

[42] 3GPP, "Draft Meeting Report," 3rd Generation Partnership Project (3GPP), Tech. Rep., Mar. 2020, Available: https://www.3gpp.org/ftp/TSG_RAN/TSG_RAN/TSGR_87e/Report/.

[43] 3GPP RP-193251, "New WID on Enhancements to Integrated Access and Backhaul," 3rd Generation Partnership Project (3GPP), Tech. Rep. Meeting #86, Sitges, Spain, Dec. 2019.

[44] 3GPP R4-1907825, "WF on simulation assumptions for IAB co-existence study," 3rd Generation Partnership Project (3GPP), Tech. Rep. Meeting RAN4 #91, Reno, United States, May 2019.

[45] S. M. Azimi-Abarghouyi, B. Makki, M. Nasiri-Kenari, and T. Svensson, "Stochastic Geometry Modeling and Analysis of Finite Millimeter Wave Wireless Networks," *IEEE Trans. Veh. Technol.*, vol. 68, no. 2, pp. 1378–1393, Feb. 2019.

[46] B. Błaszczyszyn, *Lecture Notes on Random Geometric Models: Random Graphs, Point Processes, and Stochastic Geometry*, Online Lecture Notes, 2017.

[47] T. S. Rappaport, Y. Xing, G. R. MacCartney, A. F. Molisch, E. Mellios, and J. Zhang, "Overview of Millimeter Wave Communications for Fifth-Generation (5G) Wireless Networks—With a Focus on Propagation Models," *IEEE Trans. Antennas Propag.*, vol. 65, no. 12, pp. 6213–6230, Dec. 2017.

[48] 3GPP TR 25.814, "Physical Layer Aspects for Evolved UTRA," 3rd Generation Partnership Project (3GPP), Tech. Rep., Apr. 2020.

[49] I. Rec, "P. 838-3:'Specific attenuation model for rain for use in prediction methods'," *International Telecommunications Union*, 2006.

[50] P. J. Diggle, *Some statistical aspects of spatial distribution models for plants and trees*. SLU, 1982.

[51] M. A. Abu-Rgheff, *5G Physical Layer Technologies*. John Wiley & Sons, Nov. 2019, pp. 303-313.

[52] A. Thornburg, T. Bai, and R. W. Heath, "Interference statistics in a random mmWave ad hoc network," in *Proc. IEEE ICASSP'2015*, Brisbane, QLD, 2015, pp. 2904–2908.

[53] M. Rebato, M. Mezzavilla, S. Rangan, F. Boccardi, and M. Zorzi, "Understanding Noise and Interference Regimes in 5G Millimeter-Wave Cellular Networks," in *Proc. European Wireless'2016*, Oulu, Finland, 2016, pp. 1–5.

[54] T. A. Khan, A. Alkhateeb, and R. W. Heath, "Millimeter Wave Energy Harvesting," *IEEE Trans. Wireless Commun.*, vol. 15, no. 9, pp. 6048–6062, Jun. 2016.

[55] T. K. Vu, M. Bennis, S. Samarakoon, M. Debbah, and M. Latva-aho, "Joint Load Balancing and Interference Mitigation in 5G Heterogeneous Networks," *IEEE Trans. Wirel. Commun.*, vol. 16, no. 9, pp. 6032–6046, 2017.

[56] T. M. Shami, D. Grace, A. Burr, and J. S. Vardakas, "Load balancing and control with interference mitigation in 5G heterogeneous networks," *EURASIP Journal on Wireless Communications and Networking*, vol. 2019, no. 1, p. 177, 2019.

[57] E. J. Oughton and Z. Frias, "Exploring the cost, coverage and rollout implications of 5G in Britain," *Cambridge: Centre for Risk Studies, Cambridge Judge Business School*, 2016.

[58] 5G NORMA., "Deliverable D2.1: Use Cases, Scenarios and Requirements," 5G PPP., Technical Specification (TS), 2015.

[59] H. A. Willebrand and B. S. Ghuman, "Fiber optics without fiber," *IEEE Spectrum*, vol. 38, no. 8, pp. 40–45, Aug. 2001.

[60] GSMA, *Mobile backhaul: An overview*, GSMA.com, Available: https://www.gsma.com/futurenetworks/wiki/mobile-backhaul-an-overview/ (accessed May. 1, 2020).

[61] *AT&T and Verizon to use Integrated Access and Backhaul for 2021 5G networks*, Available: https://techblog.comsoc.org/2019/12/16/att-and-verizon-to-use-integrated-access-and-backhaul-for-2021-5G-networks, Dec. 2019.

[62] *Verizon to Use 'Integrated Access Backhaul' for Fiber-Less 5G*, Available: https://www.lightreading.com/mobile/5G/verizon-to-use-integrated-access-backhaul-for-fiber-less-5G/d/d-id/754752, Oct. 2019.

[63] 3GPP R4-2008767, "WF on IAB-MT class descriptions," 3rd Generation Partnership Project (3GPP), Tech. Rep. Meeting #95-e, 25th May-5th Jun. 2015.

[64] X. Lin and J. G. Andrews, "Connectivity of millimeter wave networks with multi-hop relaying," *IEEE Wireless Commun. Lett.*, vol. 4, no. 2, pp. 209–212, 2015.

[65] S. Sharma, Y. Shi, Y. T. Hou, H. D. Sherali, S. Kompella, and S. F. Midkiff, "Joint flow routing and relay node assignment in cooperative multi-hop networks," *IEEE J. Sel. Areas Commun.*, vol. 30, no. 2, pp. 254–262, 2012.

[66] M. Movahednasab, B. Makki, N. Omidvar, M. R. Pakravan, T. Svensson, and M. Zorzi, "An energy-efficient controller for wirelessly-powered communication networks," *IEEE Trans. Wirel. Commun.*, vol. 68, no. 8, pp. 4986–5002, 2020.

PAPER B

On Topology Optimization and Routing in Integrated Access and Backhaul Networks: a Genetic Algorithm-Based Approach

C. Madapatha, B. Makki, A. Muhammad, E. Dahlman, M. -S. Alouini, and T. Svensson

IEEE Open Journal of the Communications Society, Sep. 2021

The layout has been revised.

Abstract

In this paper, we study the problem of topology optimization and routing in integrated access and backhaul (IAB) networks, as one of the promising techniques for evolving 5G networks. We study the problem from different perspectives. We develop efficient genetic algorithm-based schemes for both IAB node placement and non-IAB backhaul link distribution, and evaluate the effect of routing on bypassing temporal blockages. Here, concentrating on millimeter wave-based communications, we study the service coverage probability, defined as the probability of the event that the user equipments' (UEs) minimum rate requirements are satisfied. Moreover, we study the effect of different parameters such as the antenna gain, blockage, and tree foliage on the system performance. Finally, we summarize the recent Rel-16 as well as the upcoming Rel-17 3GPP discussions on routing in IAB networks, and discuss the main challenges for enabling mesh-based IAB networks. As we show, with a proper network topology, IAB is an attractive approach to enable the network densification required by 5G and beyond.

Index terms— Integrated access and backhaul, IAB, Genetic algorithm, Node selection, Topology optimization, Densification, Millimeter wave, (mmWave) communications, 3GPP, Stochastic geometry, Poisson point process, Coverage probability, Germ-grain model, Wireless backhaul, 5G NR, Blockage, Relay, Routing, Tree foliage, Machine learning

1 INTRODUCTION

Several reports have shown an exponential growth of demand on wireless communications, the trend which is expected to continue in the future [1]. To cope with such demands, 5G and beyond networks propose various methods for capacity and spectral efficiency improvement. Here, one of the promising techniques is network densification, i.e., the deployment of many base stations (BSs) of different types such that there are more resource blocks per unit area [2],[3], [4], [5] [6].

The BSs need to be connected to the operators' core network via a transport network, the problem which becomes challenging as the number of BSs increases. Such a transport network may be provided via wireless or wired connections. Wired (fiber) connections are typically used for transport closer to the core network and in the core network, where we need to handle aggregated traffic from multiple BSs. Wireless connections, on the other hand, are used for backhaul transport in the radio access network (RAN) closer to the BSs.

As reported in [2], the backhaul technology has large regional variations. However, on a global scale, wireless microwave technology has been a dominating media for the last few decades. Recently, there is an increase in fiber deployments attributed to geopolitical decisions and major governmental investments. Thus, going forward, it is expected that microwave and fiber will be two dominating backhaul technologies.

Fiber offers reliable connection with high peak data rates. However, 1) the deployment of fiber requires a noteworthy initial investment for trenching and installation, 2) may take a long installation time, 3) may be even not allowed in, e.g., metropolitan areas. Wireless backhaul using microwave is a well-established alternative to fiber, providing 10's of Gbps in commercial deployments[1]. Importantly, microwave is a scalable and economical backhaul technique that can meet the increasing requirements of 5G networks. Compared to fiber, wireless backhauling comes with significantly lower cost and time-to-market as well as higher flexibility, with no digging, no intrusion or disruption of infrastructure, and is possible to deploy in principle everywhere [8].

With the same reasoning and motivated by availability of massive bandwidth in millimeter wave (mmWave) spectrum/network densification, integrated access and backhaul (IAB) network has recently received considerable attention [9], [10], [11]. With IAB, the goal is to provide flexible wireless backhauling using 3GPP new radio (NR) technology in international mobile telecommunications bands, and provide not only backhaul but also the existing cellular services in the same node and via the same hardware. This, in addition to creating more flexibility and reducing the time-to-market, is generally to reduce the cost for a wired backhaul, which in certain deployments could impose a large cost for the installation and operation of the BS. Importantly,

- Internal evaluations at Ericsson shows that, even in the presence of dark fiber, the deployment of IAB network gives an opportunity to reduce the total cost of ownership in urban/suburban areas. This is partly because the same hardware can be used both for access and backhaul, i.e., less extra equipment is required especially for in-band backhauling.

- An integrated access/backhaul solution improves the possibilities for pooling of spectrum where it can be up to the operator to decide what spectrum resources to use for access and backhaul, rather than having this decided in an essentially static manner by spectrum regulators.

In this way, IAB serves as a complement to microwave and fiber backhaul specially in dense urban and suburban deployments.

Although IAB can in principle operate in every spectrum for which NR operation is specified, the focus of the 3GPP work on IAB has been on mmWave spectrum. This is intuitive because of the access to wide bandwidth in mmWave spectrum,

[1]Recent results demonstrate even more than 100 Gbps over MIMO backhaul links [7].

while the existing LTE spectrum is very expensive to be used for backhauling. With a mmWave spectrum, however, blockage and tree foliage may be challenging, as they reduce the achievable rate significantly. Properly planned and optimized networks could reap higher performances, and save costs to network operators as they can avoid static blockages such as buildings/trees [12], [13]. On the other hand, along with enabling traffic-based load balancing, routing can well compensate for temporal blockages, e.g., busses/trucks passing by. However, as the network size increases in dense areas, which is the main point of interest in IAB networks, deriving closed-form solutions for optimal network topology/routing becomes infeasible.

It should be mentioned that the network deployment optimization can be done offline, and recalculated whenever there are substantial changes in the blocking situations, service rate requirements, and addition of new set of BSs. Still, the optimization problem quickly becomes very large, thus motivating a potentially suboptimal machine learning approach, since an exhaustive search over all possible deployment options quickly becomes infeasible (see Section 5 for further details). In such cases, machine learning techniques give effective (sub)optimal solutions with reasonable implementation complexity.

1.1 Literature Review

The performance of IAB networks have been studied from different perspectives. Particularly, [14], [15], [16], [17], [18], develop various resource allocation schemes, and [19], [20] study the effect of time/frequency division duplex based resource allocation on the throughput of IAB networks. Moreover, [21], [22], [23] utilize infinite Poisson point processes (PPPs) to evaluate the coverage probability of multi-hop IAB networks. Then, [24], [25] investigate the feasibility/challenges of mmWave-based IAB networks via end-to-end simulations. Also, [26] and [27] evaluate the potentials of using IAB in fixed wireless access and unmanned aerial vehicle-based communication setups, respectively. In [28] and [29], we provide an overview of 3GPP Rel-16 discussions on IAB. Moreover, [29] uses a FHPPP (FH: finite homogeneous), i.e., a PPP with a constant density and random distributions of the nodes in a finite region, to analyze the performance between the IAB and fiber-connected networks, and verify the robustness of IAB to various environmental effects. Finally, [30] develops simulated annealing algorithms for joint scheduling and power allocation, and [31] designs a joint precoder design and power allocation scheme maximizing the network sum rate.

The problem of routing in IAB networks has been previously studied in the cases with different numbers of hops [14], [15], [16], [17], [18], [32], [33], [34]. Also, [28] develops a cost-optimal node placement scheme, and [35] proposes a joint node placement and resource allocation scheme maximizing the downlink sum rate of IAB networks. On the other hand, with different (non-IAB) network topologies/use-cases, various machine-learning based solutions have been previously proposed for topol-

ogy optimization. For instance, [36], [37], [38], [39], [40], [41], [42], [43], [44], [45] develop deep reinforcement (DR) algorithm-based solutions for topology optimization of different network configurations. Deep Q-learning is used in [46] to evaluate the cumulative transmission rate in vehicular networks. Spectrum allocation and access mode selection evaluations are considered in [47], while the potential of using K-means clustering algorithm to design ultra-reliable and low-latency wireless sensor networks is evaluated in [48]. In addition, [49] and [50] use DR learning-based algorithms to solve the large-scale load balancing problem for ultra-dense networks.

Note that the mentioned works neither consider the non-IAB backhaul links distribution optimization nor the joint optimization of the non-IAB backhaul links distribution and the IAB nodes placement. This, although is of interest in practice, may be due to the fact that such optimization problems are NP-hard with a large search space. Therefore, one needs to design efficient algorithms which can find (semi)optimal solutions within a limited simulation period. Moreover, [14]-[50] concentrate on multi-hop communications, while the usefulness and challenges of meshed-based IAB have not yet been studied. Here, it is important to consider both the performance evaluations and the standardization issues, as meshed IAB has not yet been discussed in 3GPP 5G NR. These are the motivations for our work as presented in the following.

1.2 Contributions

In this paper, we study the problem of topology optimization and routing in IAB networks. We study the problem from different points of views:

- We design effective genetic algorithm (GA)-based techniques not only for IAB node placement but also for dedicated non-IAB backhaul connection distribution. Here, concentrating on the characteristics of mmWave communications, we present the results for the cases with an FHPPP-based stochastic geometry model [21], [51]. As the metric of interest, we consider the network service coverage probability which is defined as the probability of the event that the UEs' minimum data rate requirements are satisfied.

- We study the effect of temporal blockages and routing on the coverage probability. In this way, one can avoid both the long-term and temporal blockages via topology optimization and routing, respectively. Also, the setup gives hints on the effectiveness of mesh-based communication in IAB networks, although it is not yet considered by 3GPP IAB standardization.

- We summarize the main 3GPP Rel-16 agreements as well as the upcoming Rel-17 discussions on routing, and highlight the main challenges which need to be solved before meshed IAB can be implemented.

- We study the effect of different parameters such as antenna gain, blockage and tree foliage on the system performance in both cases with well-planned and random network deployments.

- Finally, we compare the performance of the GA-based scheme with different state-of-the-art topology optimization methods. Also, we study the efficiency of the deployment optimization in the cases with constraint on the network topology, where the IAB nodes and the non-IAB backhaul links can not be freely deployed in every place.

Compared to the related literature, e.g., [12]-[51], we consider more realistic algorithms and network configurations. Moreover, our discussions on the effect of environmental parameters/deployment constraints on the system performance as well as the 3GPP agreements on IAB-based routing have not been presented before. Also, we optimize the IAB network for both node locations and non-IAB backhaul link placement independently, as well as jointly which further improves the coverage probability. We compare the performance of the proposed algorithms with different state-of-the-art schemes. These make our discussions and the conclusions completely different from those presented in the state-of-the-art works.

As we show, machine learning techniques provide effective solutions for deployment optimization which can be easily adapted for different channel models, constraints and metrics of interest with no need for mathematical analysis. Moreover, compared to random deployment, deployment planning increases the coverage probability of the IAB networks significantly. On the other hand, with a well-planned network and for a broad range of blockage/tree foliage densities, the network can well handle these blockages with small routing updates. Finally, while the service coverage probability of the IAB network is slightly affected by stationary/temporal blockages in urban areas, for a broad range of parameter settings, the blockage is not problematic for well-planned routing-enabled IAB networks, in the sense that its impact on the coverage probability is negligible. On the other hand, high levels of tree foliage may reduce the coverage probability of the network in suburban areas; the problem which can be solved by proper deployment planning.

2 IAB in 3GPP

IAB was introduced as part of Rel-16 of the 5G NR specification, with the specification finalized in fall 2020 [52]. Currently, Rel-17 work item on IAB enhancements is going on, which is expected to finish in early 2022 [53].

The overall architecture for IAB is based on the CU/DU split of the gNB, introduced already in 3GPP Rel-15. With such architecture, a gNB consists of two functionally different parts with a standardized interface (referred to as the F1 interface) in between:

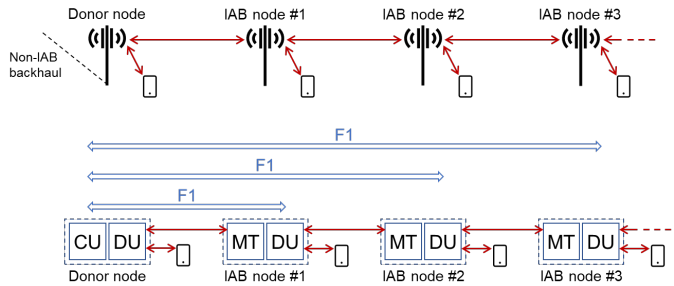

Figure 1: Types of network nodes.

- A Centralized Unit (CU) including the packet data convergence protocol (PDCP) and radio resource control (RRC) protocols,
- One or several Distributed Units (DUs) consisting of radio link control (RLC), medium access control (MAC), and physical layer protocols.

IAB specifies two types of network nodes (see also Fig. 1):

- The IAB-Donor-node is the node consisting of CU and DU functionalities, and connects to the core network via non-IAB, for example fiber, backhaul.
- The IAB node includes two modules, namely, DU and mobile terminal (MT). IAB-DU serves UEs as well as, potentially, downstream IAB nodes in case of multi-hop wireless backhauling. At its other side, an IAB-MT is the unit that connects an IAB node with the DU of the parent/upstream node.

The IAB architecture is thus based on a hierarchical or, at least, a-cyclical structure where it is well-defined if a certain node is "above" or "below" a certain other node and where information flows in well-defined down-stream and up-stream directions. The possibility for a more mesh-like structure with no well-defined hierarchy was briefly discussed during the initial phase of the 3GPP work on IAB. However, majority of the companies discard the idea owing to its complexity and no clear benefits.

When it comes to the connectivity with the parent node, the IAB-MT connects to the DU of its parent node essentially as a normal UE. The Uu interface, i.e., the link between the parent node DU and the MT of the IAB node then provides the lower-layer functionality and relays the F1 messages between the donor-node CU and the IAB-node DU. The specification of the F1 interface only defines the higher-layer protocols, for example, the signaling messages between the CU and DU, but is agnostic to the lower-layer (i.e., transport network layer) protocols. With IAB, the NR radio-access technology (the RLC, MAC, and physical layer protocols) together with some IAB-specific protocols, provides the lower-layer functionality on top of

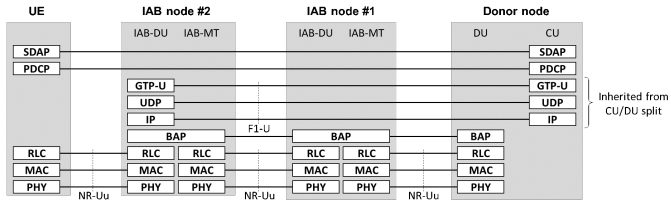

Figure 2: IAB protocol stack of the user-plane.

which the F1 interface is implemented. See Fig. 2 showing the user-plane protocols of a multi-hop IAB network (the control plane has a similar structure).

2.1 Backhaul Adaptation Protocol

Backhaul adaptation protocol (BAP) is a new IAB-specific protocol responsible for routing and bearer mapping of packets in the IAB network. More specifically, the BAP layer is responsible for forwarding of the packets in the intermediate nodes/hops between the IAB-donor-DU and the access IAB-node. For the downstream traffic, the BAP layer of the IAB-Donor-DU will add a BAP header to packets received from the upper layer. Similarly, for the upstream traffic, the BAP layer of the access IAB-node will add a BAP header to the upper layer packets. Figure 3 shows the structure for the BAP header, which contains a 10-bit BAP address field and a 10-bit BAP path ID field apart from 1-bit flag and 3 reserve bits for future use. Note that 3GPP specifications use the BAP Routing ID as a cover term for BAP address and BAP path ID fields. The purpose of the BAP address field is to carry the address of the destination IAB-node, while the Path ID field contains the path identity to be used for traversing the packets towards the destination IAB-node. This latter field is important for situations where multiple paths are configured for an IAB-node to improve network robustness/resilience and achieve load balancing by transporting a part of the traffic via each path towards the IAB-node.

To illustrate the above concept, figure 4 shows an example topology for IAB network where two paths (i.e., Path 1 and Path 2) have been configured for IAB-node 5 by the IAB-donor-CU. This means that the routing tables in the BAP layer of all the intermediate IAB-nodes (i.e., IAB1, IAB2, IAB3, etc.) are properly configured with next-hop link information for all the BAP addresses and BAP path IDs carried in the packets BAP header that these nodes will route in the network. Furthermore, the IAB-donor-DU will have mapping rules (configured by the donor-CU) how to select the BAP address and BAP path ID fields for packets from the upper layer based on the information in the IP address fields (i.e., DS/DSCP) of the F1-AP signaling.

Suppose the IAB-donor-DU receives a packet with IP address fields marked with information that is mapped to BAP address 5 and BAP path ID 1, the donor-DU will

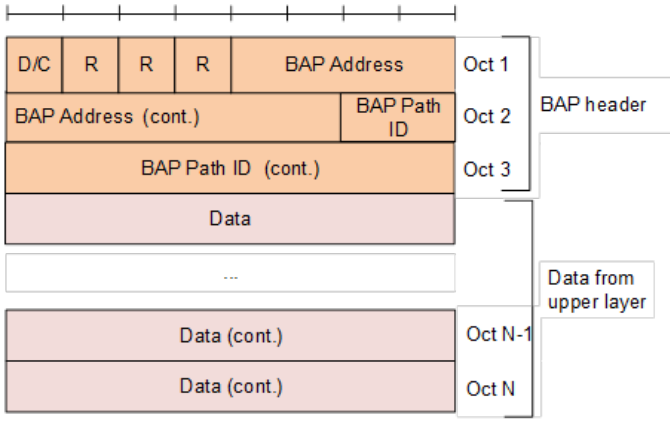

Figure 3: Structure for the BAP header.

add a BAP header with proper field values (i.e., address 5 and path ID 1) and will forward the packet to IAB2. Once IAB2 receives the packet, the node will examine the BAP header of the packet and based on the BAP address (carried in the packet) and its routing table information will transmit the packet towards IAB4. Similarly, IAB4 will route the packet to IAB5, where the IAB5 upon examining the BAP header field of the packet will notice that the packet is destined for it. Hence, IAB4 will remove the BAP header before delivering the packet to its upper layer for further processing.

In another scenario, if IAB1 receives a packet (from IAB-donor-DU) with BAP header containing BAP address 5 and path ID 2, IAB1 will forward the packet towards IAB3 instead of IAB2, and so on IAB3 will forward the packet to IAB4. When it comes to the upstream traffic, the BAP layer of IAB5 will add a BAP header containing IAB-donor-DU BAP address and appropriate path ID (either path ID 1 or path ID 2 based on the configuration information) to packets received from the upper layer. Next, IAB5 will forward the packets to IAB4, which will be further forwarded by IAB4 either to IAB1 or IAB2 depending on the path ID field value carried in the packets BAP headers. Once the packets reach IAB-donor-DU, the DU will remove the BAP header before delivering the packets to the upper layer for subsequent processing.

2.2 IAB extensions in 3GPP release 17

3GPP is considering further extensions and enhancements to IAB as part of NR Rel-17. One topic for Rel-17 is to look further into the support for dual-connectivity scenarios for IAB. For the regular network-to-device link, dual-connectivity, supported for both NR and 4G/LTE, implies that a device has established a link to

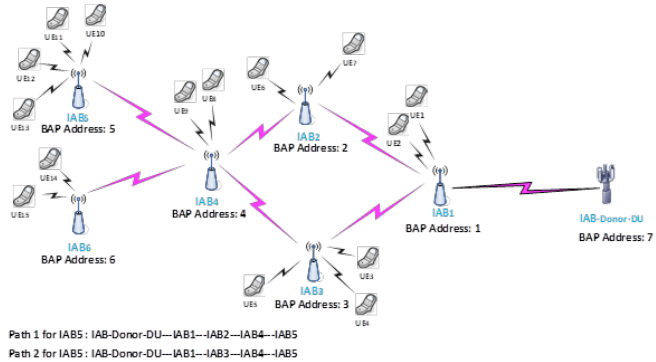

Figure 4: Example of routing in IAB network.

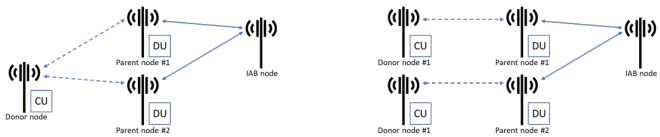

Figure 5: Intra-CU dual connectivity vs inter-CU dual-connectivity

multiple cells operating on different carrier frequencies. In the context of IAB, dual-connectivity like-wise implies that an IAB-DU is connected to multiple parent nodes via its collocated IAB-MT. Such IAB dual connectivity can be either intra-CU, that is, the same donor node is serving both parent nodes. Alternatively, dual-connectivity can be inter-CU, that is, there are multiple IAB-Donor-nodes (see Fig. 5). Clearly, the inter-CU dual-connectivity has a larger impact on the IAB network in terms of specification work and complexity.

IAB dual-connectivity is envisioned to provide higher reliability due to an additional redundancy in the wireless backhaul. It may also enable additional possibilities for load-balancing within the wireless backhaul, i.e., the possibility to more dynamically route data via different paths depending on the instantaneous load conditions on different links.

3 System Model

This section presents the system model, including the channel model, the considered UE association rule as well as the achievable data rates in the backhaul and access links. Table 1 summarizes the parameters used in the analysis.

Consider a dense urban area with a two-tier heterogeneous network (HetNet), i.e., a two-hop IAB network, where multiple MBSs (M: macro) and SBSs (S: small) serve

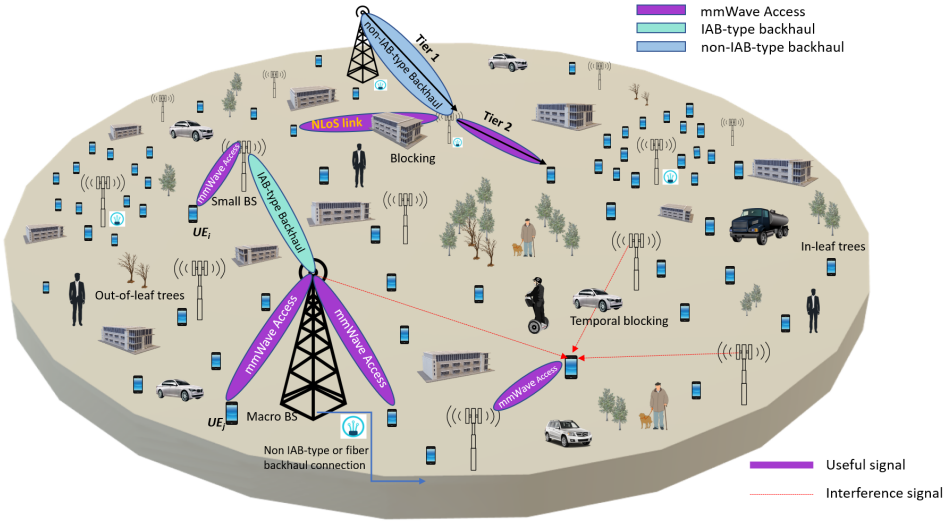

Figure 6: Schematic of the considered IAB network. A majority of the SBSs rely on IAB for backhauling. A small fraction of the SBSs, however, may have non-IAB type backhaul where such a backhauling can be provided by fiber or wirelessly.

the UEs (see Fig. 6). In this way, following the 3GPP definitions (see Section 2), the MBSs and the SBSs represent the donor and the child IABs, respectively, and throughout the paper we may use the terminologies MBS/SBS and donor IAB/IAB interchangeably. With the IAB setup, both the MBSs and the SBSs are used for both access and backhaul. However, the donor IABs, i.e., the MBSs, are non-IAB backhauled to the core network.

Note. In practice, a majority of the SBSs receive IAB-type backhaul from the MBSs wirelessly. However, a fraction of the SBSs may have access to non-IAB type dedicated backhaul connections, where such a backhaul can be provided either by fiber or a wireless radio link operating on a different frequency than the IAB network (see Fig. 6). In this paper, along with optimizing the SBSs' locations, one of our goals is to determine the proper nodes with non-IAB type backhauling such that the coverage probability is maximized. In terms of performance evaluation, our analysis does not depend on if these non-IAB backhaul links are provided by fiber or wirelessly. In practice, however, the network performance may depend on the type of such non-IAB links; Wireless radio backhaul link is quite flexible, and one can provide an SBS with wireless non-IAB backhaul as long as there is a strong LoS connection between the SBS and an MBS. Fiber connections, on the other hand, may be available in specific areas, and there may be low flexibility in fiber distribution between the nodes. In summary, depending on the type of the non-IAB backhaul links, to the SBSs, our non-IAB backhaul link distribution method, presented in Algorithm 1,

may give an ultimate opportunistic potential of the network performance.

Note that the consideration of two-hop network, e.g., [19], [20], [21], [29], [6], [54], in our work is motivated by the fact that, although the 3GPP standardization does not limit the possible number of hops, as also reported in, e.g., [28], [55], [56], [57], traffic aggregation in the backhaul links and end-to-end latency become challenging as the number of hops increases. Moreover, because IAB is of most interest in dense metropolitan areas with already existing limited number of fiber links, in most cases appropriate coverage can be provided with a maximum of two hops (For instance, see the Ericsson simulation results in the London area [[58], Fig. 3] where the required QoS is satisfied mostly by only a single backhaul hop).

We model the IAB network using an FHPPP based random distribution of the nodes in a finite region [21], [22], [23], [31]. Particularly, without topology optimization, which we use as the benchmark to evaluate the performance of planned networks, the FHPPPs $\chi_{\mathrm{M}}, \chi_{\mathrm{S}}, \chi_{\mathrm{U}}$ with densities, $\lambda_{\mathrm{M}}, \lambda_{\mathrm{S}}$ and λ_{U}, respectively, are used to model the spatial distributions of the MBSs, the SBSs and the UEs, respectively. With our topology optimization, however, while the number of nodes are still determined based on some random process, the locations of the SBSs as well as the location of the non-IAB backhaul connections to a fraction of the SBSs are optimized, in terms of network service coverage probability (see Section 5 for the details).

In our setup, in-band communication is considered where both the access and backhaul links share and operate in the same mmWave spectrum band. This is motivated by the fact that in-band communication gives better flexibility for resource allocation, at the cost of coordination complexity. For simplicity, assume the network to be distributed over a circular disk D. However, the model can be well applied on every arbitrary region D.

For the blockage, we use the well-known germ grain model described in [59, Chapter 14], which provides accurate blind spot prediction, compared to stochastic models that assume independant blocking. Particularly, the model takes induced blocking correlation into account and, thus, suits well for environments with large obstacles. Here, an FHPPP χ_{bl} models the blockage distribution in the area D with λ_{bl} denoting the density. The blockings are considered to be walls of length l_{bl} and independantly and identically distributed orientation θ_{bl}. Later, we use a GA-based approach to optimize the SBSs locations inside the region D to preferably avoid blockage in the backhaul links.

Following the state-of-the-art mmWave channel model, e.g., [60], the received power at each node can be expressed as

$$P_{\mathrm{r}} = P_{\mathrm{t}} h_{\mathrm{t,r}} G_{\mathrm{t,r}} \gamma_{(1\mathrm{m})} \gamma_{\mathrm{t,r}} \left|\left|x_{\mathrm{t}} - x_{\mathrm{r}}\right|\right|^{-1} \kappa_{\mathrm{t,r}}. \tag{B.1}$$

Here, P_{t} represents the transmit power in each link, and $h_{\mathrm{t,r}}$ denotes the independant small-scale fading in individual links. Particularly, in our study Rayleigh fading is considered for small-scale fading. Thereby, $G_{\mathrm{t,r}}$ denotes the combined antenna

Table 1: Definition of Parameters

Parameter	Definition	Parameter	Definition
χ_{M}	FHPPP of the MBSs	χ_{U}	FHPPP of the UEs
χ_{S}	FHPPP of the SBSs	χ_{bl}	FHPPP of the blockings
χ_{T}	FHPPP of the tree lines	λ_{U}	UE density
λ_{M}	MBS density	λ_{S}	SBS density
λ_{bl}	Blocking density	λ_{T}	Tree density
ρ	Service coverage probability	d	Vegetation depth
θ	Orientation of the blocking wall	φ	Angle between transmitter and receiver
D	Circular disk	R	Radius of the disk
P_{t}	Transmission power	P_{r}	Received power
h	Fading coefficient	G	Antenna gain
$\gamma_{(\mathrm{1m})}$	Reference path loss at 1 meter	γ	Propagation path loss
x	Location of the node	r	Propagation distance between nodes
α	Path loss exponent	N	Number of connected UEs
f_{c}	Carrier frequency	R_{th}	Minimum data rate threshold
w_{u}	Associated cell	w_{s}	Associated BS in backhaul link
N_{f}	Number of non-IAB backhauled SBSs	κ	Tree foliage loss
N_{s}	Number of SBSs	S_c	Number of possible solution checkings
l_{T}	Tree line length	l_{h}	Hop length
λ_{temp}	Temporal blocking density	K	Number of random sets in the GA
J	Number of sets around the Queen in GA	N_{it}	Number of iterations in the GA
B	Bandwidth	ψ	Percentage of bandwidth resources on backhaul

gain of the transmitter and receiver in the link, $\gamma_{\mathrm{t,r}}$ is the propagation path loss, and $\gamma_{(1m)}$ is the reference path loss at one meter distance while $\kappa_{\mathrm{t,r}}$ is the tree foliage loss.

The total path loss, in dB, is characterized according to the 5GCM UMa close-in model described in [61]. Here, the path loss is characterized by

$$\mathrm{PL} = 32.4 + 10\log_{10}(r)^{\alpha} + 20\log_{10}(f_{\mathrm{c}}), \tag{B.2}$$

where f_c is the carrier frequency, r is the propagation distance between the nodes, and α is the path loss exponent. Depending on the blockage, line-of-sight (LoS) and NLoS (N: Non) links are affected by different path loss exponents. The propagation loss of the path loss model is given by

$$\gamma_{\mathrm{t,r}} = \begin{cases} r^{\alpha_{\mathrm{L}}}, & \text{if LoS,} \\ r^{\alpha_{\mathrm{N}}}, & \text{if NLoS,} \end{cases} \tag{B.3}$$

where α_{L} and α_{N} denote path loss exponents for the LoS and NLoS scenarios, respectively.

5G and beyond systems are equipped with large antenna arrays which are used to minimize the propagation loss. We use the sectored-pattern antenna array model to characterize the beam pattern and antenna gain, which is given by

$$G_{\mathrm{t,r}}(\varphi) = \begin{cases} G_0 & \frac{-\theta_{\mathrm{HPBW}}}{2} \leq \varphi \leq \frac{\theta_{\mathrm{HPBW}}}{2} \\ g(\varphi) & \text{otherwise.} \end{cases} \tag{B.4}$$

Here, φ represents the angle between the transmit and receive antennas. Furthermore, θ_{HPBW} is the half power beamwidth, and G_0 denotes the main lobe gain of the antenna while $g(\varphi)$ is the side lobe gain [60]. Finally, as in, e.g., [21], [23], [29], for tractability we assume that the UE antenna gain to be 0 dB due to its omni-directional beam pattern, although UE beamforming in mmWave is an interesting future work to incorporate.

Unless otherwise stated and in harmony with, e.g.,[21], [22], [23],[29], we assume that the backhaul links are noise-limited. This assumption, which has been verified in [29], is motivated by the high beamforming capacity in the inter IAB backhaul links and the fact that simultaneous transmission/reception is not considered in our setup. Then, Section 5 validates this assumption, and we verify the effect of the backhaul interference on the coverage probability. Also, the inter-UE interference is neglected with the assumption of sufficient isolation and low power of the UEs [26]. Particularly, the interference model focuses on the aggregated interference on the

access links, caused by the neighbouring interferers, which for UE u is expressed as

$$I_u = \sum_{\mathbf{i},\, \mathbf{u} \in \chi_{i,u} \setminus \{\mathbf{w}_u\}} P_i h_{i,u} G_{i,u} \gamma_{(1\mathrm{m})} \gamma_{x_i,x_u} \|\mathbf{x}_i - \mathbf{x}_u\|^{-1}, \tag{B.5}$$

where i denotes the set of BSs excluding the associated BS w_{u} of user u. Also, for SBS s, the aggregated interference on the backhaul links is given by

$$I_s = \sum_{\mathbf{j},\, \mathbf{s} \in \chi_{j,s} \setminus \{\mathbf{w}_s\}} P_j h_{j,s} G_{j,s} \gamma_{(1\mathrm{m})} \gamma_{x_j,x_s} \|\mathbf{x}_j - \mathbf{x}_s\|^{-1}, \tag{B.6}$$

where j denotes the set of transmitting BSs excluding the associated BS w_{s} of SBS s.

We use an FHPPP denoted by χ_{T} with density λ_{T} to model the spatial distribution of the tree lines of length l_{T} [62]. The tree foliage loss is estimated using the Fitted International Telecommunication Union-Radio (FITU-R) tree foliage model [63, Chapter 7]. The model is well known for its applicability in cases with non-uniform vegetation and frequency dependancy within 10-40 GHz range. Particularly, considering both in-leaf and out-of-leaf, vegetation states, the tree foliage loss in (B.1) is expressed as

$$\kappa = \begin{cases} 0.39 f_{\mathrm{c}}^{0.39} d^{0.25}, \text{ in-leaf} \\ 0.37 f_{\mathrm{c}}^{0.18} d^{0.59}, \text{ out-of-leaf,} \end{cases} \tag{B.7}$$

where d is the vegetation depth measured in meter.

In our setup, each UE has the ability to be connected to either an MBS or an SBS depending on the maximum average received power. Let $a_u \in \{0, 1\}$ be a binary variable indicating the association with 1, while 0 representing the opposite. Thus, for the access links

$$a_u = \begin{cases} 1 & \text{if } P_i G_{z,x} h_{z,x} \gamma_{(1m)} \gamma_{\mathrm{z,x}} (\|\mathbf{z} - \mathbf{x}\|)^{-1} \\ & \quad \geq P_j G_j h_{z,y} \gamma_{(1m)} \gamma_{\mathrm{z,y}} (\|\mathbf{z} - \mathbf{y}\|)^{-1}, \\ & \quad \forall\, \mathbf{y} \in \chi_j, j \in \{\mathrm{m}, \mathrm{s}\} | \mathbf{x} \in \chi_i, \\ 0, & \text{otherwise,} \end{cases} \tag{B.8}$$

where i, j denote the BS indices, i.e., MBS or SBS. As in (3) for each UE u, the association binary variable a_u becomes 1 for the cell giving the maximum received power at the UE, while for all other cells it is 0, as the UE can only be connected to one IAB node.

Since the MBSs and the SBSs have large antenna arrays and can beamform towards the desired direction, the antenna gain over the backhaul links can be assumed to be the same, and backhaul link association can be well determined based on the

minimum path loss rule, i.e., by

$$a_{b,m} = \begin{cases} 1 & \text{if } \gamma_{\mathrm{b_m}}(\|\mathbf{z}-\mathbf{x}\|)^{-1} \geq \gamma_{\mathrm{b_m}}(\|\mathbf{z}-\mathbf{y}\|)^{-1}, \\ & \qquad \forall\ \mathbf{y} \in \chi_{\mathrm{m}} | \mathbf{x} \in \chi_{\mathrm{m}}, \\ 0, & \text{otherwise.} \end{cases} \tag{B.9}$$

For resource allocation, on the other hand, the mmWave spectrum available is partitioned into the access and backhaul links such that

$$\begin{cases} B_{\mathrm{Backhaul}} = \psi B, \\ B_{\mathrm{Access}} = (1-\psi)B, \end{cases} \tag{B.10}$$

In practice, along with the MBSs which are non-IAB backhaul-connected, a portion of the SBSs may have dedicated non-IAB backhaul connections, resulting in a hybrid IAB network. Therefore, in our deployment, some of the SBSs are IAB backhauled wirelessly and the others are connected to dedicated non-IAB backhaul links.

Let us initially concentrate on the IAB-type backhauled SBSs. Also, let, B_{backhaul} and B_{access} denote the backhaul and the access bandwidths, respectively, while total bandwidth is $B = B_{\mathrm{backhaul}} + B_{\mathrm{access}}$. The bandwidth allocated for each IAB-type wirelessly backhauled SBS, namely, child IAB, by the MBS, i.e., IAB donor, is proportional to its load and the number of UEs in the access link. The resource allocation is determined based on the instantaneous load where each IAB-type backhauled SBS informs its current load to the associated MBS each time. Thus, the backhaul-related bandwidth for the j-th IAB node, if it does not have dedicated non-IAB backhaul connection, is given by

$$B_{\mathrm{backhaul},j} = \frac{\psi B N_j}{\sum\limits_{\forall\ j} N_j}, \forall j, \tag{B.11}$$

where N_j denotes the number of UEs connected to the j-th IAB-type backhauled node and $\psi \in [0,1]$ is the fraction of the bandwidth resources on backhauling. Therefore, the bandwidth allocated to the j-th IAB-type backhauled node is proportional to the ratio between its load, and the total load of its connected IAB donor. Meanwhile, the access spectrum is equally shared among the connected UEs at the IAB node according to

$$B_{\mathrm{access},u} = \frac{(1-\psi)B}{\sum\limits_{\forall\ u} N_{j,u}}, \forall u, \tag{B.12}$$

where u denotes the UEs indices, and j represents each IAB-type backhauled node. Moreover, $N_{j,u}$ is the number of UEs connected to the j-th IAB-type backhauled node to which UE u is connected. Finally, the signal-to-interference-plus-noise ratio

(SINR) is obtained in accordance with (B.5) by

$$\mathrm{SINR} = P_{\mathrm{r}}/(I_u + \sigma^2), \tag{B.13}$$

where σ^2 is the noise power.

With our setup, the network may have three forms of access connections, i.e., MBS-UE, IAB-type backhauled SBS-UE, non-IAB backhauled SBS-UE, and the individual data rates will behave according to the form in which the UE's connection has been established. Particularly, the rates experienced by the UEs in access links that are connected to MBSs or to the IAB type-backhauled SBSs are given by

$$R_u = \begin{cases} \frac{(1-\psi)B}{N_m}\log(1+\mathrm{SINR}(x_u)), & \text{if } \mathbf{w}_{\mathrm{u}} \in \chi_{\mathrm{m}}, \\ \min\Bigg(\frac{(1-\psi)BN}{\sum\limits_{\forall\, u} N_{j,u}}\log(1+\mathrm{SINR}(x_u)), \\ \qquad \frac{\psi BN}{\sum\limits_{\forall\, j} N_j}\log(1+\mathrm{SINR}(x_{\mathrm{b}}))\Bigg), \text{if } \mathbf{w}_{\mathrm{u}} \in \chi_{\mathrm{s}}, \end{cases} \tag{B.14}$$

where j represents each IAB-type backhauled SBS connected to the MBS. Then, m gives the associated MBS, s denotes the SBS, and u represents the UEs' indices. Unlike an MBS which shares some of its bandwidth with IAB-type backhauled SBSs, a non-IAB backhauled SBS has a bandwidth of B for access, and does not need to share its bandwidth for backhauling. Thus, the UEs connected to a non-IAB backhauled SBS experience the rate given by

$$R_u = \frac{B}{N_{\mathrm{u}}}\log(1+\mathrm{SINR}(x_{\mathrm{u}})), \text{if } \mathbf{w}_{\mathrm{u}} \in \chi_{\mathrm{s}}, \tag{B.15}$$

where N_u denotes the total number of UEs connected to the non-IAB backhauled SBS of which the considered UE is associated. Depending on the associated cell, there are three possible cases for the data rate of the UEs. First is the case when the UEs are connected to the MBSs, i.e., IAB donor, as denoted by $w_{\mathrm{u}} \in \chi_{\mathrm{m}}$ in (B.14). Since the MBSs have non-IAB backhaul connection, the rate will only depend on the access bandwidth available at the UE. In the second case, the UEs are connected to the IAB-type backhauled SBSs, as denoted by $w_{\mathrm{u}} \in \chi_{\mathrm{s}}$ in (B.14). Here, the SBSs have shared backhaul bandwidth from the IAB-Donor-nodes i.e., MBSs, and thus the UEs data rates depend on the backhaul rate of the connected IAB-type backhauled SBS as well. Thus, in this case the UE is bounded to get the minimum between backhaul and access rate. Then, the third case is when the UEs are associates with the non-IAB backhauled SBSs as denoted in (B.15). Unlike in the previous case, here the SBSs have full bandwidth B which is not shared with backhauling.

In the following, we present the GA-based schemes to optimize the locations of

the SBSs as well as the non-IAB backhaul link distribution to a fraction of the SBSs such that the network service coverage probability is maximized.

4 Proposed Algorithm

In general, Rel-16 IAB network supports NLoS backhauling. However, the performance of the IAB networks is considerably affected by the quality of the backhaul links, where, if possible, it is preferred to have IAB-IAB channels with strong LoS signal strength. Also, in hybrid networks where a fraction of the SBS nodes may be backhauled via dedicated non-IAB backhaul links, it is important to obtain the set of SBSs that are critical to be non-IAB backhaul-connected for optimal performance. However, depending on the network size, it may be difficult to obtain the appropriate location of the SBSs and/or the non-IAB backhaul link placement scheme for SBSs analytically.

For instance, with N_{s} SBSs and a budget of having N_{f} non-IAB backhauled SBSs, there are $\binom{N_{\mathrm{s}}}{N_{\mathrm{f}}}$ possible combinations of non-IAB backhauled SBS selections. Therefore, the optimal set of SBSs suitable for non-IAB backhaul link placement can indeed be obtained via exhaustive search for the cases with few SBSs. However, as the network size increases, it is not feasible to search over all possible solutions. The problem becomes even more challenging with determining the optimal locations of the SBSs as they can be distributed in the whole network area. Thus, it is important to design efficient algorithms to obtain the (sub)optimal SBS locations as well as dedicated non-IAB backhaul link placement with low complexity.

With this background, the state-of-the-art works mainly concentrate on either modeling the network by placing the BSs on a grid or distribute them randomly based on stochastic geometry models. However, none of these models are accurate, as they give an optimistic or a pessimistic estimate of the network performance, respectively. Also, in practice, the network may be well planed such that, at least, high-quality backhaul links are guaranteed. This is the motivation for our GA-based approach in which we propose a fairly simple network deployment optimization algorithm with no need for detailed mathematical analysis. This is important specially because

- as we show in the following, with a well-planned network topology the need for routing, to compensate for temporal blockages, decreases which results in considerable implementation complexity reduction.

- Moreover, with our proposed GA-based approach it is possible to scale the network with proper deployment as more IAB nodes/non-IAB backhaul link connections are added to the network.

- Finally, due to the generic characteristics of machine learning schemes, one can apply the same technique as our proposed GA method for both non-IAB

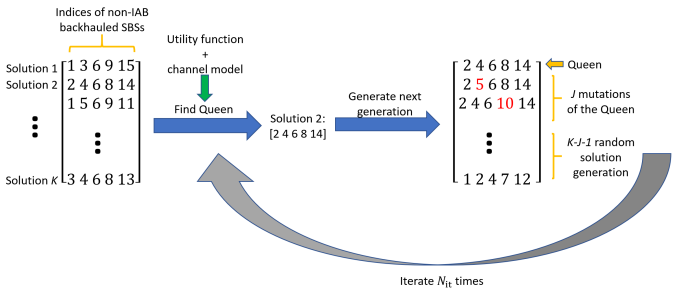

Figure 7: An example of the proposed GA in Algorithm 1 for non-IAB backhaul link distribution between a fraction of the SBSs. In each iteration, the best solution (the Queen) is regenerated. Then, J solutions are generated by small mutations in the Queen and $K - J - 1$ possible solutions are generated randomly to avoid local minimums. The iterations continue for a number of times and the Queen of the last round is returned as the final solution.

backhaul link placement and SBS location optimization, as well as for the cases with different channel models/metrics of interest.

It should be noted that, we are interested in the potential of optimal partial non-IAB type backhaul connections in order to find an upper bound on the performance of any real network that might be constrained. Such a constrained partial non-IAB type backhaul link deployment optimization would also be an interesting extension of this work, and any such network performance would be in between the optimized and the random partial non-IAB type backhaul link deployment.

Particularly, in this paper, we propose two GA-based approaches [64] to identify the optimal SBSs to be non-IAB backhaul-connected and the optimal locations for the SBSs, as explained in Algorithms 1 and 2, respectively. The algorithms are used to maximize the service coverage probability defined as the fraction of the UEs which have instantaneous UE data rates higher than or equal to a threshold R_{th}. That is, using (B.14) and (B.15), the service coverage probability is given by

$$\rho = \Pr(R_{\text{U}} \geq \eta). \tag{B.16}$$

In words, both algorithms are based on the procedure described below. As shown in Fig. 7, we start the algorithm by considering K possible selection strategies. For instance, Algorithm 1 considers K possible SBS sets for non-IAB backhaul link placement and Algorithm 2 considers K possible location sets for the SBSs. Then, in each iteration, we find the best strategy, i.e., selected solution, that maximizes the considered utility function, compared to the other $K - 1$ selected strategies. This best strategy is referred to as the Queen. The Queen is considered as one of the possible solutions in the next iteration of the algorithm to guarantee the

monotonic improvement of the algorithm performance in successive iterations. That is, the Queen represents the regeneration operator in GA. Also, for each iteration we create $J < K$ sets around the Queen. These matrices are created by applying slight modifications to the Queen, i.e., as a kind of mutation. For example, changing few SBSs of the set associated with the Queen generates these new sets needed for optimal SBS selection for non-IAB backhaul link placement in Algorithm 1. Also, in each iteration $K - J - 1$ sets of selection strategies are generated randomly, to avoid the network to be trapped in a local minimum, and the iterations continue for N_{it} iterations decided by the network designer depending on the problem at hand (See Section 5). After running all considered iterations, the ultimate Queen is returned as the best selection rule for the current network instance. Particularly, Algorithm 1 returns the optimal SBS selection rule for non-IAB backhaul link placement, while Algorithm 2 returns the optimal SBS location selection rule. The suitable parameter setting for K, J and N_{it} in the algorithms can be obtained by the designer.

Considering Algorithms 1 and 2, the following points are interesting to note:

- Our proposed algorithms result in significantly lower complexity, in comparison with the exhaustive search, as it only checks KN_{it} number of possible solutions (see Section 5).
- Moreover, due to Step 7 of the algorithms, where $K - J - 1$ random possible solutions are checked in each iteration, the proposed algorithms mimic the exhaustive search if $N_{\text{it}} \to \infty$, and they reach the globally optimal selection rule if asymptotically many iterations are considered [64].
- Unlike typical GAs, we do not use the crossover operation and instead evaluate a few random solutions in each iteration. This is because the proposed algorithms work well with no need for the additional complexity of the crossover operation, and converge with a few iterations (see Section 5). However, it is straightforward to include the crossover into the proposed algorithms where, for instance, the Queen and the next best solutions are combined to generate new possible solutions.
- The proposed algorithms optimize the network deployment off-line. However, it is straightforward to scale the network and adapt the algorithm in an on-line manner. For instance, adding new set of SBSs to an already-planned network deployment, one can rerun the algorithm for only a few iterations with the initial considered solutions not randomly but based on the Queen of the already-planned network.

Since the considered problem is polynomial time reducible, it is NP-hard [65], [66]. Moreover, unless for the cases with very small networks, the search space increases rapidly with the network density which makes exhaustive search based optimization infeasible. As an example, the number of possible solution checkings of exhaustive

Algorithm 7 GA-based non-IAB Backhaul Link Placement.

In each network instance with a budget for N_{f} non-IAB backhaul-connected SBSs, and $N_{\mathrm{s}} > N_{\mathrm{f}}$ SBSs, do the followings:

I. Consider K sets of N_{f} non-IAB backhaul-connected SBSs, F_k, and for each set create the corresponding channel matrix. Then, for each matrix H_k, $k = 1..., K$, implement the system model in Section 3.

II. For each selected possible solution F_k, evaluate the objective function U_k, $k = 1, ..., K$. For instance, considering the service coverage probability ρ as the objective function, U_k is given by (B.16).

III. Find the set of the SBSs among the considered solutions $F_k, \forall k$, which gives in the best value of the objective function, service coverage probability (the Queen), e.g., F_i where $\rho(H_k) \leq \rho(H_i)$, $\forall k = 1, ..., K$.

IV. $F_1 \longleftarrow F_i$

V. Generate $J < K$, sets of SBSs F_j^{new}, $j = 1, ..., J$, around the Queen, i.e., F_i. These sets of SBSs are generated by making small changes to the Queen, for instance, by replacing few SBSs with other SBSs.

VI. $F_{j+1} \longleftarrow F_j^{\mathrm{new}}$, $j = 1, ..., J$.

VII. Use the same procedure as in Step 1 and regenerate the remaining sets $F_j, j = J + 2, ..., K$, randomly.

VIII. Proceed to Step 2 and continue the process for N_{it} iterations pre-considered by the network designer.
Return the Queen as the optimal SBS selection rule for non-IAB backhaul link placement.

=0

search when optimizing the selection of non-IAB backhaul connected SBSs in a fixed network area is given by

$$S_c = \binom{N_\mathrm{s}}{N_\mathrm{f}}, \tag{B.17}$$

where $\binom{n}{k}$ denotes the "n choose k" operator. In this way, for moderate/large values of N_f and/or N_s, the search space soon becomes so large that exhaustive search is not feasible. However, the complexity of Algorithm 1 for a similar use case will be in the linear order of KN_it, reducing the complexity compared to exhaustive search significantly.

Finally, it should be noted that:

- Depending on the infrastructures and the availability of non-IAB backhaul link connection, in practice it may not be possible to provide some SBSs with a non-IAB backhaul link connection (either fiber or a dedicated LoS nonIAB wireless backhaul). This is because the those connections may be available in specific areas. In this way, as explained in Section 3, Algorithm 1 gives an optimistic ultimate network performance, as we consider no limitation for non-IAB backhaul link distribution among the SBSs. Then, depending on the specific network deployment, it is straightforward to adapt Algorithm 1 to consider restrictions on non-IAB backhaul link distribution among the SBSs.

- According to the 3GPP discussions, one can consider two different, namely, wide-area and local-area, IAB network deployments. Local-area IAB deployment refers to the cases with an unplanned network where the mobile terminal (MT) module of the IAB nodes have UE-type functionality, in terms of transmit power etc. Wide-area IAB network, on the other hand, refers to the cases with well-planned deployment and gNB-type functionalities for the IAB nodes. In this way, the proposed scheme mainly concentrates on the wide-area IAB network deployment, as the main use-case of the IAB networks.

5 Performance Evaluation Of Deployment Optimization

The simulation results and discussions are divided into three main areas in which 1) we evaluate the convergence behaviour of the proposed algorithms, and we study their effect on optimizing the IAB network performance, 2) verify the effect of environmental parameters on the coverage probability, and 3) evaluate the system performance for different transmission capabilities of the nodes. Then, in Section 6, we investigate the effect of routing on the performance of IAB networks experiencing temporal blockings.

The general system parameters are presented in Table 2 and, in each figure, we give the detailed system parameters in the figure captions. The IAB network is deployed

Algorithm 8 GA-based SBS Location Selection.

In each network instance with N_s SBSs, from all possible locations in the space, do the followings:

I. Consider K sets of L_k locations, and for each set create the corresponding channel matrix H_k, $k = 1..., K$, according to the system model in Section 5.

II. Evaluate the objective function for each set, i.e., U_k, $k = 1, ..., K$. For instance, considering the service coverage probability ρ as the objective function, U_k is given by (B.16).

III. Find the Queen, i.e., the set of locations which gives the best value of the objective function, i.e., service coverage probability, among the considered sets, e.g., L_i where $\rho(H_k) \leq \rho(H_i)$, $\forall k = 1, ..., K$,

IV. $L_1 \longleftarrow L_i$

V. Generate $J < K$, sets of locations L_j^{new}, $j = 1, ..., J$, around L_i. These sets of locations are generated by making small changes to the Queen, for instance, by replacing few locations with another sets of locations.

VI. $L_{j+1} \longleftarrow L_j^{\text{new}}$, $j = 1, ..., J$.

VII. Use the same procedure as in Step 1 and regenerate the remaining sets $L_j, j = J + 2, ..., K$, randomly.

VIII. Proceed to Step 2 and continue the process for N_{it} iterations pre-considered by the network designer.
Return the Queen as the optimal SBS location selection rule.

=0

Table 2: Simulation Parameters

Parameter	**Value**
Carrier frequency	28 GHz
Bandwidth	1 GHz
IAB node and UEs density	(MBS, SBS, UE) = (2, 50, 500) /km^2
Blocking density	500 /km^2
Path loss exponents	(LoS, NLoS) = (3, 4)
Main lobe antenna gains	(MBS, SBS, UE) = (18, 18, 0) dBi
Side lobe antenna gains	(MBS, SBS, UE) = (-2, -2, 0) dBi
Half power beamwidth	30°
Noise power	5 dB
Percentage of non-IAB backhauled SBS nodes	10%
In-leaf percentage	15%
Tree depth	7.5 m

in a 2D disk, in which the blockage, and the tree distributions are also modelled using statistical models described in Section 3. In particular, the network is a hybrid IAB deployment, of which a fraction of the SBSs will be non-IAB backhaul-connected while the others are backhauled using IAB. In all figures, except for Fig. 13 which studies the system performance in suburban areas, we focus on dense areas as the most important use-case in IAB networks. Also, in all figures, except in Fig. 15, we ignore interference in the backhaul links, and assume them to be noise-limited. In Figs. 8,12, 13-10, we study the system performance in the cases with non-IAB backhaul link placement optimization (Algorithm 1). Figures 9, 14, 11 and 17 present the results for the cases with Algorithm 2 optimizing the SBSs locations.

5.1 On the Performance of the Proposed Algorithms

In Figs. 8-9, we study the convergence performance of the proposed algorithms, and compare the results with the cases having only MBSs or random network deployment. Figure. 8 shows the service coverage probability achieved for different numbers of iterations in Algorithm 1 with optimal non-IAB backhaul link connection distribution and different algorithm parameters K and J. Here, the results are presented for the cases with 10% of the SBSs having the possibility to be non-IAB backhaul-connected. Then, Fig. 9 demonstrates the IAB network service coverage probability as a function of the number of iterations in Algorithm 2, and compares the results with the benchmark schemes using only MBSs or random network deployment of

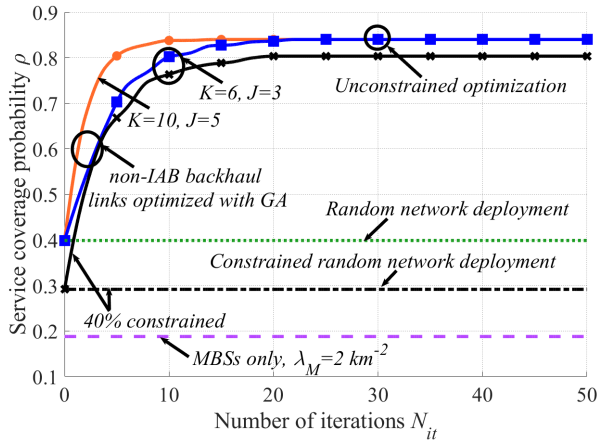

Figure 8: Service coverage probability as a function of the number of iterations in Algorithm 1 with non-IAB backhaul link connection distribution, and $P_{\mathrm{m}}, P_{\mathrm{s}}, P_{\mathrm{u}} = (40, 24, 0)$ dBm. The parameters are set to $\lambda_{\mathrm{M}} = 2$ km^{-2}, $\lambda_{\mathrm{S}} = 50$ km^{-2} and $\lambda_{\mathrm{U}} = 500$ km^{-2}. The results are presented in both cases with constrained and free non-IAB backhaul link distribution in the coverage area.

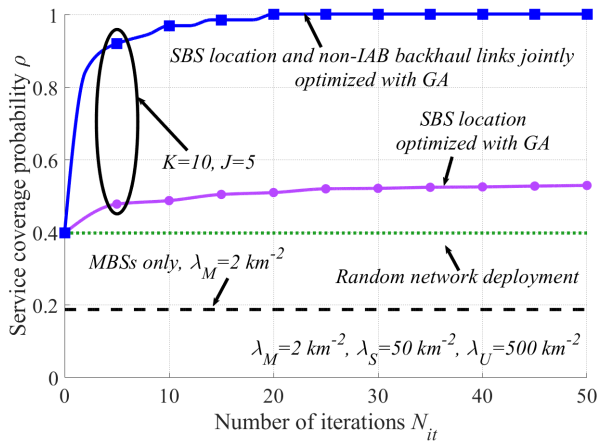

Figure 9: Service coverage probability as a function of the number of iterations in Algorithm 2 with IAB node placement optimization, IAB node placement and non-IAB backhaul links joint optimization and $P_{\mathrm{m}}, P_{\mathrm{s}}, P_{\mathrm{u}} = (40, 24, 0)$ dBm. The parameters are set to $\lambda_{\mathrm{M}} = 2$ km^{-2}, $\lambda_{\mathrm{S}} = 50$ km^{-2} and $\lambda_{\mathrm{U}} = 500$ km^{-2}.

which 10% of the SBSs are non-IAB backhaul-connected.

As in every machine learning-based algorithm applied in large systems, the main challenge of the proposed scheme is to achieve reasonably good results within limited iterations. This is challenging specially in the cases with large network density and/or joint optimization of the non-IAB backhaul links distribution and IAB nodes placements, as the search space increases rapidly. However, as shown in the evaluations (Figs. 8-9), with a proper setting of the algorithms parameters, the GA converges with a few number of iterations.

As seen in Figs. 8 and 9, the developed Algorithms 1 and 2 converge rapidly to give a maximum service coverage probability. For example, Fig. 8 converges with almost $N_{\text{it}} = 20$ iterations which, with $K = 6$, leads to a total of 120 possible solution checkings. As a result, the proposed algorithm reduces the complexity compared to exhaustive search significantly because with $\lambda_{\text{s}} = 50$ km^{-2} and the network area of 1 km^{-2} exhaustive search requires $\binom{50}{5} \simeq 2 \times 10^6$ solution checkings, i.e. $\simeq 17000$ times larger search than those in our proposed scheme. In particular, the proposed algorithms have improved the service coverage probability, compared to the IAB network with random node locations and random non-IAB backhaul connections, significantly. For instance, with the parameter settings of Fig. 8, optimizing the non-IAB backhaul link distribution among 10% of the SBSs increases the coverage probability from 40% with random non-IAB backhaul link distribution to 85%. Moreover, with the parameter settings of Fig. 9, optimizing the SBSs location leads to a coverage probability increment from 40% with random network deployment to 55%, while the joint optimization of non-IAB backhaul link distribution and SBS location further improves the coverage probability reaching the maximum of 100%.

In the simulations, we considered no constraints on the SBSs and non-IAB backhaul links locations. However, in practice, it may not be possible to place the SBSs and the non-IAB backhaul links freely. To evaluate this point, in Fig. 8 we study the system performance in the cases with constraints on the non-IAB backhaul link distribution. Particularly, Fig. 8 shows the coverage probability in the cases where the non-IAB backhaul links can not be placed in 40% of the area selected randomly. Here, the results presented for both cases with random and optimized distributions of the non-IAB backhaul links in the 60% of the coverage area. As seen in Fig. 8, although the constraint on topology optimization may limit the benefit of IAB, still the system performance is improved compared to the cases with only MBSs. Also, for a broad range of parameter settings, the effect of topology constraints on the network performance is not significant.

Finally, as expected and also demonstrated in Figs. 8-9, as the UEs density increases, MBSs alone can not support the UEs' coverage probability requirements, and indeed we need to densify the network using (IAB) nodes of different types. In this way, as also experienced in practical network implementations, a well-planned network deployment results in significant performance improvement, which reduces

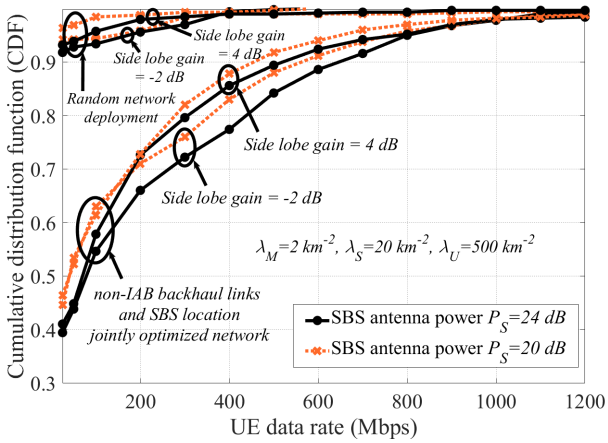

Figure 10: CDF of the achievable rates with $P_{\mathrm{m}}, P_{\mathrm{u}} = (40, 0)$ dBm for SBS location and non-IAB backhaul links joint optimization. The parameters are set to $\lambda_{\mathrm{M}} = 2$ km^{-2}, $\lambda_{\mathrm{S}} = 20$ km^{-2} and $\lambda_{\mathrm{U}} = 500$ km^{-2}.

the need for high network node density as well as the implementation cost.

Note that, while Figs. 8-9 show monotonic improvement of the system performance in successive iterations, in some iterations the proposed algorithms may follow a ladder-shape convergence pattern. This is because the service coverage probability does not necessarily improve in each iteration, and there is a possibility to reach a local optimum in some iterations. However, we always elude the local minima due to Step 7 of Algorithms 1 and 2. Thus, given that sufficiently large number of iterations are carried out, the algorithm converges to a (sub)optimal solution.

In Figs. 10 and 11, we study the cumulative distribution function (CDF) of the UEs achievable data rates in the cases with SBS location optimization as well as joint non-IAB backhaul link distribution and SBS location optimization, and compare the results with random network deployment. Here, the parameters are set to $\lambda_{\mathrm{M}} = 2$ km^{-2}, $\lambda_{\mathrm{S}} = 20$ km^{-2} and $\lambda_{\mathrm{U}} = 500$ km^{-2}, and in all cases 10% of the SBSs are non-IAB backhaul-connected. Also, the joint optimization follows the same setup as in Algorithms 1-2.

As can be seen in Fig. 10, with a random deployment and the parameter settings of the figure, (almost) all UEs maximum achievable rates are below 400 Mbps, the result which holds for both considered values of the IAB nodes transmit powers and side lobe gains. On the other hand, jointly optimizing the non-IAB backhaul link distribution and SBSs locations gives the chance to support higher access data rates, depending on the UEs position and their associated backhaul links qualities. For instance, as opposed to the cases with random network deployment, with $P_{\mathrm{s}} = 24$ dBm around 25% of the UEs may experience > 400 Mbps access rates, if the non-IAB

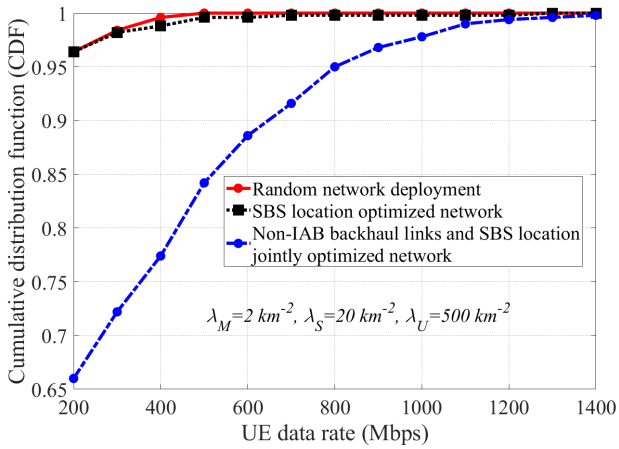

Figure 11: CDF of the achievable rates with $P_{\mathrm{m}}, P_{\mathrm{u}} = (40, 0)$ dBm for SBS location optimization, SBS location and non-IAB backhaul links joint optimization. The parameters are set to $\lambda_{\mathrm{M}} = 2$ km^{-2}, $\lambda_{\mathrm{S}} = 20$ km^{-2} and $\lambda_{\mathrm{U}} = 500$ km^{-2}.

backhaul link distribution and the SBSs locations are properly planned (Fig. 10).

In our simulations, we consider relatively low side lobe gains, compared to the main lobe gain. This is motivated by the fact that, to guarantee high-rate reliable backhaul performance at mmw spectrum, IAB nodes are expected to be equipped with a large number of antennas and be capable of directional beamforming. However, depending on the hardware properties, in practice there may be cases with relatively high side lobe gains [67]. For this reason, in Fig. 10 we study the effect of the side lobe gain on the network performance, and verify the coverage probability for different values of side lobe gains. As demonstrated in the figure, while the coverage probability is slightly reduced by increasing the side lobe gain, for a broad range of parameter settings, the relative performance loss is negligible.

In harmony with Fig. 10, Fig. 11 shows that, the SBS location-optimized network can support UEs data rates up to 1200 Mbps while non-IAB backhaul link distribution and SBS locations jointly optimized network can support UEs data rates up to around 1400 Mbps. In this way, the joint optimization improves the performance, compared to optimizing one of the parameters, at the cost of higher computational complexity. Finally, note that, along with simplifying the optimization process, one of the motivations for separate optimization of the SBSs locations and non-IAB backhaul links distribution is that in practice the SBSs and the non-IAB backhaul links many be deployed by different companies or in different times, which makes joint optimization difficult.

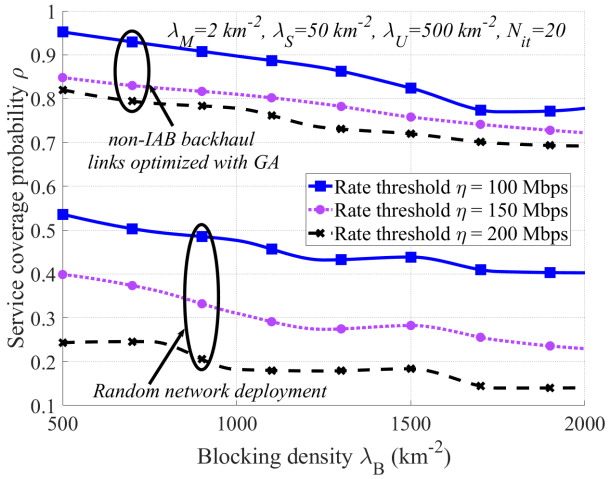

Figure 12: Service coverage probability of the IAB network as a function of the blocking density λ_{B}, with $P_{\mathrm{m}}, P_{\mathrm{s}}, P_{\mathrm{u}} = (40, 24, 0)$ dBm and different methods of non-IAB backhaul link connection distribution among 10% of the SBSs. The parameters are set to $\lambda_{\mathrm{M}} = 2$ km^{-2}, $\lambda_{\mathrm{S}} = 50$ km^{-2}, $\lambda_{\mathrm{U}} = 500$ km^{-2} and $N_{\mathrm{it}} = 20$.

5.2 Effect of Blocking and Tree Foliage

In contrast to the non-IAB backhaul-connected networks, IAB networks may be affected by environmental effects specially the blockage and the tree foliage[2]. In Figs. 12 and 13, we respectively study the effect of the blockage and tree foliage on the coverage probability of the IAB network with random deployment or GA-optimized non-IAB backhaul link distribution. Here, the results are presented for different rate thresholds of the UEs, i.e., η in (15). In particular, Fig. 12 shows the service coverage probability considering the FHPPP-based germ-grain blockage model for different blocking densities.

Although urban areas are the main point of interest for IAB network, to study the potentials of its usage in suburban areas, in Fig. 13 we demonstrate the service coverage probability as a function of the tree density in the suburban areas. Here, we present the results for the average hop distance $l_{\mathrm{h}} = 450$ m corresponding to SBSs density, $\lambda_{\mathrm{S}} = 8$ km^{-2}. This is motivated by, e.g., [68], reporting the tree foliage as one of the main challenges of IAB in suburban areas. According to Figs. 12-13, the following points can be concluded:

- The GA-based planned deployment shows significant improvement and resilience to blockage and tree foliage, compared to random deployment, where

[2]As reported in [25], with the typical hop lengths of the IAB networks and 28 GHz, the effect of the rain on the coverage probability of IAB network is negligible.

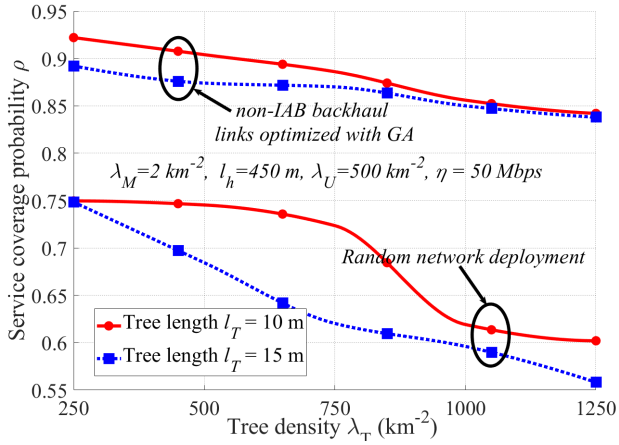

Figure 13: Service coverage probability of the IAB network as a function of tree density λ_{T}, with $P_{\mathrm{m}}, P_{\mathrm{s}}, P_{\mathrm{u}} = (40, 33, 0)$ dBm and different methods of non-IAB backhaul link connection distribution among 10% of the SBSs. The parameters are set to $\lambda_{\mathrm{M}} = 2$ km^{-2}, $l_{\mathrm{h}} = 450$ m, $\lambda_{\mathrm{U}} = 500$ km^{-2} and $\eta = 50$ Mbps.

the coverage probability is not much affected by the blockage (Fig. 12). For instance, with the given system configuration in Fig. 12, the GA optimized setup shows 0.85 service coverage probability at $\eta = 150$ Mbps, $\lambda_{\mathrm{B}} = 1000$ km^{-2}, while the coverage probability reduces to 0.72 at $\lambda_{\mathrm{B}} = 2000$ km^{-2}, i.e., only 15% coverage loss by doubling the blockage density. On the other hand, with a random network deployment, $\eta = 150$ Mbps and $\lambda_{\mathrm{B}} = 1000$, the coverage probability is only 0.4 and it is dropped to 0.23, i.e., 42% performance degradation, as the blockage density increases to $\lambda_{\mathrm{B}} = 2000$ km^{-2}.

- In suburban area and with a random network deployment, the coverage probability is considerably affected by the tree foliage, especially when the trees density and/or length increase. However, we note that the introduction of GA optimization on selecting the SBSs with non-IAB backhaul-connection has brought resilience to the tree foliage. This is due to the fact that the algorithm finds the optimum set of nodes minimizing the SBS links with high losses due to tree foliage. For instance, considering the settings of Fig. 13 and the random FHPPP model with $l_T = 15$ m, the service coverage probability drops from 0.75 to 0.55 (26% coverage degradation) when the tree density is increased from 250 to 1250 km^{-2}. However, the same tree density increase at $l_T = 15$ m in GA-optimized network gives a drop only from 0.88 till 0.83, i.e., only 5% performance drop, the result which is almost independent of the tree length.

In general, the robustness of IAB in the presence of tree foliage is hard to predict

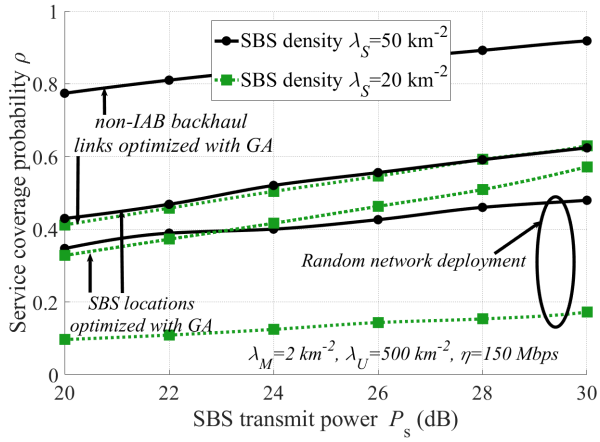

Figure 14: Service coverage probability of the IAB network as a function of the SBSs transmit power P_{s}, with $P_{\mathrm{m}}, P_{\mathrm{u}} = (40, 0)$ dBm for both non-IAB backhaul link location and node placement optimization methods, $\lambda_{\mathrm{M}} = 2$ km^{-2}, $\lambda_{\mathrm{U}} = 500$ km^{-2} and $\eta = 150$ Mbps.

due to the fact that the link quality can vary depending on the characteristics of the tree lines. Particularly, the backhaul links quality may change due to wet trees, snow on the trees, wind and varying percentage of leaves in different seasons. However, we conclude that, although the IAB is prone to medium/highly densified tree foliage in suburban areas, network planning can reduce much of its adverse effect, and the mmWave IAB is expected to work well for areas with low/moderate foliage level.

5.3 Effect of Antenna Gain and Transmit Power

In Fig. 14, we demonstrate the service coverage probability as a function of the SBS transmit power for three scenarios, namely, random FHPPP-based deployment, GA-based non-IAB backhaul link distribution and GA-based SBS location optimization. Also, Fig. 15 shows the service coverage probability as a function of the SBS antenna gain for random FHPPP-based deployment with 10% non-IAB backhaul-connected SBSs, macro-only network and GA-optimized non-IAB backhaul link distribution between 10% of the SBSs. In addition, to verify the effect of interference in the backhaul links, the figure shows the service coverage probability in the presence of both noise-limited and noise plus interference limited backhaul links. Here, we increase the SBS antennas' main lobe gain, while fixing the side lobe gain at -2 dB.

As we observe in Fig. 14, both GA-optimization methods used for selecting the dedicated non-IAB backhauled nodes and selecting SBSs locations have significantly increased the system coverage probability, compared to random deployment, and the

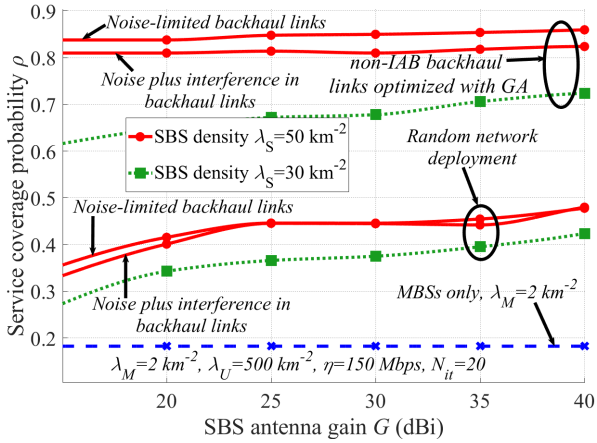

Figure 15: Service coverage probability of the IAB network as a function of the SBSs antenna gain G, with $P_{\mathrm{m}}, P_{\mathrm{s}}, P_{\mathrm{u}} = (40, 24, 0)$ dBm for non-IAB backhaul link location optimization, $\lambda_{\mathrm{M}} = 2$ km^{-2}, $\lambda_{\mathrm{U}} = 500$ km^{-2}, $\eta = 150$ Mbps and $N_{\mathrm{it}} = 20$.

relative effect of network planning increases with the SBSs' transmit power (Fig. 14). Moreover, with different deployment conditions and the considered range of transmit powers, the coverage probability increases almost linearly with the SBSs transmit power, while the relative benefit of the transmit power increment increases in the cases with a well-planned network (Fig. 14). Also, Fig. 15 demonstrates that, for the considered parameter setting of the figure and moderate/high antenna gains, the system performance is almost insensitive to the antenna gain specially if the network is well planned. Finally, as seen in Fig. 15, the impact of the interference in the backhaul links is negligible, and thus, the backhaul links can be well assumed to be noise-limited (Also, see [21], [22], [23], [29] for further discussions).

In Fig. 16, we compare the coverage probability of the proposed GA-based scheme with those obtained by different state-of-the-art algorithms including exhaustive search, Tabu algorithm [69] and Greedy algorithm [70]. Note that Tabu is an evolutionary algorithm with a specific method of producing the generations (see [71] for details) while with Greedy algorithm, e.g., the non-IAB backhaul links locations are determined one-by-one [70]. Here, the parameters are set to $\lambda_{\mathrm{M}} = 2$ km^{-2}, $\lambda_{\mathrm{U}} = 500$ km^{-2}, and in all cases 10% of the SBSs are non-IAB backhaul-connected. Thereby, we optimize the non-IAB backhaul links distribution and, as can be seen in Fig. 16, the GA converges rapidly with limited iterations to the maximum coverage probability achieved by exhaustive search. This is an indication of the efficiency of the proposed method with considerably lower complexity, compared to exhaustive search. Moreover, for a given number of iterations, the GA outperforms the greedy

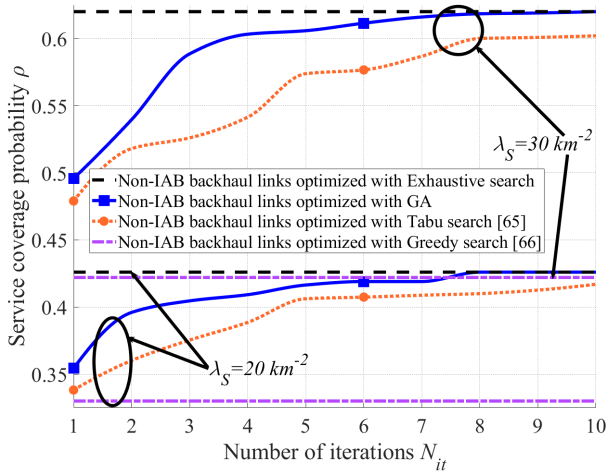

Figure 16: Service coverage probability as a function of the number of iterations in Algorithm 1 with non-IAB backhaul links optimization. The parameters are set to $P_{\mathrm{m}}, P_{\mathrm{s}}, P_{\mathrm{u}} = (40, 24, 0)$ dBm, $\lambda_{\mathrm{M}} = 2$ km^{-2}, and $\lambda_{\mathrm{U}} = 500$ km^{-2}.

and the Tabu algorithms, in terms of coverage probability. Note that, while the greedy algorithm is easy to implement, it may not always lead to the global optimum due to the fact that it does not consider the entire search space. Finally, note that the results of Fig. 16 are presented for a given example channel realization for which one can run the exhaustive search in limited time[3]. However, the effectiveness of semi-optimal algorithms is more visible when studying the average system performance over multiple channel realizations, where running exhaustive search is not feasible within limited time.

[3]We have checked the results of Fig. 16 for a number of channel realizations and observed the same qualitative conclusions.

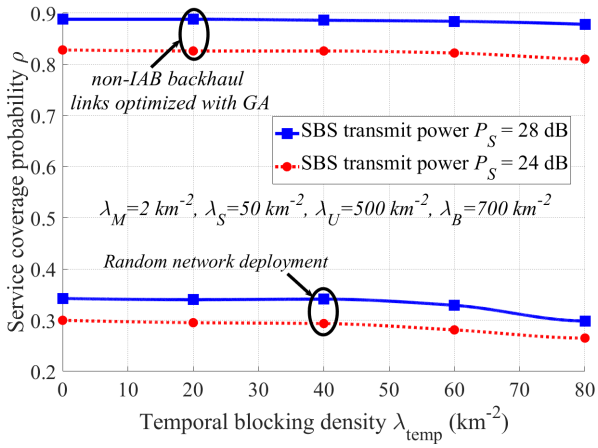

Figure 17: Service coverage probability of the IAB network as a function of the temporal blocking density λ_{temp}, with $P_{\text{m}}, P_{\text{u}} = (40, 0)$. The parameters are set to $\lambda_{\text{M}} = 2$ km^{-2}, $\lambda_{\text{S}} = 50$ km^{-2}, $\lambda_{\text{U}} = 500$ km^{-2} and $\lambda_{\text{B}} = 700$ km^{-2}

6 On the Effect of Routing

As demonstrated, deployment planning can compensate for stationary blockages/tree foliage. On the other hand, depending on, e.g., the height of the SBSs, the (backhaul) links may be temporally blocked by, for instance, trucks passing by. In such cases, routing can be used to reduce the coverage probability degradation. For this reason, in this section, we study the effect of routing on the performance of IAB networks (see Section 2 for 3GPP standardization agreements on routing). Note that, in general, routing can be utilized not only for temporal blockages but also for load balancing in the cases with varying data traffic. In this paper, we concentrate on temporal blockage, and load balancing-based routing is out of the scope of our work. Note that, here, the network deployment is first optimized based on static blockages/tree foliage. Then, by temporal blockage we refer to the blockages that are added to the network after the deployment optimization is performed.

Figure 17 shows the service coverage probability considering a static blocking density $\lambda_{\text{B}} = 700$ km^{-2} for different temporal blocking densities. In addition, to understand the IAB sensitivity for temporal blockings and the effect of the routing, in Fig. 18, we plot the percentage of the links that have been updated by routing as a function of the density of the temporal blockings added to the network. The results are presented for various cases with random deployment, GA-optimized non-IAB backhaul link distribution or GA-optimized SBS locations. Here, by routing, the received powers are recalculated, the association matrix is re-updated and thereby the data rates are calculated again, i.e., (8), (9), (13) and (14), are adapted based on

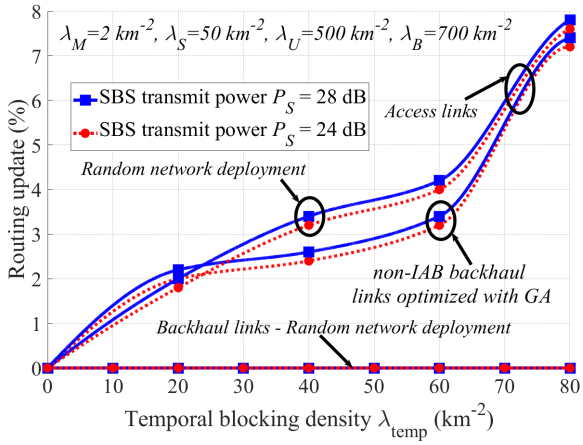

Figure 18: Percentage of routing updating of the IAB network as a function of the temporal blocking density λ_{temp} with P_{m}, $P_{\text{u}} = (40, 0)$. The parameters are set to $\lambda_{\text{M}} = 2$ km^{-2}, $\lambda_{\text{S}} = 50$ km^{-2}, $\lambda_{\text{U}} = 500$ km^{-2} and $\lambda_{\text{B}} = 700$ km^{-2}

the presence of temporal blockages such that the coverage probability degradation is minimized. Also, by percentage of routing update we refer to the fraction of links in the network that have changed their associated BS, both in the access and backhaul links. Here, the results are demonstrated for different transmit powers of the SBSs. According to Fig. 17-18 the following points can be concluded.

- Unless for high densities of temporal blockings, the service coverage probability of the IAB network is not degraded much by temporal blockage (Fig. 17). Also, the introduction of GA to optimize the dedicated non-IAB backhaul connections has brought further resilience in the network to temporal blockage. Finally, the sensitivity to temporal blockage increases slightly at low SBS transmit powers (Fig. 17).

- As demonstrated in Fig. 18, with temporal blockage, the routing scheme may update the access links of the UEs to the IAB nodes. However, 1) for a broad of temporal blockage densities for both non-IAB backhaul connection-optimized and random deployments, the access links updates are less than 10%. Also, 2) in all considered cases, the backhaul links do not need to be updated due to temporal blockage. This is intuitively because the IAB donor-IAB backhaul links are strong to support the required rates and the presence of temporal blockage does not affect their efficiency much unless for high temporal blockage densities. Finally, compared to random network deployment, optimizing the non-IAB backhaul link distribution among 10% of the SBSs with GA has slightly reduced the percentage of routing update with the addition of tempo-

ral blockings. For instance, with the parameter settings of Fig. 18, $\lambda_{\text{temp}} = 50$ km^{-2}, and $P_{\text{s}} = 28$ dBm, in random network deployment one may need a routing update of 3.6%, while in the GA-optimized network it is only 2.9%.

In this way, the results indicate that, while deployment optimization can well robustify the network to static blockages, with a well-planned network the system performance is almost insensitive to low/moderate temporal blockages, and routing may not be required unless for high temporal blockage densities/severe coverage probability requirements. On the other hand, depending on the data traffic variation and the number of hops in the IAB network, the routing may be of interest in load balancing.

7 Conclusion

We studied the problem of deployment optimization and routing in IAB networks to guarantee high coverage probability in the presence of tree foliage/blockage. Moreover, we reviewed the recent 3GPP agreements on IAB-based routing, as well as the key challenges to enable meshed IAB.

As we showed, machine-learning techniques can be effectively utilized for deployment optimization, with no need for mathematical analysis and with the capability to be adapted for different channel models/constraints/metrics of interest. Particularly, the proposed algorithm reduces the complexity compared to exhaustive search significantly because with typical network area our proposed scheme requires orders of magnitude less solution checkings compared to exhaustive search. Also, while deployment planning boosts the coverage probability of IAB networks, compared to random deployment, significantly, for a broad range of coverage constraints/blockage densities, the impact of routing to increase redundancy may be negligible. Indeed, routing may be of interest in the cases with severe availability constraints/high blockage densities as well as for load balancing. Finally, in practice, deployment planning may be affected by, e.g., the availability of non-IAB backhaul connection in specific areas, and the designer may consider, e.g., seasonal tree foliage variations, rental costs and/or foreseen infrastructure changes.

Reference

[1] P. Cerwall, “Mobile data traffic growth outlook,” Jun. 2018.

[2] Ericsson, “Mobile data traffic growth outlook,” 2018.

[3] M. Agiwal, A. Roy, and N. Saxena, *Next generation 5g wireless networks: A comprehensive survey*, 2016.

[4] S. Dang, O. Amin, B. Shihada, and M.-S. Alouini, "What should 6G be?" *Nature Electronics*, vol. 3, no. 1, pp. 20–29, Jan. 2020.

[5] X. Gao, O. Edfors, F. Tufvesson, and E. G. Larsson, "Massive mimo in real propagation environments: Do all antennas contribute equally?" *IEEE Trans. Wirel. Commun.*, vol. 63, no. 11, pp. 3917–3928, Jul. 2015.

[6] Ericsson, "Mobile data traffic growth outlook," *Ericsson Mobility Report*, 2018.

[7] C. Czegledi et al., "Demonstrating 139 Gbps and 55.6 bps/Hz Spectrum Efficiency Using 8x8 MIMO over a 1.5 km Link at 73.5 GHz," accepted for presentation in IMS2020, CA, USA, Aug. 2020.

[8] Ericsson, "Mobile data traffic growth outlook," 2023.

[9] C. Dehos, J. L. González, A. D. Domenico, D. Kténas, and L. Dussopt, "Millimeter-wave access and backhauling: the solution to the exponential data traffic increase in 5G mobile communications systems?" *IEEE Commun. Mag.*, vol. 52, no. 9, pp. 88–95, Sept. 2014.

[10] Y. Li, E. Pateromichelakis, N. Vucic, J. Luo, W. Xu, and G. Caire, "Radio Resource Management Considerations for 5G Millimeter Wave Backhaul and Access Networks," *IEEE Commun. Mag.*, vol. 55, no. 6, pp. 86–92, Jun. 2017.

[11] N. Rajatheva et al., "Scoring the terabit/s goal: Broadband connectivity in 6G," *arXiv preprint arXiv:2008.07220*, 2020.

[12] K. N. R. S. V. Prasad, H. K. Rath, and A. Simha, "Wireless mobile network planning and optimization," in *Proc. IEEE COMSNETS'2014*, Bangalore, India, 2014, pp. 1–4.

[13] A. Al-Dulaimi, S. Al-Rubaye, J. Cosmas, and A. Anpalagan, "Planning of ultra-dense wireless networks," *IEEE Network*, vol. 31, no. 2, pp. 90–96, Mar. 2017.

[14] M. N. Islam, S. Subramanian, and A. Sampath, "Integrated Access Backhaul in Millimeter Wave Networks," in *Proc. IEEE WCNC'2017*, CA, USA, Mar. 2017, pp. 1–6.

[15] M. N. Islam, N. Abedini, G. Hampel, S. Subramanian, and J. Li, "Investigation of performance in integrated access and backhaul networks," in *Proc. IEEE INFOCOM WKSHPS'2018*, HI, USA, Apr. 2018, pp. 597–602.

[16] Y. Li, J. Luo, R. A. Stirling-Gallacher, and G. Caire, "Integrated access and backhaul optimization for millimeter wave heterogeneous networks," *arXiv*, 2019.

[17] Y. Liu, A. Tang, and X. Wang, "Joint Incentive and Resource Allocation Design for User Provided Network Under 5G Integrated Access and Backhaul Networks," *IEEE Trans. Netw. Sci. Eng.*, vol. 7, no. 2, pp. 673–685, Apr. 2020.

[18] N. Tafintsev et al., "Reinforcement learning for improved uav-based integrated access and backhaul operation," in *Proc. IEEE ICC Workshops'2017*, 2020, pp. 1–7.

[19] M. N. Kulkarni, J. G. Andrews, and A. Ghosh, "Performance of Dynamic and Static TDD in Self-Backhauled Millimeter Wave Cellular Networks," *IEEE Trans. Wireless Commun.*, vol. 16, no. 10, pp. 6460–6478, Oct. 2017.

[20] B. Makki, M. Hashemi, L. Bao, and M. Coldrey, "On the Performance of FDD and TDD Systems in Different Data Traffics: Finite Block-Length Analysis," in *Proc. VTC-Fall'2018*, IL, USA, Aug. 2018, pp. 1–5.

[21] C. Saha, M. Afshang, and H. S. Dhillon, "Integrated mmWave Access and Backhaul in 5G: Bandwidth Partitioning and Downlink Analysis," in *Proc. ICC'2018*, MO, USA, May 2018, pp. 1–6.

[22] S. Singh, M. N. Kulkarni, A. Ghosh, and J. G. Andrews, "Tractable Model for Rate in Self-Backhauled Millimeter Wave Cellular Networks," *IEEE J. Sel. Areas Commun.*, vol. 33, no. 10, pp. 2196–2211, Oct. 2015.

[23] C. Saha and H. S. Dhillon, "Millimeter Wave Integrated Access and Backhaul in 5G: Performance Analysis and Design Insights," *arXiv*, 2019.

[24] M. Polese, M. Giordani, A. Roy, S. Goyal, D. Castor, and M. Zorzi, "End-to-End Simulation of Integrated Access and Backhaul at mmWaves," in *Proc. IEEE CAMAD'2018*, Barcelona, Spain, Sep. 2018, pp. 1–7.

[25] M. Polese et al., "Integrated Access and Backhaul in 5G mmWave Networks: Potential and Challenges," *IEEE Commun. Mag.*, vol. 58, no. 3, pp. 62–68, Mar. 2020.

[26] M. Hashemi, M. Coldrey, M. Johansson, and S. Petersson, "Integrated Access and Backhaul in Fixed Wireless Access Systems," in *Proc. VTC-Fall'2017*, Toronto, Canada, Sep. 2017, pp. 1–5.

[27] N. Tafintsev et al., "Aerial Access and Backhaul in mmWave B5G Systems: Performance Dynamics and Optimization," *IEEE Commun. Mag.*, vol. 58, no. 2, pp. 93–99, Feb. 2020.

[28] O. Teyeb, A. Muhammad, G. Mildh, E. Dahlman, F. Barac, and B. Makki, "Integrated Access Backhauled Networks," in *Proc. VTC2019-Fall'2019*, Honolulu, HI, USA, Sep. 2019, pp. 1–5.

[29] C. Madapatha et al., "On integrated access and backhaul networks: Current status and potentials," *IEEE open j. Commun. Soc.*, pp. 1–1, Sep. 2020.

[30] F. Gómez-Cuba and M. Zorzi, "Twice simulated annealing resource allocation for mmWave multi-hop networks with interference.," in *Proc. IEEE ICC'2020*, Dublin, Ireland, 2020, pp. 1–7.

[31] A. Fouda, A. S. Ibrahim, I. Guvenc, and M. Ghosh, "UAV-Based In-Band Integrated Access and Backhaul for 5G Communications," in *Proc. IEEE VTC-Fall'2018*, IL, USA, Aug. 2018, pp. 1–5.

[32] A. HasanzadeZonuzy, I. Hou, and S. Shakkottai, "Broadcasting Real-Time Flows in Integrated Backhaul and Access 5G Networks," in *Proc. IEEE WiOPT'2019*, Avignon, France, 2019, pp. 1–8.

[33] M. Polese, M. Giordani, A. Roy, D. Castor, and M. Zorzi, "Distributed Path Selection Strategies for Integrated Access and Backhaul at mmWaves," in *Proc. IEEE GLOBECOM'2018*, Abu Dhabi, United Arab Emirates, Dec. 2018, pp. 1–7.

[34] B. Zhai, M. Yu, A. Tang, and X. Wang, "Mesh architecture for efficient integrated access and backhaul networking," in *Proc. IEEE WCNC'2020*, Seoul, Korea (South), May 2020, pp. 1–6.

[35] J. Y. Lai, W. Wu, and Y. T. Su, "Resource allocation and node placement in multi-hop heterogeneous integrated-access-and-backhaul networks," *IEEE Access*, vol. 8, pp. 122 937–122 958, Jul. 2020.

[36] N. Chen, T. Qiu, X. Zhou, K. Li, and M. Atiquzzaman, "An intelligent robust networking mechanism for the internet of things," *IEEE Commun. Mag.*, vol. 57, no. 11, pp. 91–95, Nov. 2019.

[37] X. Meng, H. Inaltekin, and B. Krongold, "Deep reinforcement learning-based topology optimization for self-organized wireless sensor networks," in *Proc. IEEE GLOBECOM'2019*, HI, USA, Dec. 2019, pp. 1–6.

[38] X. Fu, F. R. Yu, J. Wang, Q. Qi, and J. Liao, "Dynamic service function chain embedding for nfv-enabled iot: A deep reinforcement learning approach," *IEEE Trans. Wirel. Commun.*, vol. 19, no. 1, pp. 507–519, Oct. 2019.

[39] P. Sun, Y. Hu, J. Lan, L. Tian, and M. Chen, "Tide: Time-relevant deep reinforcement learning for routing optimization," *Future Generation Computer Systems*, vol. 99, pp. 401–409, Oct. 2019.

[40] M. Wang et al., "Neural network meets dcn: Traffic-driven topology adaptation with deep learning," *Proceedings of the ACM on Measurement and Analysis of Computing Systems*, vol. 2, no. 2, pp. 1–25, Jun. 2018.

[41] S. Zhang, B. Yin, and Y. Cheng, "Topology aware deep learning for wireless network optimization," *arXiv preprint arXiv:1912.08336*, 2019.

[42] P. V. Klaine, M. A. Imran, O. Onireti, and R. D. Souza, "A survey of machine learning techniques applied to self-organizing cellular networks," *Commun. Surv. Tutor.*, vol. 19, no. 4, pp. 2392–2431, Jul. 2017.

[43] Q. Mao, F. Hu, and Q. Hao, "Deep learning for intelligent wireless networks: A comprehensive survey," *Commun. Surv. Tutor.*, vol. 20, no. 4, pp. 2595–2621, Jun. 2018.

[44] S. Troia, R. Alvizu, and G. Maier, "Reinforcement learning for service function chain reconfiguration in nfv-sdn metro-core optical networks," *IEEE Access*, vol. 7, pp. 167 944–167 957, Nov. 2019.

[45] S. Wang and T. Lv, "Deep reinforcement learning for demand-aware joint vnf placement-and-routing," in *Proc. IEEE GC Wkshps'2019*, HI, USA, 2019, pp. 1–6.

[46] X. Du, H. Van Nguyen, C. Jiang, Y. Li, F. R. Yu, and Z. Han, "Virtual relay selection in lte-v: A deep reinforcement learning approach to heterogeneous data," *IEEE Access*, May 2020.

[47] S. Yan, X. Zhang, H. Xiang, and W. Wu, "Joint access mode selection and spectrum allocation for fog computing based vehicular networks," *IEEE Access*, vol. 7, pp. 17 725–17 735, Jan. 2019.

[48] Y. Chang, X. Yuan, B. Li, D. Niyato, and N. Al-Dhahir, "Machine-learning-based parallel genetic algorithms for multi-objective optimization in ultra-reliable low-latency wsns," *IEEE Access*, vol. 7, pp. 4913–4926, Dec. 2018.

[49] Y. Xu, W. Xu, Z. Wang, J. Lin, and S. Cui, "Load balancing for ultradense networks: A deep reinforcement learning-based approach," *IEEE Internet Things J.*, vol. 6, no. 6, pp. 9399–9412, Aug. 2019.

[50] X. Chen, R. Proietti, H. Lu, A. Castro, and S. J. B. Yoo, "Knowledge-based autonomous service provisioning in multi-domain elastic optical networks," *IEEE Commun. Mag.*, vol. 56, no. 8, pp. 152–158, Aug. 2018.

[51] S. M. Azimi-Abarghouyi, B. Makki, M. Haenggi, M. Nasiri-Kenari, and T. Svensson, "Coverage analysis of finite cellular networks: A stochastic geometry approach," in *Proc. IEEE IWCIT'2018*, Tehran, Iran, Apr. 2018, pp. 1–5.

[52] 3GPP RP-201756, "Revised WID: Integrated Access and Backhaul for NR," 3rd Generation Partnership Project (3GPP), WID revised Meeting RAN#89e, Electronic Meeting, Jun. 2020.

[53] 3GPP RP-201293, "New WID on Enhancements to Integrated Access and Backhau," 3rd Generation Partnership Project (3GPP), WID revised Meeting RAN#88-e, Electronic Meeting, Sep. 2020.

[54] P. Cerwall, "Mobile data traffic growth outlook," *Ericsson Mobility Report*, Jun. 2018.

[55] M. N. Kulkarni, A. Ghosh, and J. G. Andrews, "Max-min rates in self-backhauled millimeter wave cellular networks," *arXiv*, 2018.

[56] F. Gomez-Cuba and M. Zorzi, "Optimal link scheduling in millimeter wave multi-hop networks with space division multiple access," in *Proc. IEEE ITA'2016*, La Jolla, CA, Feb. 2016, pp. 1–9.

[57] J. Y. Lai, W. Wu, and Y. T. Su, "Resource allocation and node placement in multi-hop heterogeneous integrated-access-and-backhaul networks," vol. 8, Jul. 2020, pp. 122 937–122 958.

[58] M. Agiwal, A. Roy, and N. Saxena, "Next Generation 5G Wireless Networks: A Comprehensive Survey," *Commun. Surv. Tutor.*, vol. 18, no. 3, pp. 1617–1655, Feb. 2016.

[59] B. Błaszczyszyn, "Lecture Notes on Random Geometric Models—Random Graphs, Point Processes and Stochastic Geometry," 2017.

[60] S. M. Azimi-Abarghouyi, B. Makki, M. Nasiri-Kenari, and T. Svensson, "Stochastic Geometry Modeling and Analysis of Finite Millimeter Wave Wireless Networks," *IEEE Trans. Veh. Technol.*, vol. 68, no. 2, pp. 1378–1393, Feb. 2019.

[61] T. S. Rappaport, Y. Xing, G. R. MacCartney, A. F. Molisch, E. Mellios, and J. Zhang, "Overview of Millimeter Wave Communications for Fifth-Generation (5G) Wireless Networks—With a Focus on Propagation Models," *IEEE Trans. Antennas Propag.*, vol. 65, no. 12, pp. 6213–6230, Dec. 2017.

[62] P. J. Diggle, *Some statistical aspects of spatial distribution models for plants and trees*. 1982.

[63] M. A. Abu-Rgheff, *5G Physical Layer Technologies*. John Wiley & Sons, Nov. 2019, pp. 303-313.

[64] B. Makki, A. Ide, T. Svensson, T. Eriksson, and M. Alouini, "A genetic algorithm-based antenna selection approach for large-but-finite MIMO networks," *IEEE Trans. Veh. Technol.*, vol. 66, no. 7, pp. 6591–6595, Dec. 2017.

[65] Tutorialspoint, *NP hard and NP-complete classes*, Accessed Aug. 20, 2021.

[66] G. Panchal and D. Panchal, "Solving NP hard problems using genetic algorithm," *Transportation*, vol. 106, pp. 6–2, 2015.

[67] D. Steinmetzer, D. Wegemer, M. Schulz, J. Widmer, and M. Hollick, "Compressive millimeter-wave sector selection in off-the-shelf ieee 802.11 ad devices," in *Proc. IEEE CoNEXT'2017*, NY, USA, Nov. 2017, pp. 414–425.

[68] H. Ronkainen, J. Edstam, A. Ericsson, and C. Östberg, "Ericsson technology review,"

[69] H. Guo, B. Makki, and T. Svensson, "Genetic algorithm-based beam refinement for initial access in millimeter wave mobile networks," *Wirel. Commun. Mob. Comput.*, vol. 2018, Jun. 2018.

[70] Z. Gu, J. Zhang, and Y. Ji, "Topology optimization for FSO-based fronthaul/backhaul in 5G+ wireless networks," in *Proc. IEEE ICC Workshops'2018*, MO, USA, May 2018, pp. 1–6.

[71] X. Gao, L. Dai, C. Yuen, and Z. Wang, "Turbo-like beamforming based on tabu search algorithm for millimeter-wave massive mimo systems," *IEEE Trans. Veh. Technol.*, vol. 65, no. 7, pp. 5731–5737, 2015.

PAPER C

Constrained Deployment Optimization in Integrated Access and Backhaul Networks

C. Madapatha, B. Makki, H. Guo, and T. Svensson

IEEE Wireless Communications and Networking Conference(WCNC)'
2023, Glasgow, United Kingdom.

The layout has been revised.

Abstract

Integrated access and backhaul (IAB) is one of the promising techniques for 5G networks and beyond (6G), in which the same node/hardware is used to provide both backhaul and cellular services in a multi-hop fashion. Due to the sensitivity of the backhaul links with high rate/reliability demands, proper network planning is needed to make the IAB network performing appropriately and as good as possible. In this paper, we study the effect of deployment optimization on the coverage of IAB networks. We concentrate on the cases where, due to either geographical or interference management limitations, unconstrained IAB node placement is not feasible in some areas. To that end, we propose various millimeter wave (mmWave) blocking-aware constrained deployment optimization approaches. Our results indicate that, even with limitations on deployment optimization, network planning boosts the coverage of IAB networks considerably.

Integrated access and backhaul, IAB, Topology optimization, Densification, millimeter wave (mmWave) communications, 3GPP, Coverage, Wireless backhaul, 5G NR, 6G, Blockage, Machine learning, Network planning.

1 Introduction

The data traffic and the users' rate/reliability demands continue to steadily increase in 5G and beyond (6G) [1]. In order to meet such demands, network densification, i.e, the deployment of many base stations (BSs) of different types is one of the key enablers. These increasing number of BSs, however, need to be connected to the core network using the transport network.

According to [2], the backhaul technology varies across different regions. However, optical fiber and microwave links have been globally the dominating media for the backhaul. Recently, fiber deployments have increased due to their reliability, and have demonstrated Tbps-level data rates. On the other hand, due to low initial investment and installation time, wireless backhaul comes with considerably lower price, flexibility and time-to-market, at the cost of low peak rate.

Typical wireless backhaul technologies are mainly based on 1) point-to-point line-of-sight (LoS) communications in the range of 10-80 GHz, 2) non-standardized solutions, and 3) accurate network planning such that the interference to/from the backhaul transceivers is minimized. With 5G, however, access communication, i.e., the communication between the gNB and the user equipments (UEs), moves to the millimeter wave (mmWave) band, i.e., the band which was previously used for back-

hauling. Thus, there will be conflict of interest between access and backhaul, which requires coordination. Also, considering small access points on, e.g., lamppost, one needs to support NLoS (N: non) communication in (possibly, unplanned) backhaul networks. These are the main motivations for the so called integrated access and backhaul (IAB) where the operators can use portion of the radio network resources for wireless backhaul. That is, IAB provides not only access link cellular service but also backhaul using the same node. IAB has been standardized for 5G NR in 3GPP Release-16, Release-17 [3], [4] and, the standardization will be continued in Release-18 [5], [6], [7].

IAB network supports multi-hop communication in which an IAB donor, connected to the core network via, e.g., a fiber link, includes a central unit (CU) for the following concatenated IAB nodes which are connected to IAB donor in a multi-hop fashion (see Fig. 1). Each IAB node consists of two modules, namely, mobile termination (MT) and distributed unit (DU). The DU part of an IAB node is used to serve UEs or the MT part of *child* IAB nodes. The MT part of the IAB is used to connect the IAB node to its *parent* IAB-DU in the multi-hop chain towards the IAB donor. In general, the DU part has similar gNB functionalities, although there may be IAB-specific differences. The IAB-MT part, on the other hand, may have different capabilities, although in general it acts not differently from a UE from the point-of-view of its parent IAB.

In practice, IAB networks may face deployment constraints, where the nodes can not be deployed in some locations. Such constraints may come from two reasons: On one hand, depending on the location and regulatory restrictions in protected areas, it may not be possible/allowed to have the IAB nodes in, e.g., some areas. Although these restrictions vary based on the country and locality, all provinces have their own building and landscape protection laws. Additionally, federal laws have to be obeyed and permissions under these laws, if applicable, have to be obtained (e.g. air traffic safety, forest protection, listed buildings etc.). On the other hand, network planning may impose constraints on IAB nodes placement, e.g., to limit the interference. For instance, 3GPP has defined two categories of IAB nodes, namely, wide- and local-area IAB, with distinct properties [8], [9]. The main differences between these two categories are in the nodes capabilities and the level of required network planning.

Wide-area IAB-node can be seen as an independent IAB-node providing its own coverage, with possibly long backhaul link to connect to its parent IAB-node. Here, the goal is to extend the coverage. Due to radio frequency properties, wide-area IAB-node deployment are *well-planned*, by operators. For these type of IAB-nodes, the MT part of the IAB node looks like a normal gNB, in terms of, e.g., high transmit power, beamforming or antenna gains. In wide-area IAB networks, one may consider a minimum distance between the nodes with, e.g., LOS connections. On the other hand, the use-case for the local-area IAB-node is to boost the capacity within an already existing cell served by an IAB donor or parent IAB-node. With local-area

IAB networks, the transmit power of the MT part may range between those of UEs and gNBs. Also, the network may be fairly unplanned, while geographical-based constraints may still prevent unconstrained IAB installation in different places.

In this paper, we study the effect of network planning on the service coverage of IAB networks. We present different algorithms for constrained deployment optimization, with the constraints coming from either inter-IAB distance limitations or geographical restrictions. Moreover, we study the effect of different parameters on the network performance. As we show, even with constraints on deployment optimization, the coverage of IAB networks can be considerably improved via proper network planning.

Note that the problem of topology optimization in different IAB or non-IAB networks have been previously studied in, e.g., [10], [11], [12], [13], [14], [15]. However, compared to the literature, we present different algorithms for deployment optimization, consider different types of constraints and study the performance of IAB networks with various parameter settings, which makes our paper different from the previous works.

2 System Model

Consider downlink communication in a two-hop IAB network, where the IAB donor and its child IAB nodes serve multiple UEs [16], [17], [18], [19], [20] (see Fig. 1). Since in-band communication offers proper flexibility for resource allocation, at the cost of co-ordination complexity, we consider an in-band setup where both access and backhaul links operate over the same mmWave band.

In one scenario as shown in Fig. 1a, the IAB nodes with gNB-like IAB-MT capabilities maintain a minimum distance r_{th} between each other, i.e., the distance between every two node s should be $s > r_{\text{th}}$ where r_{th} is a threshold distance considered by the network designer, when there is no blockage in the links between IAB nodes. In another scenario shown in Fig. 1b, while the IAB nodes can be in different distances to each other, due to geographical or regulatory restrictions, it may not be possible to have the nodes in some specific areas.

We use the germ grain model [21, Chapter 14] to model the blockings which provides accurate blind spot prediction. Particularly, a finite homogeneous poisson point process (FHPPP) is used to model the blockings in an area with the blocking density λ_{bl}. The blockings are considered to be walls of length l_{bl} and orientation θ_{bl}.

Using the state-of-the-art mmWave channel model, e.g., [22], [23], the received power at each node can be described as

$$P_{\text{r}} = P_{\text{t}} h_{\text{t,r}} G_{\text{t,r}} L_{\text{t,r}} (||x_{\text{t}} - x_{\text{r}}||)^{-1}. \tag{C.1}$$

Here, P_{t} stands for the transmit power, $h_{\text{t,r}}$ denotes the small-scale fading of the

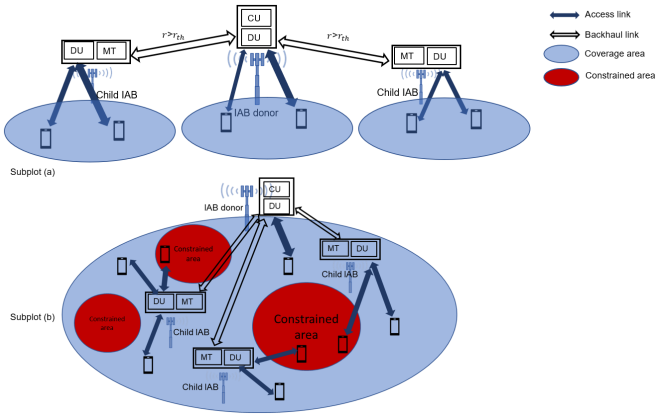

Figure 1: An illustration of the IAB netowrk. Subplot (a): An IAB network with a minimum required distance between the IAB nodes and the IAB-MTs having gNB-like capabilities. Subplot (b): An IAB network with geographical constraints on node placement and the IAB-MT being less capable compared to an gNB.

link, $L_{\mathrm{t,r}}(\cdot)$ is the path loss according to 5GCM UMa close-in model described in [24], and its path loss exponent is dependant on the LoS and NLoS state of the link which is determined by the germ grain blocking model. Particulary, the antenna gain is characterized according to sectored-pattern antenna array model by

$$G_{\mathrm{t,r}}(\alpha) = \begin{cases} G_{\mathrm{m}}, & \frac{-\alpha_{\mathrm{HP}}}{2} \leq \alpha \leq \frac{\alpha_{\mathrm{HP}}}{2} \\ G_{\mathrm{s}}, & \text{otherwise} \end{cases} \tag{C.2}$$

where G_{m} denotes the main lobe antenna gain and G_{s} represents the side lobe antenna gain. Furthermore, in our two-hop setup, each of the UEs can be connected to either the IAB donor or a child IAB, depending on the received power at the UE. Thereby, the interference observed by UE u, caused by the neighbouring interferers, is expressed as

$$I_u = \sum_{\mathbf{i} \in \chi_{i,u} \setminus \{\mathbf{w}_u\}} P_i \, h_{i,u} \, G_{i,u} \, L_{\mathrm{t,r}}(\|\mathbf{x}_i - \mathbf{x}_u\|)^{-1}, \tag{C.3}$$

where i represents the nodes excluding the associated node w_{u} of UE u. Moreover, for child IAB node c, the aggregated interference on the backhaul links is given by

$$I_c = \sum_{\mathbf{j} \in \chi_{j,c} \setminus \{\mathbf{w}_c\}} P_j \, h_{j,c} \, G_{j,c} \, L_{j,c}(\|\mathbf{x}_j - \mathbf{x}_c\|)^{-1}, \tag{C.4}$$

where j represents transmitting nodes with the exclusion of associated node w_{c} of child node c. The available mmWave spectrum is partitioned into access and backhaul

links such that

$$\begin{cases} W_{\text{Backhaul}} = \beta W \\ W_{\text{Access}} = (1-\beta)W, \end{cases} \tag{C.5}$$

where W denotes the bandwidth and $\beta \in [0,1]$ represents the bandwidth partitioning factor. With our implementation, the network may have two types of access links, i.e., IAB donor-UE or child IAB-UE, and the individual UE data rate depends on the type of the access link. In particular, the UE data rates in access links that are connected to the IAB donor or to the child IAB nodes are given by

$$R_u = \begin{cases} \frac{(1-\beta)W}{N_d} \log(1+\text{SINR}(x_u)), \quad \text{if } \mathbf{w}_\text{u} \in \chi_\text{d}, \\ \min\Bigg(\frac{(1-\beta)WN}{\sum\limits_{\forall\, u} N_{j,u}} \log(1+\text{SINR}(x_u)), \\ \qquad \frac{\beta WN}{\sum\limits_{\forall\, j} N_j} \log(1+\text{SINR}(x_\text{b}))\Bigg), \text{if } \mathbf{w}_\text{u} \in \chi_\text{c}, \end{cases} \tag{C.6}$$

where j denotes each child IAB node connected to the IAB donor d, which shares some of its bandwidth with child IAB nodes. Moreover, c denotes the child node, and u identifies the UE. Thereby, χ_d, χ_c, χ_u denote the set of IAB donors, child IAB nodes and UEs, respectively. In particular, using the rates (C.6), our goal is to perform constrained deployment optimization such that service coverage given by

$$\text{CP} = \Pr(R_\text{U} \geq \rho), \tag{C.7}$$

is maximized. Here, ρ denotes a minimum rate threshold requirement considered by the network designer.

In Algorithms 1 and 2, we propose greedy-based methods for IAB placement with minimum inter-IAB distance and geographical constraints, respectively. The algorithms are based on rejection-sampling method where multiple possible solutions are checked such that, satisfying the constraints, the service coverage is maximized.

Note that we present the algorithms for the general case where the position of both the IAB donors and the IAB nodes are optimized. However, in practice, the position of the IAB donor may be pre-determined based on, e.g., the fiber availability. Moreover, we present the algorithms for the simplest cases where each of the N_it possible set of locations is determined independently. However, one can use, e.g., genetic algorithms to generate the new set of possible solutions based on, e.g., mutation of the previously obtained solutions [12], [19]. Such more complex algorithms may also be of interest in the cases with a large number of nodes. Finally, we present the setup for the cases finding a given number of possible solutions N_it. Alternatively,

Algorithm 9 IAB placement with minimum inter-IAB distance requirement

With N_{d} IAB donors, N_{c} IAB child nodes inside the network area, do the followings:

I. Place the 1st node, $i = 1$, randomly in the considered network area.

II. Place the next node $i + 1$ where $i = 1, 2, 3, ..., (N_{\mathrm{c}} + N_{\mathrm{d}} - 1)$.

III. Find the minimum inter-node distances s_i between $(i + 1)$th node and each of other nodes.

IV. If any $s_i < r_{\mathrm{th}}$, redistribute the last node $(i + 1)$th by repeating Steps II-IV until $s_i > r_{\mathrm{th}}$.

V. For the obtained node locations, calculated the coverage. Then, proceed to Step I and continue the process for N_{it} iterations pre-considered by the network designer, saving the best set of node locations L_b among the considered solutions $L_j, \forall j, j = 1, 2, 3, ..., N_{\mathrm{it}}$, which gives in the best value of the service coverage.

Return the set of the node locations in Step V as the optimal node location set.

Algorithm 10 IAB placement in the presence of constrained areas restricting IAB node placement

With N_{d} IAB donors, N_{c} IAB child nodes and a set of constrained areas inside the network area, do the followings:

I. Place the IAB donors/IAB nodes randomly in the considered network area.

II. Identify the IAB node(s) falling inside the constrained areas.

III. For each of the nodes identified in Step II, redistribute the nodes.

IV. Proceed to Step II and continue the process until all IAB nodes fall outside the constrained areas. Save the set of locations as L_i.

V. For the saved set of node locations L_i, compute the utility function, i.e., the service coverage given by (C.7). Proceed to Step I and continue the process for N_{it} iterations pre-considered by the network designer, saving the best set of node locations L_b among the considered solutions $L_i, \forall i, i = 1, ..., N_{\mathrm{it}}$ which gives in the best value of the utility function, e.g., service coverage.

Return the set of the node locations in V as the optimal node location set.

one can run the algorithms until no further improvement is observed in a window of the obtained solutions.

3 Simulation Results and Discussion

In this section, we evaluate the effect of inter-node distance and the effect of constrained deployment optimization on the service coverage (C.7) of the IAB networks.

Figure 2b demonstrates the service coverage as a function of the distance between the IAB donor and child IAB nodes, s as of the symmetric setup shown in Fig. 2a of which the donor is located at the center and child IAB nodes are placed symmetrically besides. As shown, the service coverage improves as the IAB nodes are well distributed in the area up to certain distance. Intuitively, this is supported by the decreased interference among the nodes and also better coverage in the area. However, the coverage later starts to drop at large values of s, due to the low coverage experienced by the UEs in the middle of the IAB donor and child IAB nodes.

In Fig. 3, we study the cumulative distribution function (CDF) of the UEs achievable data rates in the cases with different antenna gains and inter-node distances, $s = 100$ m and $s = 400$ m. Here, the parameters are set to UE density = 100 km^{-2}, $P_m, P_s = 24$ dBm, and the IAB-donor is located at the center. As can be seen in Fig. 3, higher antenna gain gives the opportunity to support higher access data rates depending on the inter-node distances. For instance, with $G_m, G_s = 28$ dBi and $s = 400$ m around 20% of UEs may experience > 200 Mbps access rates, compared to the 13%, when $G_m, G_s = 24$ dBi. Moreover, the effect of the antennas gain increases with the inter-node distance (Figs. 2 and 3).

Figure 4b demonstrates the service coverage as a function of the distance between the IAB donor and child IAB nodes, s as of the symmetric setup shown in Fig. 4a of which the IAB donor is located at the center and child IAB nodes are placed symmetrically with equal distance from the donor. As shown, the service coverage increases with the node separation s, up to a point around 550 m, which is due to the decreased interference between the nodes and at the same time properly covering the area. Then, the coverage starts to slightly drop due to the coverage reduction for the UEs in between too far nodes. In this way, there is an optimal distance between the nodes maximizing the coverage. Finally, the coverage decreases significantly with increased UEs minimum rate requirements, to compensate of which one needs more resources/IAB nodes.

In Fig. 5, we study the effect of deployment optimization. Particularly, considering a minimum inter-node distance constraint, we compare the coverage of the IAB networks in the cases with optimized deployment, optimized by Algorithm 1, and the cases with hexagonal IAB deployment.

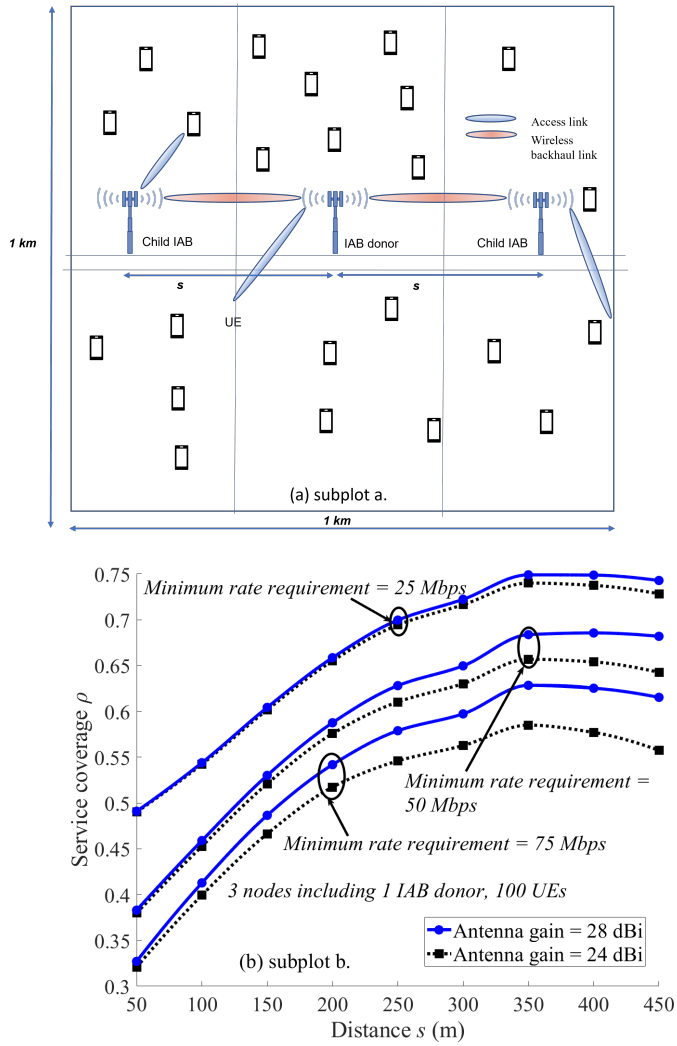

Figure 2: Service coverage as a function of the distance from IAB donor to child IAB s in subplot a with blockage $\lambda_{\text{bl}} = 500$ km^{-2}.

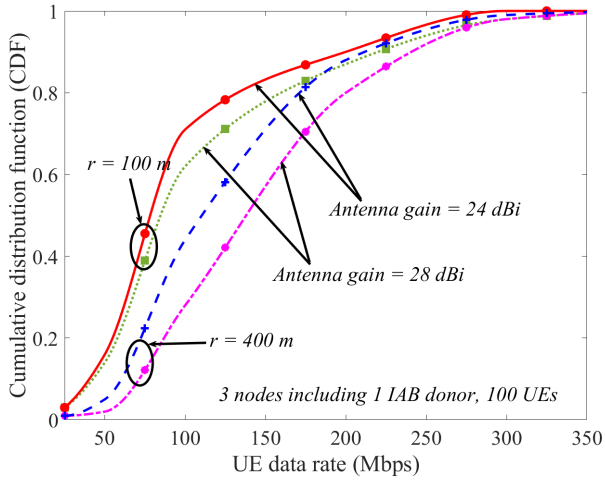

Figure 3: CDF of the achievable rates with blockage density $\lambda_{\text{bl}} = 500$ km^{-2}, and 100 UEs.

Here, the results are presented for the cases where the IAB donor has $G_m = 24$ dBi and child IAB nodes have a gain of $G_s = 18$ dBi for IAB nodes density of 20 km^{-2}. Moreover, the figure presents the results for the cases where the nodes locations are obtained only by considering the minimum distance between them or when the blockages and the backhaul links' qualities are also taken into account in the optimization. As we see, the service coverage drops when the constraint becomes tighter, however, for all considered range of constraints, compared to hexagonal deployment, constrained deployment optimization increases the network coverage significantly. Indeed, knowing the blockages locations helps in improving the deployment optimization, specially when the UE density increases. Finally, the effect of inter-node distance constraint on the coverage increases with the UE density.

Figure 6 verifies the effect of geographical constraints, on the coverage of IAB networks. Particularly, we study the coverage of the deployment-optimized IAB networks in the cases where, following Fig. 1b, the IAB nodes can not be placed in constrained areas. Here, the results are presented for a network consisting of five circular constrained areas of radius c, with blockage density $\lambda_{\text{bl}} = 500$ km^{-2}, child IAB node density $\lambda_{\text{child}} = 50$km^{-2}, and minimum rate requirement $R_U = 75$ Mbps. The results are presented for the radius of each constrained areas ranging from 100 m to 200 m which corresponds from 10% to 40% of the total disk area, respectively.

As demonstrated in Fig. 6, with low geographical constraints, network performance is not affected by the deployment constraints. However, with large area constraints, the service coverage decreases. This is intuitively because, with larger constraints for IAB placement, there is an increased chance of low coverage for users within the

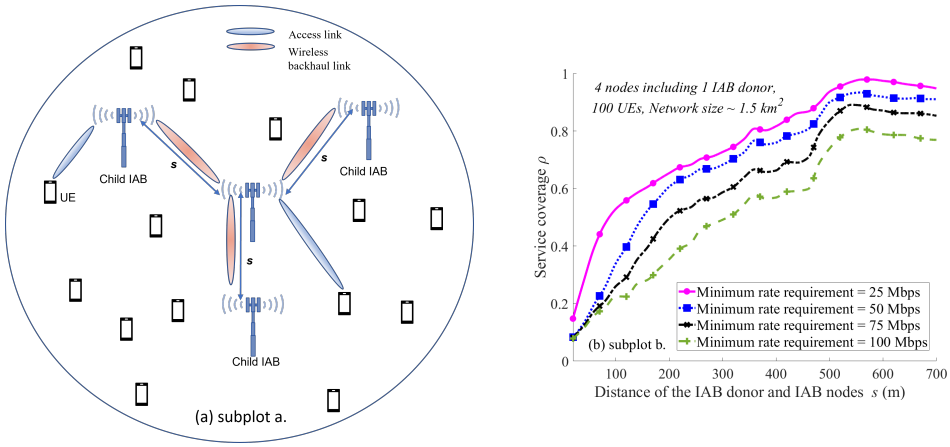

Figure 4: Service coverage as a function of the minimum distance constraint between the nodes, blockage density $\lambda_{\text{bl}} = 500$ km^{-2}, child IAB node density $\lambda_{\text{child}} = 20$ km^{-2}.

constrained areas. Also, since the IAB nodes get packed outside the constrained areas, interference levels for the UEs outside the constrained areas increases resulting in a further decrease in coverage. It can be seen in Fig. 6, where the optimized IAB network in the presence of UE density = 200 km^{-2} increases the coverage to 90.5% from the case with UE density = 400 km^{-2} with coverage of 77%. Finally, compared to random deployment, proper network planning boosts the coverage significantly. Also, compared to the case with child IAB nodes distributed randomly in the unconstrained areas, the coverage is less severely affected by geographical constraints when optimized by Algorithm 10.

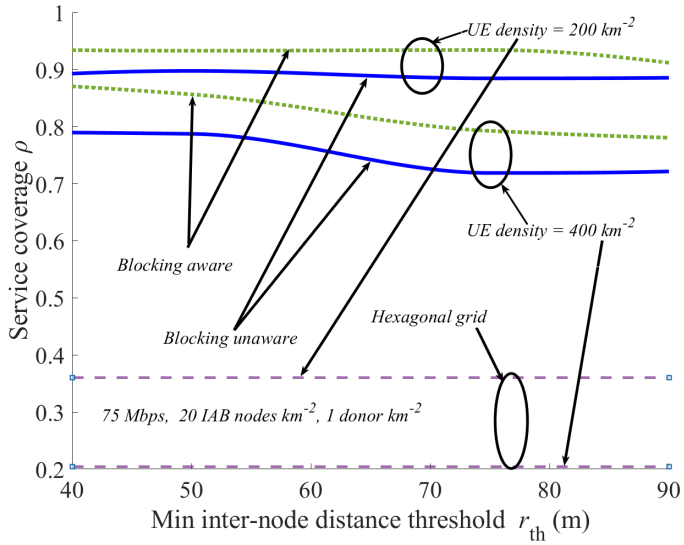

Figure 5: Service coverage as a function of the minimum distance constraint between the nodes, blockage density $\lambda_{\text{bl}} = 500$ km^{-2}, child IAB node density $\lambda_{\text{child}} = 20$ km^{-2}.

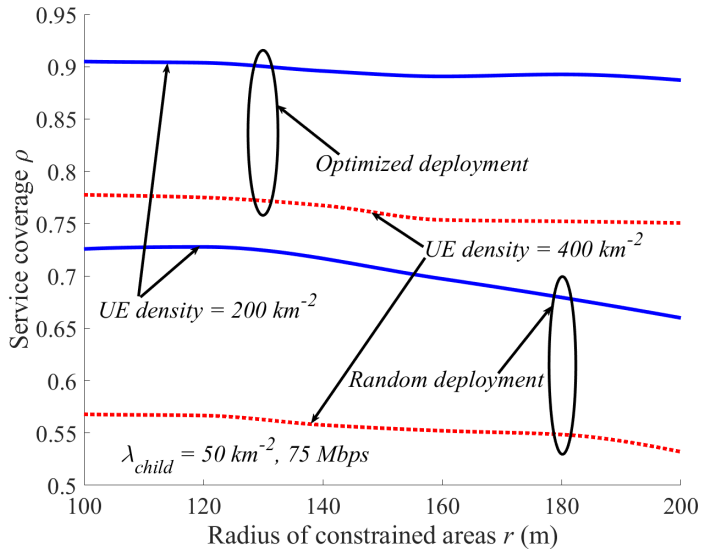

Figure 6: Service coverage as a function of the radius of the constrained areas (c), blockage density $\lambda_{\text{bl}} = 500$ km^{-2}, $\lambda_{\text{child}} = 50$ km^{-2}.

4 Conclusion

We studied the problem of IAB network deployment optimization in the cases with different deployment constraints. We proposed iterative constrained deployment optimization methods with no need for mathematical analysis and with the capability to be adapted for different channel models/constraints/metrics of interest. As demonstrated, with different geographical and inter-node distance constraints, compared to random or hexagonal deployments, proper network planning can boost the coverage of the IAB networks significantly. Finally, in practice, deployment planning may be affected by, e.g., the availability of non-IAB backhaul connection in specific areas, local authority regulations, and the designer may consider, e.g., the planned infrastructure changes, cost, seasonal variations.

Acknowledgment

This work was supported in part by the European Commission through the H2020 Project Hexa-X under Grant 101015956, and in part by the Gigahertz-ChaseOn Bridge Center at Chalmers in a project financed by Chalmers, Ericsson, and Qamcom.

Reference

[1] N. Rajatheva et al., "Scoring the terabit/s goal: Broadband connectivity in 6G," *arXiv preprint arXiv:2008.07220*, Aug. 2020.

[2] Ericsson, "Mobile data traffic growth outlook," 2018.

[3] 3GPP TR 38.874, " Study on Integrated Access and Backhaul (Release 16)," 3rd Generation Partnership Project (3GPP), Tech. Rep. V16, Dec. 2018.

[4] T. 38.300, *NR and NG-RAN overall description*, 3rd Generation Partnership Project (3GPP), V17.1.0, Jun. 2022.

[5] V. F. Monteiro et al., "TDD frame design for interference handling in mobile iab networks," *arXiv preprint arXiv:2204.13198*, Apr. 2022.

[6] 3GPP RP-222671, "New WID on Mobile IAB, 3rd Generation Partnership Project," 3rd Generation Partnership Project (3GPP), Tech. Rep., Sep. 2022.

[7] V. F. Monteiro et al., "Paving the way towards mobile IAB: Problems, Solutions and Challenges," *arXiv preprint arXiv:2206.14946*, 2022.

[8] 3GPP TS 38.174, " Integrated Access and Backhaul (IAB) radio transmission and reception," 3rd Generation Partnership Project (3GPP), Tech. Rep. V.17.0.0, Mar. 2022.

[9] H. Ronkainen, J. Edstam, C. Östberg, and A. Ericsson, "Integrated access and backhaul: A new type of wireless backhaul in 5G," *Frontiers in Communications and Networks*, vol. 2, p. 4, Apr. 2021.

[10] N. Chen, T. Qiu, X. Zhou, K. Li, and M. Atiquzzaman, "An intelligent robust networking mechanism for the internet of things," *IEEE Commun. Mag.*, vol. 57, no. 11, pp. 91–95, Nov. 2019.

[11] X. Meng, H. Inaltekin, and B. Krongold, "Deep reinforcement learning-based topology optimization for self-organized wireless sensor networks," in *Proc. IEEE GLOBECOM'2019*, HI, USA, Dec. 2019, pp. 1–6.

[12] C. Madapatha, B. Makki, A. Muhammad, E. Dahlman, M.-S. Alouini, and T. Svensson, "On topology optimization and routing in integrated access and backhaul networks: A genetic algorithm-based approach," *IEEE OJ-COMS*, vol. 2, pp. 2273–2291, Sep. 2021.

[13] C. A. Oroza, J. A. Giraldo, M. Parvania, and T. Watteyne, "Wireless-sensor network topology optimization in complex terrain: A bayesian approach," *IEEE Internet Things J.*, vol. 8, no. 24, pp. 17 429–17 435, Dec. 2021.

[14] J. Y. Lai, W.-H. Wu, and Y. T. Su, "Resource allocation and node placement in multi-hop heterogeneous integrated-access-and-backhaul networks," *IEEE Access*, vol. 8, pp. 122 937–122 958, Jul. 2020.

[15] X. Fu, F. R. Yu, J. Wang, Q. Qi, and J. Liao, "Dynamic service function chain embedding for NFV-enabled IoT: A deep reinforcement learning approach," *IEEE Trans. Wirel. Commun.*, vol. 19, no. 1, pp. 507–519, Oct. 2019.

[16] S. Singh, M. N. Kulkarni, A. Ghosh, and J. G. Andrews, "Tractable model for rate in self-backhauled millimeter wave cellular networks," *IEEE J. Sel. Areas Commun. IEEE J SEL AREA COMM*, vol. 33, no. 10, pp. 2196–2211, May 2015.

[17] C. Saha and H. S. Dhillon, "Millimeter wave integrated access and backhaul in 5G: Performance analysis and design insights," *IEEE J. Sel. Areas Commun. IEEE J SEL AREA COMM*, vol. 37, no. 12, pp. 2669–2684, 2019.

[18] N. Chen, T. Qiu, X. Zhou, K. Li, and M. Atiquzzaman, "An intelligent robust networking mechanism for the internet of things," *IEEE Commun. Mag.*, vol. 57, no. 11, pp. 91–95, Nov. 2019.

[19] O. P. Adare, H. Babbili, C. Madapatha, B. Makki, and T. Svensson, "Uplink power control in integrated access and backhaul networks," in *In Proc. DySPAN'2021*, Virtual, 2021, pp. 163–168.

[20] C. Fang, C. Madapatha, B. Makki, and T. Svensson, "Joint scheduling and throughput maximization in self-backhauled millimeter wave cellular networks," in *2021 17th International Symposium on Wireless Communication Systems (ISWCS)*, IEEE, 2021, pp. 1–6.

[21] B. Błaszczyszyn, "Lecture Notes on Random Geometric Models—Random Graphs, Point Processes and Stochastic Geometry," 2017.

[22] S. M. Azimi-Abarghouyi, B. Makki, M. Nasiri-Kenari, and T. Svensson, "Stochastic Geometry Modeling and Analysis of Finite Millimeter Wave Wireless Networks," *IEEE Trans. Veh. Technol.*, vol. 68, no. 2, pp. 1378–1393, Feb. 2019.

[23] C. Madapatha et al., "On integrated access and backhaul networks: Current status and potentials," *IEEE OJ-COMS*, vol. 1, pp. 1374–1389, Sep. 2020.

[24] T. S. Rappaport, Y. Xing, G. R. MacCartney, A. F. Molisch, E. Mellios, and J. Zhang, "Overview of Millimeter Wave Communications for Fifth-Generation (5G) Wireless Networks—With a Focus on Propagation Models," *IEEE Trans. Antennas Propag.*, vol. 65, no. 12, pp. 6213–6230, Dec. 2017.

PAPER D

Reconfigurable Intelligent Surfaces-Assisted Integrated Access and Backhaul

C. Madapatha, B. Makki, H. Guo, and T. Svensson

In Proc. IEEE International Black Sea Conference on Communications and Networking (BlackSeaCom)'
2025, Chisinau, Moldova.
Extended version included here, available Online:
`https://arxiv.org/pdf/2502.12011`.

The layout has been revised.

Abstract

In this paper, we study the impact of reconfigurable intelligent surfaces (RISs) on the coverage extension of integrated access and backhaul (IAB) networks. Particularly, using a finite stochastic geometry model, with random distributions of user equipments (UEs) in a finite region, and planned hierachical architecture for IAB, we study the service coverage probability defined as the probability of the event that the UEs' minimum rate requirements are satisfied. We present comparisons between different cases including IAB-only, IAB assisted with RIS for backhaul as well as IAB assisted by network controlled repeaters (NCRs). Our investigations focus on wide-area IAB assisted with RIS through the lens of different design architectures and deployments, revealing both conflicts and synergies for minimizing the effect of tree foliage over seasonal changes and rain. Our simulation results reveal both opportunities and challenges towards the implementation of RIS in IAB.

Integrated access and backhaul, IAB, reconfigurable intelligent surfaces, RIS, service coverage probability, 5G, 6G, tree foliage.

1 Introduction

The rapid growth in data traffic and the advent of technologies like the Internet of Things (IoT) and 5G networks necessitate innovative solutions for wireless communication systems [1]. Reconfigurable intelligent surface (RIS) and integrated access and backhaul (IAB) networks emerge as candidate techniques, offering enhanced coverage, capacity, and reliability leading to a new era in wireless network architecture.

RIS is a meta-surface with multiple passive reflective surfaces attached to each unit cell, which can coordinately align its phases using a controller and perform beamforming. In the literature, different types of RISs exist, such as passive, active, absorptive, STAR-RIS, and beyond-diagonal RIS. RISs have the potential to be deployed densely in a network with low energy consumption **10787237**, [2]. Also, the passive nature of the elements in RIS allows them to be coated to any surface without hassle, making its deployment faster [3]. Aligning the phase of RIS towards a particular user equipment (UE) requires channel state information (CSI) which is regarded as a challenge in highly dynamic propagation scenarios. The programmability of RIS also facilitates energy-efficient network operations by allowing precise control over the radio propagation environment [4]. This programmability, coupled with its adaptability, makes RIS an interesting enabler for future wireless networks.

IAB is a decode-and-forward relaying method standardized in 3GPP Releases 16-18

where an IAB node provides intermediate connections between, e.g., the IAB donor and the child nodes (in general, IAB can be a multi-hop network but practically it may be limited to 2 or 3 hops due to its latency [5], [6], [7]). According to 3GPP specifications, IAB nodes are classified into two categories: wide-area and local-area IAB. These categories differ primarily in terms of their functional capabilities and the extent of network planning required for their deployment [7], [8]. Particularly, compared to local-area IAB, wide-area IAB is a more powerful/capable node used for coverage extension in a wide area.

In particular, RIS may be helpful by providing alternative paths when the direct link from the IAB-donor to IAB-child faces deep fading and/or blockage and makes it easier to avoid such trouble. The dynamic nature of RIS deployments allows for flexibility in addressing environmental challenges including tree foliage, and propagation losses. Recent advancements highlight the growing importance of RISs and IAB networks in next-generation communication systems. For instance, RISs have demonstrated significant potential in improving signal strength and energy efficiency through passive beamforming. Integration of RIS with IAB networks capitalizes on these strengths, enabling seamless backhaul and access link operations even under challenging propagation conditions [9]. Furthermore, the integration of RIS with IAB networks enables dynamic resource management and can improve the overall network energy efficiency. As explored in the literature, the programmability and adaptability of RIS enhance the flexibility of IAB nodes, making them resilient to environmental factors such as rain and foliage. These features allow RIS to provide alternative paths for signal propagation, ensuring reliable connectivity in scenarios where direct links face challenges. The combination of RIS and IAB also aligns with the objectives of future 6G networks, which aim to optimize resource utilization and energy efficiency [10].

In this paper, we study the performance of RIS-assisted IAB networks in the cases with different environmental effects. By dynamically managing RIS elements and balancing the load between backhaul and access links, this approach addresses the growing demand for scalable, energy-efficient wireless networks capable of supporting high user densities and diverse application scenarios. This work builds on these advancements, progressing towards a framework for deploying and optimizing RIS-assisted IAB networks in real-world environments. These advancements reflect the ongoing evolution in network design with RIS. They aim to achieve highly flexible, sustainable, and energy-efficient wireless communication infrastructures, aligning with the broader goals of future 6G networks.

In particular, we study the service coverage probability as the performance metric. We consider a wide-area setup and consider RIS to improve the coverage area of the IAB in the cases with, e.g., seasonal tree foliage. Moreover, we compare the performance of RIS-assisted IAB networks with cases having only IABs or the cases where network-controlled repeaters (NCRs) are used to assist the IAB network. Also,

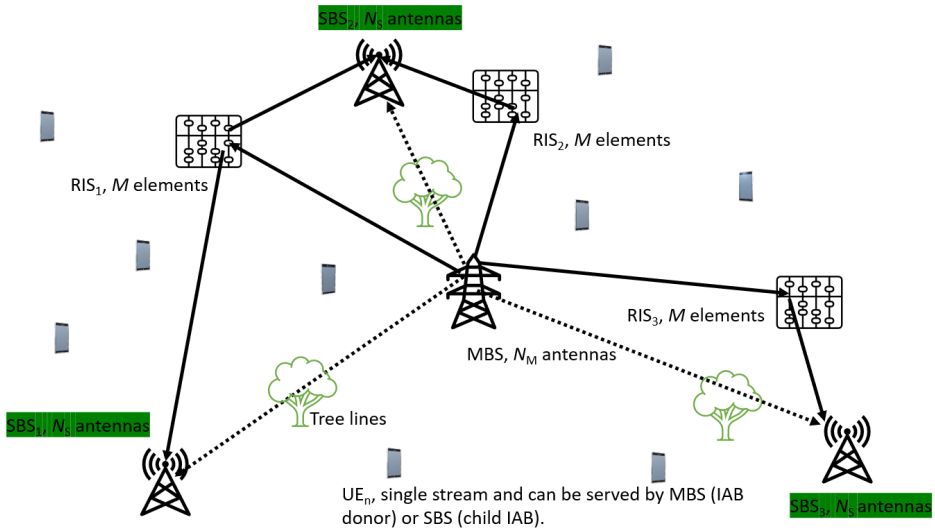

Figure 1: Illustration of the wide-area IAB assisted with RIS for backhaul links amidst seasonal tree foliage changes

we investigate the effect of rain loss on the performance of these networks. Our simulations show that the use of RISs/NCRs help to increase the service coverage probabilty in the presence of tree foliage.

2 The Integration of RIS and IAB

Consider an in-band wide-area IAB network with two-hops in downlink where the IAB donor and IAB child nodes can serve multiple UEs as shown in Fig. 1. In contrast to a local-area IAB network, this topology is designed with the intention to extend coverage focusing on sub-urban areas. Here, UEs are served either by the IAB donor or IAB child nodes, while the backhaul link can be either directly from IAB donor to IAB child node or be via RIS depending on the seasonal tree foliage level in the direct backhaul link. In particular, the direct link can be blocked by the dense tree lines while the path via the RIS does not have obstructions from tree lines. This is motivated by the fact that the effect of the tree foliage may change considerably in different seasons where, for instance, the foliage loss may increase signficantly during the spring and summer.

2.1 Backhaul via Direct links

Following the state-of-the-art mmWave channel model given in [11], the received power at each node can be expressed as

$$P_{\text{rx}} = P_{\text{tx}} h_{\text{link}} G_{\text{ant}} \eta_{\text{path}} \phi_{\text{loss}}. \tag{D.1}$$

Here, P_{tx}, h_{link}, G_{ant}, η_{path} denote the transmit power, independent small-scale fading for each link, modelled as Rayleigh fading, cumulative antenna gain of transmitter and receiver, and pathloss in linear scale, respectively while ϕ_{loss} is the tree foliage loss. Furthermore, pathloss denoted by η_{path}, can be expressed in dB, as characterized according to the 5GCM UMa close-in model described in [12] below.

$$\eta_{\text{path (dB)}} = 32.4 + 10\log_{10}(d)^{\alpha} + 20\log_{10}(f_c), \tag{D.2}$$

where f_c is the carrier frequency, d is the propagation distance between the nodes, and α is the path loss exponent. Depending on the blockage, line-of-sight (LoS) and NLoS (N: Non) links are affected by different path loss exponents. It should also be noted that 5GCM RMa close-in model is not applicable for sub-urban use cases unless the environment is clearly rural which would result in overestimation of coverage, unlike 5GCM UMa model.

5G and beyond systems are equipped with large antenna arrays which are used to minimize the propagation loss. We use the sectored-pattern antenna array model to characterize the beam pattern and antenna gain, which is given by

$$G_{\text{ant}}(\theta) = \begin{cases} G_{\text{main}} & \frac{-\theta_{\text{HPBW}}}{2} \leq \theta \leq \frac{\theta_{\text{HPBW}}}{2} \\ g_{\text{side}}(\theta) & \text{otherwise.} \end{cases} \tag{D.3}$$

Here, θ represents the angle between the transmit and receive antennas. Furthermore, θ_{HPBW} is the half power beamwidth, and G_{main} denotes the main lobe gain of the antenna while $g_{\text{side}}(\theta)$ is the side lobe gain [11]. Similar to [13], we assume an omni-directional beam pattern with UE antenna gain of 0 dB.

We assume that the inter-UE interference is negligible in the downlink with the assumption of sufficient isolation. Particularly, the interference model focuses on the aggregated interference on the access links, caused by the neighboring interferers, which for UE u is expressed as

$$I_u = \sum_{i,u \in \Lambda_{i,u} \setminus \{w_u\}} P_i h_{i,u} G_{i,u} \eta_{(1\text{m})} \eta_{x_i,x_u} \|\mathbf{x_i} - \mathbf{x_u}\|^{-1}, \tag{D.4}$$

where i denotes the set of base stations (BS)s excluding the associated BS w_u of user u. Also, for small base station (SBS) s, the aggregated interference on the backhaul

links is given by

$$I_s = \sum_{j,s \in \Lambda_{j,s} \setminus \{w_s\}} P_j h_{j,s} G_{j,s} \eta_{(1\mathrm{m})} \eta_{x_j,x_s} \|\mathbf{x_j} - \mathbf{x_s}\|^{-1}, \tag{D.5}$$

where j denotes the set of transmitting BSs excluding the associated BS w_s of SBS s.

We use a finite homogeneous Poisson point process (FHPPP) denoted by Λ_T with density λ_T to model the spatial distribution of the tree lines of length r. The tree foliage loss is estimated using the Fitted International Telecommunication Union-Radio (FITU-R) tree foliage model [14, Chapter 7]. The model is well known for its applicability in cases with non-uniform vegetation and frequency dependency within the 10-40 GHz range. Particularly, considering both in-leaf and out-of-leaf vegetation states, the tree foliage loss in (D.1) is expressed as

$$\phi_{\text{loss}} = \begin{cases} 0.39 f_{\text{c}}^{0.39} r^{0.25}, & \text{in-leaf} \\ 0.37 f_{\text{c}}^{0.18} r^{0.59}, & \text{out-of-leaf,} \end{cases} \tag{D.6}$$

where r is the vegetation depth measured in meters.

In our setup, each UE has the ability to be connected to either an MBS or an SBS depending on the maximum average received power. Let $a_u \in \{0, 1\}$ be a binary variable indicating the association with 1, while 0 representing the opposite. Thus, for the access links

$$a_u = \begin{cases} 1, & \text{if } P_i G_{z,x} h_{z,x} \eta_{z,x} (\|\mathbf{z} - \mathbf{x}\|)^{-1} \\ & \qquad \geq P_j G_j h_{z,y} \eta_{z,y} (\|\mathbf{z} - \mathbf{y}\|)^{-1}, \\ & \qquad \forall\, \mathbf{y} \in \Lambda_j, j \in \{\mathrm{m}, \mathrm{s}\} | \mathbf{x} \in \Lambda_i, \\ 0, & \text{otherwise,} \end{cases} \tag{D.7}$$

where i, j denote the BS indices, i.e., MBS or SBS. As in (7) for each UE u, the association binary variable a_u becomes 1 for the cell giving the maximum received power at the UE, while for all other cells it is 0, as the UE can only be connected to one IAB node. Here, **x, y** represent the BS locations while **z** is the location of the UE.

Since the MBSs and the SBSs have large antenna arrays and can beamform towards the desired direction, the antenna gain over the backhaul links can be assumed to be the same, and backhaul link association can be well determined based on the

minimum path loss rule, i.e., by

$$a_{\text{link}} = \begin{cases} 1, & \text{if } \eta_{\text{link}}(\|\mathbf{u}-\mathbf{v}\|)^{-1} \geq \eta_{\text{link}}(\|\mathbf{u}-\mathbf{w}\|)^{-1}, \\ & \qquad \forall\ \mathbf{w} \in \Lambda_{\text{nodes}} | \mathbf{v} \in \Lambda_{\text{nodes}}, \\ 0, & \text{otherwise.} \end{cases} \tag{D.8}$$

For resource allocation, on the other hand, the mmWave spectrum available is partitioned into the access and backhaul links such that

$$\begin{cases} B_{\text{backhaul}} = \psi B, \\ B_{\text{access}} = (1-\psi)B. \end{cases} \tag{D.9}$$

Here, B denotes the bandwidth, while ψ represents the bandwidth partitioning factor, which lies between 0 and 1. Along with the MBSs which are non-IAB backhaul-connected, a portion of the SBSs may have dedicated non-IAB backhaul connections, resulting in a hybrid IAB network. Therefore, in our deployment, some of the SBSs are IAB backhauled wirelessly and the others are connected to dedicated non-IAB backhaul links.

Let us initially concentrate on the IAB-type backhauled SBSs. Also, let, B_{backhaul} and B_{access} denote the backhaul and the access bandwidths, respectively, while total bandwidth is $B = B_{\text{backhaul}} + B_{\text{access}}$. The bandwidth allocated for each IAB-type wirelessly backhauled SBS (child IAB) by the MBS (IAB donor) is proportional to its load and the number of UEs in the access link. The resource allocation is determined based on the instantaneous load where each IAB-type backhauled SBS informs its current load to the associated MBS each time. Thus, the backhaul-related bandwidth for the k-th IAB node, if it does not have dedicated non-IAB backhaul connection, is given by

$$B_{\text{backhaul},k} = \frac{\psi B N_k}{\sum\limits_{\forall\ k} N_k}, \forall k, \tag{D.10}$$

where N_k denotes the number of UEs connected to the k-th IAB-type backhauled node and $\psi \in [0,1]$ is the fraction of the bandwidth resources on backhauling. Therefore, the bandwidth allocated to the k-th IAB-type backhauled node is proportional to the ratio between its load, and the total load of its connected IAB donor. Meanwhile, the access spectrum is equally shared among the connected UEs at the IAB node according to

$$B_{\text{access},u} = \frac{(1-\psi)B}{\sum\limits_{\forall\ u} N_{k,u}}, \forall u, \tag{D.11}$$

where u denotes the UEs indices, and k represents each IAB-type backhauled node. Moreover, $N_{k,u}$ is the number of UEs connected to the k-th IAB-type backhauled

node to which UE u is connected. Finally, the signal-to-interference-plus-noise ratio (SINR) is obtained in accordance with (D.4) by

$$\mathrm{SINR} = P_{\mathrm{rx}}/(I_u + \sigma^2), \tag{D.12}$$

where σ^2 is the noise power.

With our setup, the network may have three forms of access connections, i.e., MBS-UE, IAB-type, and non-IAB backhauled SBS-UE. The individual data rates will behave according to the form in which the UE's connection has been established. Particularly, the rates experienced by the UEs in access links that are connected to MBSs or to the IAB type-backhauled SBSs are given by

$$R_u = \begin{cases} \frac{(1-\psi)B}{N_m}\log(1+\mathrm{SINR}(v_u)), & \text{if } w_u \in \Lambda_{\mathrm{MBS}}, \\ \min\Bigg(\frac{(1-\psi)BN}{\sum\limits_{\forall\, u} N_{k,u}}\log(1+\mathrm{SINR}(v_u)), \\ \qquad \frac{\psi BN}{\sum\limits_{\forall\, k} N_k}\log(1+\mathrm{SINR}(v_b))\Bigg), \text{if } w_u \in \Lambda_{\mathrm{SBS}}, \end{cases} \tag{D.13}$$

where k represents each IAB-type backhauled SBS connected to the MBS. Then, m gives the associated MBS, s denotes the SBS, and u represents the UEs' indices.

Depending on the associated cell, there are two possible cases for the data rate of the UEs. First is the case when the UEs are connected to the MBSs, i.e., IAB donor, as denoted by $w_u \in \Lambda_{\mathrm{MBS}}$ in (D.13). Since the MBSs have non-IAB backhaul connection, the rate will only depend on the access bandwidth available at the UE. In the second case, the UEs are connected to the IAB-type backhauled SBSs, as denoted by $w_u \in \Lambda_{\mathrm{SBS}}$ in (D.13). Here, the SBSs have shared backhaul bandwidth from the IAB-Donor-nodes i.e., MBSs, and thus the UEs data rates depend on the backhaul rate of the connected IAB-type backhauled SBS as well.

2.2 Backhaul via RIS

Consider an M-element RIS assisting the backhaul between IAB donor and IAB child, where the receive signal at the RIS can be expressed in [15] as

$$y = \sqrt{P_{\mathrm{tx}}}\mathbf{g}_c\mathbf{w}_c x + z, \tag{D.14}$$

where P_{tx} is the transmit power at the donor IAB, x is the transmitted signal with a unit power, $\mathbf{w}_c \in \mathbb{C}^{N_c \times 1}$ is the beamformer of the BS-RIS link and has unit power as an upper bound, and z is the additive Gaussian noise at the receiver side.

Also, ignoring the direct IAB-donor to IAB-child link as well as the nonlinearities between adjacent reflectors, the equivalent channel $\mathbf{g} \in \mathbb{C}^{1\times N_r}$ in the RIS-assisted

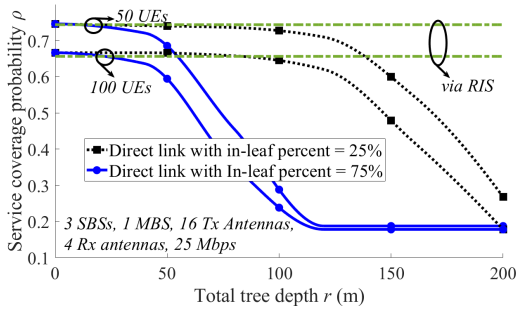

Figure 2: Network service coverage probability as a function of total tree depth.

link (BS-RIS-UE) is given by

$$\mathbf{g}_c = \mathbf{g}_{ru}\mathbf{\Omega}\mathbf{g}_{br}. \tag{D.15}$$

Here, $\mathbf{g}_{br} \in \mathbb{C}^{M\times N_r}$ and $\mathbf{g}_{ru} \in \mathbb{C}^{1\times M}$ are the channel between IAB donor-RIS and RIS-IAB child, respectively. Moreover,

$$\mathbf{\Omega} = \text{diag}(e^{j\omega_1}, \ldots, e^{j\omega_M}) \tag{D.16}$$

is the reflection coefficient matrix of the RIS. With joint BS active and RIS passive beamforming, the backhaul data rate at child IAB node with RIS assistance can be expressed as

$$R = \log\left(1 + \frac{P\left|\mathbf{g}_{ru}\mathbf{\Omega}\mathbf{g}_{br}\mathbf{w}_c\right|^2}{\sigma^2}\right). \tag{D.17}$$

To optimize the RIS matrix $\mathbf{\Omega}$, the phase shifts ω_M are adjusted to maximize the effective channel gain, $\left|\mathbf{g}_{ru}\mathbf{\Omega}\mathbf{g}_{br}\mathbf{w}_c\right|^2$ ensuring constructive signal combination at the IAB child.

3 Simulation Results and Discussion

This section evaluates the effect of RIS-assistance in mitigating the tree foliage and rain loss on the service coverage probability, ρ of IAB networks. Here, ρ can be expressed using (D.13) as $\rho = \Pr(R_{\text{u}} \geq \beta)$ where β represents the data rate threshold. The simulation results and discussions are divided into five parts to provide a comprehensive understanding of the network performance. As illustrated in Fig. 1, we consider the MBS to be located at the origin, SBSs at symmetrically with 120 degrees apart at 600 m away from the origin.

Table 1: Service coverage probability when the RIS path is impacted by tree foliage. The relative distance is the ratio between cumulative tree depth in the RIS path and the tree depth in the direct path.

Relative tree depth (%)	0%	20%	40%	60%	80%	100%
ρ at In-leaf 25%, 100 UEs	0.680	0.676	0.663	0.648	0.515	0.281
ρ at In-leaf 75%, 100 UES	0.680	0.415	0.187	0.185	0.178	0.170

Impact of Tree Foliage on Service Coverage

Figure 2 illustrates the network service coverage probability as a function of total tree depth, r, for different percentages of in-leaf conditions and the inclusion of RIS-assisted links. The parameters are set to 1 MBS, 3 SBSs, 16 Tx antennas and 4 Rx antennas, and in all cases the minimum UE data rate threshold requirement is kept at 25 Mbps. For both 50 and 100 UEs, it is observed that the direct link's performance deteriorates significantly as the tree depth increases, especially under 75% in-leaf conditions. For instance, with a total tree depth of 150 m, service coverage probability drops below 0.3 for the 75% in-leaf scenario, compared to approximately 0.6 for the 25% in-leaf case. Also, for small values of total tree depth r, the traditional IAB network is depicting similar performance to an RIS-aided network. However, as the r becomes larger, the RIS-aided network outperforms the IAB only backhauled network. This is because, with larger r it is more likely for the backhaul links to be affected by tree foliage than the double path-loss of RIS-aided backhaul link. The RIS-assisted links provide substantial improvement in coverage by bypassing the obstructions caused by dense foliage. As seen, service coverage probability for RIS-assisted communication remains above 0.7, even at a tree depth of 200 m, highlighting the robustness of this solution. This improvement underscores the RIS's capability to mitigate coverage issues in foliage-heavy environments.

The RIS-assisted backhaul links can usually be pre-planned to maximize LoS and reduce tree foliage impact. In Table 1, we depict how unplanned RIS-assisted links affect the performance. Here, we consider the ratio of tree line depth between the RIS assisted backhaul path and direct link path. As seen, for cases with in-leaf percentage of the vegetation is at 75%, the RIS assisted link starts to degrade significantly when the relative tree line depth reaches 40%. This shows the importance of tree foliage-aware RIS placement, particularly in dense suburban or rural deployments.

Carrier Frequency and User Density Effects

Figure 3 evaluates the service coverage probability as a function of the number of UEs for two carrier frequencies, 28 GHz and 38 GHz. Across all scenarios, service coverage probability decreases with an increasing number of UEs due to higher competition for resources. However, the performance at 28 GHz consistently outperforms 38 GHz, attributed to lower path loss at lower carrier frequencies. In reality, networks

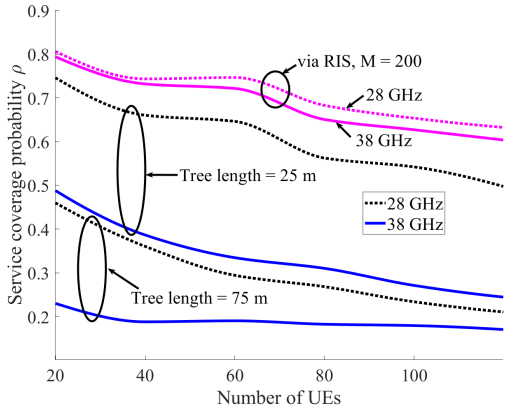

Figure 3: Network service coverage probability for different carrier frequencies as a function of number of UEs, N.

often use multiple frequency bands for complementary purposes (e.g., combining the strengths of 28 GHz for extended coverage with the higher capacity of 38 GHz in small cells).

As we see, with 60 UEs and a tree line depth of 25 m, service coverage probability is approximately 0.6 for 28 GHz but drops to about 0.3 for 38 GHz. This disparity becomes more significant as the user density increases. Moreover, increasing the tree line depth to 75 m significantly affects coverage, reducing service coverage probability by nearly 50% for both frequencies. These results emphasize the trade-offs between carrier frequency and user density in designing robust IAB networks.

Rain Intensity and Tree Foliage Combined Effect

In Fig. 4, we investigate the combined impact of rain intensity and tree foliage on service coverage probability. As rain intensity increases, service coverage probability declines for all configurations, with direct links under 75% in-leaf conditions showing the worst performance. At a rain intensity of 10 mm/hr, service coverage probability is below 0.2 for this scenario, indicating severe degradation. The inclusion of RIS or SBS mitigates this issue significantly. For instance, RIS-assisted communication with 200 reflecting elements maintains service coverage probability above 0.6 across all rain intensities, demonstrating its resilience. Similarly, SBSs provide consistent improvement, although their performance is slightly less robust compared to RIS. These results suggest that deploying RIS in combination with SBSs can effectively counteract adverse environmental conditions, ensuring reliable service coverage.

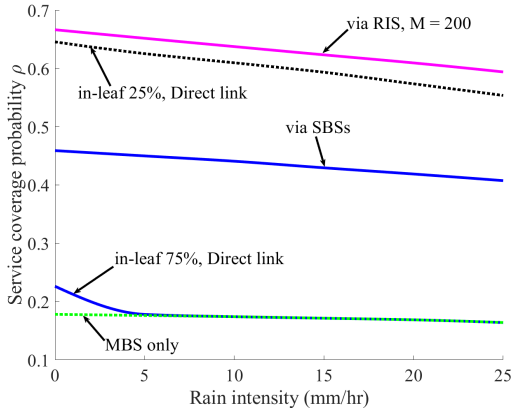

Figure 4: Network service coverage probability as a function of rain intensity in the presence of tree foliage.

Influence of Main Lobe Antenna Gain

Figure 5 illustrates the effect of main lobe antenna gain on service coverage probability for two tree depths: 50 m and 100 m. The results reveal a significant improvement in service coverage probability with increasing antenna gain. For a tree depth of 50 m, service coverage probability reaches 0.7 at a main lobe gain of approximately 25 dB and saturates near 0.8 at higher gains. In contrast, for a tree depth of 100 m, service coverage probability shows a slower improvement, reaching only about 0.6 at a gain of 30 dB. This disparity highlights the compounded effect of tree depth and antenna gain. Higher antenna gains effectively compensate for the path loss caused by tree obstructions, but their impact diminishes as tree depth increases. These findings emphasize the need for optimal antenna design and deployment strategies to enhance coverage in dense foliage environments.

Also, as seen in Fig. 5, the use of NCR enhances service coverage probability compared to backhaul via direct links, particularly in low main lobe antenna gain scenarios. However, as the main lobe antenna gain increases, the direct link surpasses NCR, indicating that the effectiveness of NCR is higher in environments with lower antenna gain and higher tree depth. Here, the NCRs are placed at the same locations as of RISs and the maximum output power constraint, amplification gain are set to 40 dBm and 100 dB, respectively. In particular, NCR and RIS have similar functionalities while there are detailed differences between them such as high power amplification and additional beamforming capabilities at the NCR (see [16] for details about the NCR).

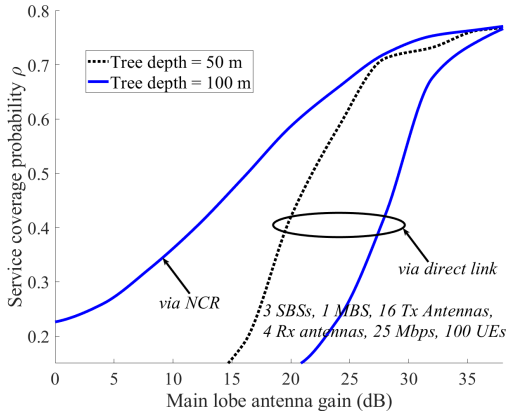

Figure 5: Network service coverage probability as a function of main lobe antenna gain.

Practical Implications

Deploying RISs and SBS nodes effectively mitigates the adverse impacts of foliage, by maintaining service coverage where direct links fail. RISs promise to provide cost-efficient backhaul solutions, while SBSs enhance reliability by distributing the network load. Also, we see the importance of selecting suitable frequencies based on deployment scenarios. Lower mmWave frequencies, such as 28 GHz, offer better coverage in dense environments, while higher frequencies, like 38 GHz, provide higher capacity but are more sensitive to obstructions. Optimizing antenna gains improve coverage, particularly in moderate foliage conditions. However, high obstructions require additional measures like RISs or SBSs for effective performance. Overall, we suggest that combining RISs, SBSs, selection of suitable carrier frequency, and advanced antenna designs ensures reliable connectivity especially in sub-urban wide-area IAB networks.

4 Conclusion

We studied the problem of RIS-assited IAB network to counter tree foliage loss over several seasons. This study provides valuable insights into the design of reliable and efficient IAB networks in challenging environments. The results demonstrate that deploying RISs/NCRs are useful for mitigating the effects of foliage, rain, and other environmental factors, ensuring robust service coverage, especially in wide-area IAB networks. The comparative analysis of 28 GHz and 38 GHz frequencies highlights the trade-offs between coverage and capacity, emphasizing the need for strategic frequency selection based on deployment scenarios. Additionally, optimizing the main lobe antenna gain further enhances coverage, particularly in moderate obstruction

conditions. By integrating these strategies, one can achieve cost-effective and resilient IAB networks, catering to both urban and sub-urban deployment needs. Also, the proposed RIS-assisted scheme improves the service coverage probability throughout the year, regardless of the season and the carrier frequency used.

Acknowledgments

This work was supported by the European Commission through the Horizon Europe/JU SNS project Hexa-X-II (Grant Agreement no. 101095759).

Reference

[1] Ericsson, "Mobile data traffic growth outlook," 2023.

[2] A. V. Parambath, J. Flordelis, C. Madapatha, F. Rusek, E. Bengtsson, and T. Svensson, "Integrating reconfigurable intelligent surfaces (riss) into indoor d-mimo networks for 6G," in *2024 IEEE 100th Vehicular Technology Conference (VTC2024-Fall)*, IEEE, 2024, pp. 1–6.

[3] R. Wang, Y. Yang, B. Makki, and A. Shamim, "A wideband reconfigurable intelligent surface for 5G millimeter-wave applications," *IEEE Trans. Antennas Propag.*, 2024.

[4] G. C. Alexandropoulos et al., "Ris-enabled smart wireless environments: Deployment scenarios, network architecture, bandwidth and area of influence," *EURASIP Journal on Wireless Communications and Networking*, vol. 2023, no. 1, p. 103, 2023.

[5] C. Fang, C. Madapatha, B. Makki, and T. Svensson, "Joint scheduling and throughput maximization in self-backhauled millimeter wave cellular networks," in *2021 17th International Symposium on Wireless Communication Systems (ISWCS)*, IEEE, Virtual, 2021, pp. 1–6.

[6] C. Madapatha, B. Makki, A. Muhammad, E. Dahlman, M.-S. Alouini, and T. Svensson, "On topology optimization and routing in integrated access and backhaul networks: A genetic algorithm-based approach," *IEEE OJ-COMS*, vol. 2, pp. 2273–2291, Sep. 2021.

[7] C. Madapatha, B. Makki, H. Guo, and T. Svensson, "Constrained deployment optimization in integrated access and backhaul networks," in *2023 IEEE Wireless Communications and Networking Conference (WCNC)*, IEEE, 2023, pp. 1–6.

[8] O. Teyeb, A. Muhammad, G. Mildh, E. Dahlman, F. Barac, and B. Makki, "Integrated access backhauled networks," in *2019 IEEE 90th Vehicular Technology Conference (VTC2019-Fall)*, IEEE, 2019, pp. 1–5.

[9] 6G Research Consortium, "Deliverable D4.3: Early Results of 6G Radio Key Enablers," 6G Project, Technical Report, Apr. 2024.

[10] M. Diamanti, P. Charatsaris, E. E. Tsiropoulou, and S. Papavassiliou, "The prospect of reconfigurable intelligent surfaces in integrated access and backhaul networks," *IEEE trans. green commun.*, vol. 6, no. 2, pp. 859–872, 2022.

[11] S. M. Azimi-Abarghouyi, B. Makki, M. Nasiri-Kenari, and T. Svensson, "Stochastic Geometry Modeling and Analysis of Finite Millimeter Wave Wireless Networks," *IEEE Trans. Veh. Technol.*, vol. 68, no. 2, pp. 1378–1393, Feb. 2019.

[12] T. S. Rappaport, Y. Xing, G. R. MacCartney, A. F. Molisch, E. Mellios, and J. Zhang, "Overview of Millimeter Wave Communications for Fifth-Generation (5G) Wireless Networks—With a Focus on Propagation Models," *IEEE Trans. Antennas Propag.*, vol. 65, no. 12, pp. 6213–6230, Dec. 2017.

[13] C. Saha and H. S. Dhillon, "Millimeter Wave Integrated Access and Backhaul in 5G: Performance Analysis and Design Insights," *arXiv*, 2019.

[14] M. A. Abu-Rgheff, *5G Physical Layer Technologies*. John Wiley & Sons, Nov. 2019, pp. 303-313.

[15] H. Guo et al., "A comparison between network-controlled repeaters and reconfigurable intelligent surfaces," *arXiv preprint arXiv:2211.06974*, 2022.

[16] F. Carvalho et al., "Network-controlled repeater–an introduction," *arXiv preprint arXiv:2403.09601*, 2024.

PAPER E

Joint Fiber and Free Space Optical Infrastructure Planning for Hybrid Integrated Access and Backhaul Networks

C. Madapatha, P. Lechowicz, C. Natalino, P. Monti, and T. Svensson

Accepted at IEEE International Symposium on Personal, Indoor and Mobile Radio Communications (PIMRC)
2025, Istanbul, Turkey.

The layout has been revised.

Abstract

Integrated access and backhaul (IAB) is one of the promising techniques for 5G networks and beyond (6G), in which the same node/hardware is used to provide both backhaul and cellular services in a multi-hop architecture. Due to the sensitivity of the backhaul links with high rate/reliability demands, proper network planning is needed to ensure the IAB network performs with the desired performance levels. In this paper, we study the effect of infrastructure planning and optimization on the coverage of IAB networks. We concentrate on the cases where the fiber connectivity to the nodes is constrained due to cost. Thereby, we study the performance gains and energy efficiency in the presence of free-space optical (FSO) communication links. Our results indicate hybrid fiber/FSO deployments offer substantial cost savings compared to fully fibered networks, suggesting a beneficial trade-off for strategic link deployment while improving the service coverage probability. As we show, with proper network planning, the service coverage, energy efficiency, and cost efficiency can be improved.

Integrated access and backhaul, IAB, Topology optimization, fiber, millimeter wave (mmWave), 3GPP, Coverage, Wireless backhaul, 5G NR, 6G, Free Space Optical, FSO, Network planning.

1 Introduction

The rapid growth in mobile data traffic, fueled by the rise of smart devices, immersive applications, and the Internet of Things (IoTs), has significantly increased the demand for high-speed, low-latency, and ultra-reliable communication networks. To meet this growing need, network densification has emerged as a key strategy in the evolution of 5G and the development toward future 6G [1]. This approach involves deploying many low-power, small base stations (SBSs), access points (APs) or reconfigurable intelligent surfaces (RISs) within a geographical area. The primary objectives are enhancing spatial frequency reuse, increasing capacity, and reducing end-to-end latency by bringing the network infrastructure closer to end users [2]. Realizing the full benefits of network densification introduces challenges concerning backhauling, i.e., the process of connecting distributed access points to the core network. Traditional backhaul solutions, such as fiber optics and microwave links, each come with their own advantages and disadvantages [3].

Fiber optics offer high throughput and reliability but have high deployment costs and extended installation times, posing challenges for rapid expansion in dense urban

areas or hard-to-reach rural locations [4]. On the other hand, microwave links offer faster deployment and greater flexibility in network topology. However, they are constrained by the availability of licensed spectrum and can be affected by interference and weather-related fading, particularly in the millimeter-wave (mmWave) bands, which may impair performance [5]. To tackle these challenges, Integrated Access and Backhaul (IAB) has emerged as a crucial solution for cost-effective and scalable network expansion. Standardized in 3GPP Release 16 and later, IAB uses the same radio access technology and spectrum for both user access and backhaul transmission, significantly reducing the need for wired infrastructure. IAB nodes operate as relay points, creating multi-hop wireless mesh topologies that extend coverage and capacity in a self-organizing and adaptive way. However, despite these advantages, IAB systems are still susceptible to the limitations of wireless backhaul links, especially in situations involving line-of-sight (LoS) blockages, weather conditions (e.g., rain fade), and complexities introduced by dynamic urban environments [6].

In response to these vulnerabilities, researchers and industry stakeholders have focused on hybrid backhaul architectures, more specifically those where IAB is integrated with Free-Space Optical (FSO) communication and fiber. FSO systems use tightly focused light beams, typically in the infrared or visible spectrum, to transmit high-speed data wirelessly without needing physical cables. These systems offer several significant advantages, including multi-Gbps throughput, immunity to electromagnetic interference, enhanced security due to their narrow beamwidths, and operation within license-free spectrum bands. Additionally, employing FSO links can alleviate congestion in the radio frequency (RF) spectrum and serve as a complementary backhaul path for mmWave IAB systems, providing a high-capacity alternative, especially where a fiber deployment is too costly.

FSO links are highly vulnerable to atmospheric conditions (e.g., fog, heavy rain, dust), which can lead to significant signal loss and outages. To address these challenges, advanced adaptive link management strategies have been proposed. These include dynamic on-off switching, load balancing, and dual-mode transceivers that can switch between FSO and RF backhaul based on real-time link quality metrics and environmental sensing. These strategies enhance the backhaul network's resilience and reliability while allowing for context-aware resource allocation and quality of service (QoS) provisioning [7].

Although there is growing interest in IAB and FSO technologies, much of the existing literature treats them separately. Studies focused on IAB usually examine aspects such as optimal node placement, routing algorithms, and scheduling, often under idealized channel conditions and without considering the integration of optical links [8], [9]. On the other hand, research related to FSO emphasizes channel modelling, beam alignment, and techniques for atmospheric compensation, but not many address how these systems can be incorporated into broader radio access network (RAN) architectures. This fragmented approach creates a significant gap in devel-

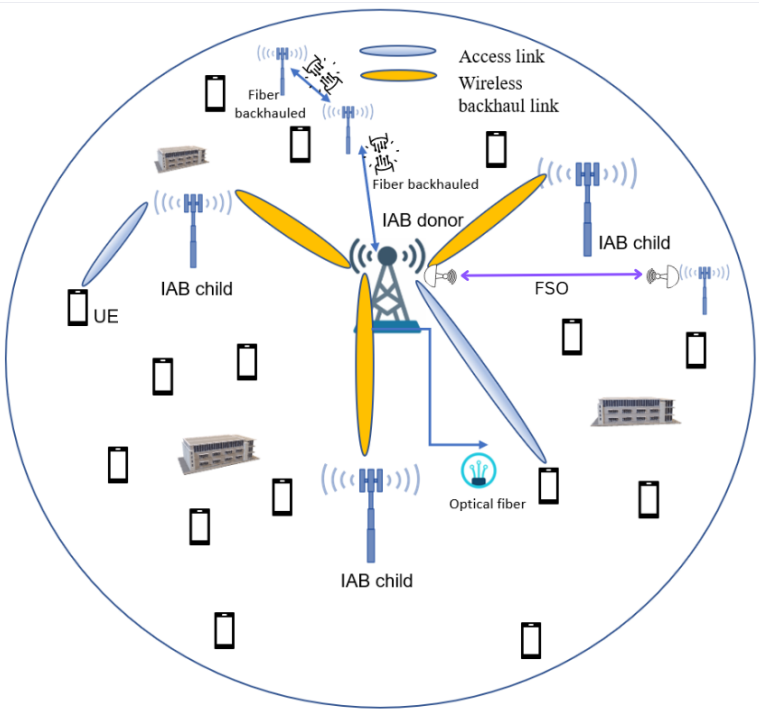

Figure 1: Schematic of the hybrid IAB system model.

oping comprehensive hybrid fiber/FSO backhaul solutions. To address this issue, we propose a unified and intelligent backhaul framework, one that seamlessly integrates IAB, FSO, and fiber optics based on real-time conditions, network demands, and service requirements. This framework would utilize the strengths of each technology, i.e., to use the widespread applicability and scalability of IAB, the ultra-high capacity of FSO, and the reliability of fiber. By implementing such solutions, next-generation wireless networks can achieve enhanced performance, adaptability, sustainability, and cost-effectiveness.

In this paper, we study the effect of network planning on the service coverage probability of IAB networks assisted with fiber/FSOs. We present fiber/FSO deployment algorithms that jointly optimize the inter-node fiber distance and cost. Moreover, we study the effect of different parameters on the network performance focusing on the service coverage probability and energy efficiency. As we show, the coverage and cost efficiency of IAB networks can be considerably improved via proper network planning.

2 System Model

We consider the downlink of a two-hop IAB network, where an MBS, i.e., IAB donor and its associated SBS, i.e., IAB child nodes serve a set of UEs as illustrated in Fig. 1 [6], [10], [11], [12]. Particularly, finite homogeneous Poisson point processes (FHPPPs) are used to model the spatial distributions of the MBSs, SBSs, and UEs. An in-band mmWave communication framework is assumed, where both access and backhaul links share the same frequency band. While this setup increases coordination complexity, it offers flexible spectrum utilization without requiring dedicated frequency channels. We adopt the LoS probability model for urban macro (UMa) scenario as detailed in 3GPP TR 38.901, [13], for blockage, and the 5GCM UMa close-in channel model [6], [14] to characterize mmWave propagation. The received power at node r from transmitter t is modeled as:

$$P_{\text{rx}} = P_{\text{tx}} h_{t,r} G_{t,r} L_{t,r}(\|x_t - x_r\|)^{-1}, \tag{E.1}$$

where P_{tx} is the transmit power, $h_{t,r}$ denotes small-scale fading modelled as a normalized Rayleigh random variable, $G_{t,r}$ is the combined antenna gain, and $L_{t,r}(\cdot)$ represents path loss, which depends on LoS or Non-LoS (NLoS) conditions determined by the blockage model.

The antenna gain $G_{t,r}$ follows a simplified sector antenna pattern:

$$G_{t,r}(\theta) = \begin{cases} G_{\text{main}}, & |\theta| \leq \frac{\theta_{\text{HP}}}{2} \\ G_{\text{side}}, & \text{otherwise} \end{cases}, \tag{E.2}$$

where θ_{HP} is the half-power beamwidth, and G_{main}, G_{side} denote the main-lobe and side-lobe gains, respectively [15].

Each UE u associates with either the IAB donor or one of the child IAB nodes based on received power. The interference at UE u is defined as:

$$I_u = \sum_{i \in \Phi_u \setminus \{w_u\}} P_i h_{i,u} G_{i,u} L_{i,u}(\|x_i - x_u\|)^{-1}, \tag{E.3}$$

where w_u is the serving node of UE u, and Φ_u is the set of all potential interferers.

Similarly, the aggregate interference experienced by a child IAB node c on its backhaul link is:

$$I_c = \sum_{j \in \Phi_c \setminus \{w_c\}} P_j h_{j,c} G_{j,c} L_{j,c}(\|x_j - x_c\|)^{-1}, \tag{E.4}$$

where w_c denotes the IAB donor serving the IAB child node c. The available mmWave

bandwidth W is partitioned between access and backhaul links as:

$$\begin{aligned} W_{\text{bh}} &= \beta W, \\ W_{\text{ac}} &= (1-\beta)W, \end{aligned} \tag{E.5}$$

where $\beta \in [0,1]$ denotes the backhaul bandwidth allocation factor.

Let $\mathcal{D}$, $\mathcal{C}$, and $\mathcal{U}$ denote the sets of IAB donors, child IAB nodes, and UEs, respectively. Each UE $u \in \mathcal{U}$ may be served either directly by the IAB donor or through a child IAB node. Accordingly, the downlink rate R_u for UE u is given by:

$$R_u = \begin{cases} \dfrac{W_{\text{ac}}}{N_d} \log_2(1+\text{SINR}_u), & w_u \in \mathcal{D}, \\ \min\left\{ \dfrac{W_{\text{ac}}}{N_{c,u}} \log_2(1+\text{SINR}_u), \\ \dfrac{W_{\text{bh}}}{N_c} \log_2(1+\text{SINR}_c) \right\}, & w_u \in \mathcal{C} \end{cases}, \tag{E.6}$$

where N_d is the number of UEs directly served by the donor, $N_{c,u}$ is the number of UEs served by child IAB node c (to which u is associated), and N_c is the total number of child IAB nodes. In addition, for UEs served by SBSs with non-IAB backhaul (e.g., fiber or FSO-connected), the downlink rate is expressed as:

$$R_u = \frac{W}{N_u} \log_2(1+\text{SINR}_u), \quad \text{if } w_u \in \mathcal{S}, \tag{E.7}$$

where N_u denotes the total number of UEs connected to the non-IAB backhauled SBS of which the considered UE is associated.

Our design objective is to optimize node deployment and bandwidth allocation to maximize service coverage probability, given by $\Pr(R_u \geq \eta)$ and defined as the fraction of UEs whose instantaneous rate exceeds a target threshold η.

Algorithm 11 Plan connected fiber-backhaul topology

$\Gamma = (V, E)$: Initial disconnected graph (e.g., only MBS ring) Γ: Connected graph with all nodes reachable $V_0 \leftarrow \{v \in V : \deg(v) = 0\}$ *Nodes with no connections

while $V_0 \neq \varnothing$ **do** Select random node $v \in V_0$ $u \leftarrow \arg\min_{w \in V \setminus V_0} dist(v, w)$ *Closest connected node Add edge (v, u) to Γ $V_0 \leftarrow V_0 \setminus \{v\}$ Γ

2.1 Fiber Backhaul Connection Placement Algorithm

We model the base station fiber-backhaul planning as a graph $\Gamma = (V, E)$, where V represents the set of base stations and E the set of fiber links interconnecting them. Base stations are classified as main base stations (MBSs) V_m or small base stations (SBSs) V_s. SBSs may be connected via either IAB $V_{IAB} \subset V_s$ or fiber $V_{Fib} \subset V_s$.

Algorithm 12 Fiber-backhaul connection placement FBCP(α)

$\Gamma = (V, E)$: network topology with MBS ring; V_m: MBSs; $V_{IAB} \subset V_s$ SBSs with IAB backhaul; $V_{Fib} \subset V$ SBSs with fiber backhaul; N: number of SBSs to connect with fiber; $\alpha \in [0, 1]$: Weight parameter for separation vs. cost Updated graph Γ with N additional fiber-connected SBSs
$\Gamma_{design} \leftarrow$ Connected reference graph from Algorithm 11

for $i \leftarrow 1$ N **do** $v \in V_{IAB}$ $p^* \leftarrow$ null *Best path to an MBS $v_m \in V_m$ $p_{v,v_m} \leftarrow$ Shortest path from v to v_m in Γ_{design}

  if $p^* =$ null **or** $l(p_{v,v_m}) < l(p^*)$ **then** $p^* \leftarrow p_{v,v_m}$
$E' \leftarrow$ Edges in p^* not already in Γ
$\Gamma'[v] \leftarrow$ Updated graph Γ with edges E'
$cost[v] \leftarrow \beta_{dig} \cdot l(E') + \beta_{fiber} \cdot l(p^*) + 2 \cdot \beta_{trx}$, cost of moving from Γ to Γ'
$sep[v] \leftarrow \sum_{u \in V_{Fib} \cup V_m} \frac{1}{dist(v,u)}$
Normalize $cost[v]$ and $sep[v]$ for all $v \in V_{IAB}$
$v \in V_c$ $weight[v] \leftarrow \alpha \cdot sep[v] + (1 - \alpha) \cdot cost[v]$ $v^* \leftarrow \arg\min_{v \in V_{IAB}} weight[v]$
$\Gamma \leftarrow \Gamma'[v^*]$ $V_{IAB} \leftarrow V_{IAB} \setminus \{v^*\}$ $V_{Fib} \leftarrow V_{Fib} \cup \{v^*\}$ Γ, V_{IAB}, V_{Fib}

MBSs V_m are interconnected by fiber links $E_m \subset E$ that form a ring topology and serve as IAB donor nodes. Let $l(P)$ denote the total length of fibers along path P, and let $dist(v, u)$ denote the Euclidean distance between base stations v and u.

Although the long-term goal is to connect all nodes via fiber, in practice, this deployment occurs incrementally to amortize the cost over time. The eventual fiber-connected network is designed using the Algorithm 11, which incrementally expands an initially connected subgraph. Disconnected nodes are processed in random order and connected to their nearest already connected neighbor. In our case, the initial subgraph is the ring topology formed by the MBSs V_m. The aim is to minimize the deployment cost and maximize the average SNR, which both are scaling with respect to distance [16].

We assume the primary costs in optical network deployment arise from trenching, optical fiber, and transceivers. The MBSs V_m are interconnected in a ring topology, while each fiber-connected SBS $v \in V_{Fib}$ is linked to its nearest MBS via a dedicated point-to-point fiber. The full deployment follows the structure produced by Algorithm 11. We further assume that multiple fiber links can share a trench. All cost metrics are normalized relative to the cost of a 10G transceiver ($\beta_{trx} = 1$), with trenching cost set at $\beta_{dig} = 2.4$ units per meter and fiber cost at $\beta_{fiber} = 0.006$ units per meter [17]. We express the potential cost of an FSO link within the range $\beta_{FSO} = [1, 100]$.

While the long-term infrastructure plan assumes full fiber connectivity, mid-term decisions about which SBSs should be fiber-connected remain unresolved. To address this, we propose Fiber-Backhaul Connection Placement algorithm (FBCP, Algorithm 12) connects N SBSs with fiber links, guided by a weighting parameter

α. This parameter balances minimizing deployment cost (α=0) and maximizing the spatial separation among fiber-connected SBSs (α=1) to improve coverage. The algorithm starts with the initial ring topology Γ composed of the MBSs V_m and incrementally connects SBSs until N nodes are fiber-connected.

At each step, the algorithm evaluates all currently unconnected SBSs V_{IAB} (line 3). For each node $v \in V_{IAB}$, it computes the shortest path to the closest IAB donor in V_m, using the design graph Γ_{design} (lines 4–8). Let E' denote the set of edges required to connect node v to the existing graph Γ. The cost of connecting v is computed in line 11. The inverse separation is calculated as the sum of inverse Euclidean distances from node v to all currently fiber-connected nodes (line 12). After normalizing both cost and separation metrics, the node minimizing the weighted objective is selected (lines 13–16). This node is then connected via fiber according to Γ_{design}, and the process repeats until N SBSs are connected.

3 Simulation Results and Discussion

In this section, we evaluate the effect of fiber/FSO deployment strategies on the cost, service coverage probability, and energy efficiency of the IAB networks. Here, the nodes are connected according to FBCP (Algorithm 12) with separation-cost weight parameter α, where α=1 corresponds to scenario focused on increasing nodes separation solely and *cost sort*, i.e., minimizing cost with α=0). We consider an IAB network operating at 28 GHz, with $W = 1$ GHz, $G_{\text{main}} = 24$ dBm, $G_{\text{side}} = -2$ dBm and $\eta = 100$ Mbps. The network consists 5 MBSs, i.e., IAB donors, 80 SBSs, i.e., IAB child nodes and 1000 UEs, for the evaluations, unless otherwise stated.

3.1 Cost Behavior of Fiber-Connected SBSs

Fig. 2 presents the cost as the number of SBSs connected with fiber. This plot compares six distinct strategies: FBCP focusing on the deployment cost (α=0.0), random (RND), and four spatial diversity-based FBCP schemes defined by α parameters ranging from 0.25 to 1.0. All strategies start at a base cost of approximately 5,600 units when no SBS is fiber-connected.

The FBCP(α=0) strategy, which prioritizes the least expensive SBSs to connect, consistently yields the lowest cost across all connection levels. At 40 connected SBSs, the cost incurred is about 13,300 units under FBCP(α=0), compared to approximately 19,600 units for the RND strategy, and over 20,750 units for the most spatially diverse configuration FBCP(α=1). This demonstrates that enforcing spatial diversity in SBS placement while potentially beneficial for coverage can increase deployment cost by more than 60%. All strategies converge to a total cost of around 24,000 as they are using the same long-term fiber placement planning strategy according to Algorithm 11.

3.2 Hybrid Fiber-FSO Backhaul Strategies

Fig. 3 illustrates the total cost of connecting 60 SBSs as a function of the FSO-to-10G transceiver cost ratio β_{FSO}. Two scenarios are examined: (i) all 60 SBSs are fiber-backhauled (solid lines), and (ii) 40 SBSs are fiber-backhauled while 20 SBSs utilize FSO backhaul (dashed lines). These scenarios are evaluated for three FBCP methods with α values of 0.0, 0.5, and 1.0. For each FBCP method, a crossover point is evident, indicating the β_{FSO} value beyond which connecting additional SBSs with FSO incurs a lower cost than using fiber. For FBCP(α=0) , which solely prioritizes cost, this crossover occurs at approximately β_{FSO}=70. n contrast, for the FBCP(α=1), method, which emphasizes spatial separation, the crossover point appears at a lower β_{FSO} value of around 47, suggesting that a focus on cost minimization also indirectly mitigates the higher relative cost of FSO backhauling.

Fig. 4 (top) demonstrates the topologies connecting fiber and FSOs in the backhaul, while Fig. 4 (bottom) examines the cost efficiency of hybrid deployments for FBCP(α=0.5), as a function of connected SBSs. The blue solid line (*Fiber connected*) represents the scenario where all connected SBSs are fiber-backhauled. The other dashed lines depict cases with a fixed number of fiber-connected SBSs, with the remaining SBSs being FSO-connected. The fully fibered scenario reaches the maximum cost of approximately 24,00 units, while the fully FSO-based configuration (*FSO & 0-fiber connected*) has the lowest cost, roughly 8,800 units. Hybrid approaches show nearly linear cost growth. When 20 SBSs are fiber-connected (and remaining 59 are FSOs connected), the total cost rises to around 12,800 units. This increases to 18,100 units for 40 fiber-connected SBSs, and to approximately 21,200 units at 60. The top of the figure illustrates the placement of fiber and FSO links for two cases: (i) 20 SBSs connected solely with fiber, and (ii) 20 SBSs fiber-backhauled and 20 SBSs FSO-backhauled. These trends highlight the cost benefit of selective fiber deployment. For example, opting for a hybrid model with 40 fiber-connected SBSs can yield over 30% cost savings compared to a fully fibered network, while enabling strategic use of reliable links where most needed.

3.3 Impact of Fiber-Connected SBSs on Service Coverage Probability

In Fig. 5, we present the impact of the number of fiber-connected SBSs on service coverage probability under various deployment strategies. As we see, the *cost sort*, i.e., α=0) scheme for low UE density (50 UEs) achieves nearly ideal performance, maintaining a service coverage probability of 0.99 or higher regardless of the number of fiber-connected SBSs.

As the UE density increases from 1,000 to 1,500, the service coverage probability decreases, however, connecting more SBSs with fiber gradually increases performance. For instance, with 1,000 UEs, the coverage improves from approximately 0.4 with no

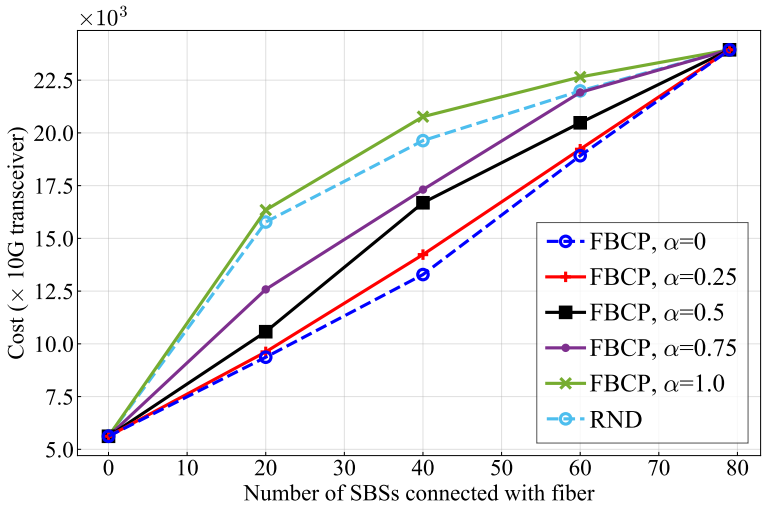

Figure 2: Cost as a function of the number of SBSs connected with fiber.

fiber-connected SBSs to over 0.76 with 80 SBSs connected. These trends show the scalability and efficiency of the cost-aware SBS selection approach.

In contrast, random SBS selection with 1000 UEs performs sub-optimally, particularly when smaller number of SBSs are fiber-connected out of the possible 80. However, when the number of SBSs fiber-connected surpasses about 26-30, the service coverage probability outperforms other deployment strategies. When the number of SBSs to be fiber-connected is small (e.g., 26-30), the number of possible random configurations is high. This high variability leads to a wider range of possible outcomes, including many suboptimal configurations where, fiber-connected SBSs may be too concentrated in certain areas and edges, leaving coverage gaps. Some SBSs with high UE density may not be selected for fiber connection, resulting in poor service coverage. However, when the number of fiber-connected SBSs increases, it results in a reduced configuration space. Since fewer SBSs are remaining to choose from, the random selection becomes less variable, and the likelihood of forming effective configurations increases. Also, with more SBSs connected to fiber, the network is closer to achieving coverage saturation, meaning that most critical areas already have a fiber-connected SBS. The spatial separation strategies ($\alpha = 0.5$ and $\alpha = 0.75$) align closely with that of *cost sort*, i.e., $\alpha = 0$. While increasing α introduces spatial diversity, it often incurs higher deployment cost, making the deployments less favorable compared to *cost sort*, i.e., $\alpha = 0$ scenario. As we see, targeted FBCP deployment, potentially augmented by spatial considerations, emerges as a robust strategy for maintaining service coverage probability.

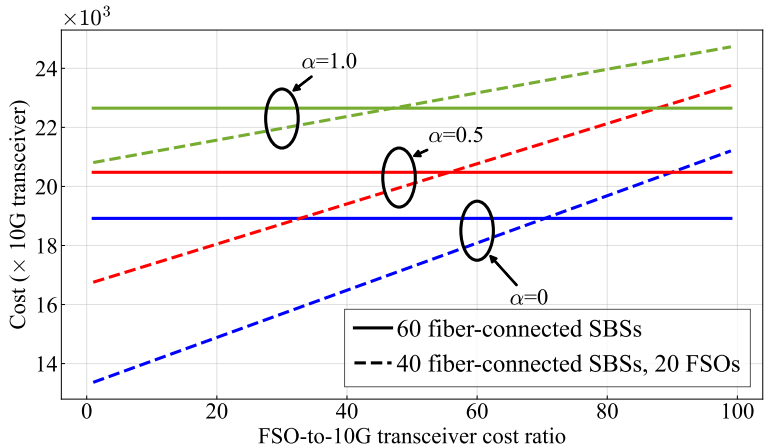

Figure 3: Cost as a function of the FSO-to-10G transceiver cost ratio for 60 connected SBSs.

3.4 Impact on the energy efficiency

Fig. 6 depicts the network energy efficiency, measured in bits per second per watt (bps/W), as a function of the transmit power of SBSs, P_{SBS}, across four different deployment scenarios. These include *cost sort*, i.e., $\alpha = 0$, strategy with 20 and 60 SBSs that are fiber-connected, and FBCP($\alpha = 0.75$), using the same SBS counts.

Here, the energy efficiency is given by $\text{EE} = \frac{R_{\text{total}}}{P_{\text{total}}}$, where the total achievable system throughput is represented by R_{total}, while the total power consumed across the network is denoted by P_{total}, which can be expressed as:

$$P_{\text{total}} = P_{\text{MBS}} + P_{\text{SBS, wireless}} + P_{\text{SBS, fibered}}. \tag{E.8}$$

In all configurations, energy efficiency increases initially with P_{SBS}, peaks around 15-20 dBm, and then decreases. This trend highlights the trade-off between increased throughput and rising power consumption. As transmit power increases, user data rates improve due to stronger desired signals, but the associated increase in network power consumption eventually dominates, reducing overall efficiency.

Among the schemes, separation-based deployment ($\alpha = 0.75$) with 60 SBSs achieve the highest energy efficiency, peaking above 1.2×10^7 bps/W. The *cost sort* strategy (when $\alpha = 0$) with 60 SBSs also performs comparably well, indicating that optimized SBS placement either by cost or spatial diversity yields energy-efficient performance. In contrast, the $\alpha = 0$ and $\alpha = 0.75$ deployments with only 20 SBSs demonstrate lower efficiency. This highlights the role of SBS density in achieving energy-efficient coverage, as fewer nodes lead to higher per-node loads and less spatial reuse. Overall, we see that moderate transmit powers combined with intelligent SBS selection

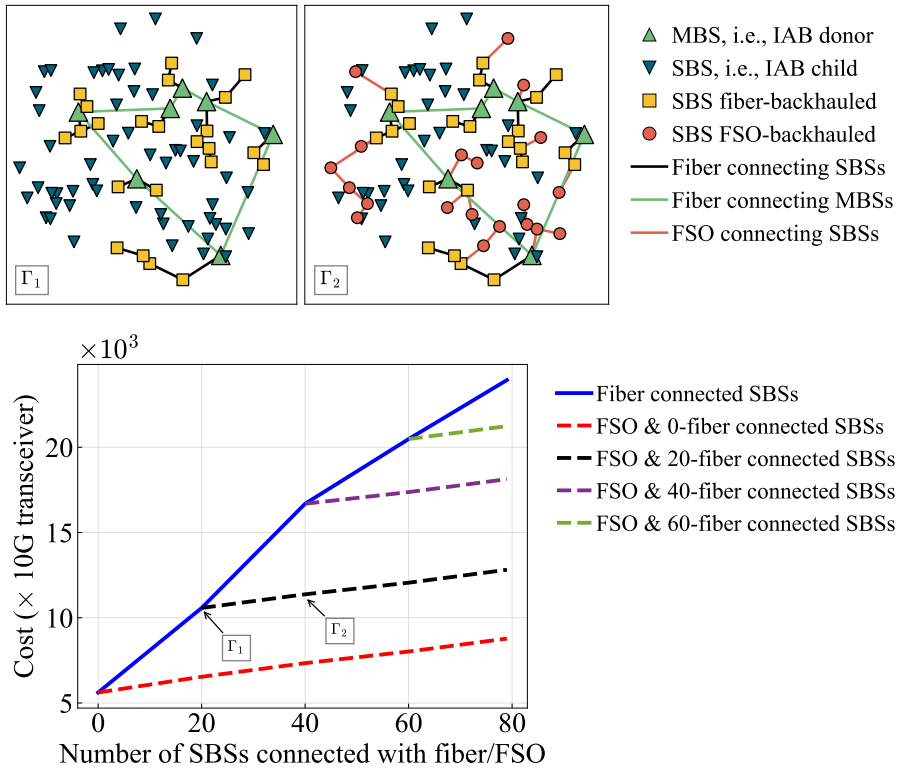

Figure 4: Cost and corresponding topologies for SBSs connected with fiber and FSOs for FBCP(α=0.5); (a) Topologies connecting 20 SBSs with fiber (left); 20 SBSs with fiber and 20 SBSs with FSOs (right); (b) Cost as a function of the number of SBSs connected with fiber and FSOs

strategies (cost-aware or spatially diverse) can significantly boost energy efficiency in dense small-cell networks, of IAB type.

4 Conclusion

We studied the problem of IAB network infrastructure optimization with fiber/FSO assisted backhaul. We proposed a fiber backhaul connection placement algorithm for planning fiber rollout according to separation vs. cost weighting parameter. As demonstrated, proper backhaul network planning can boost the IAB networks' coverage, reduce the cost of deployment, and energy efficiency. In practice, factors such as the availability of non-IAB backhaul connections in certain regions and local regulatory constraints may significantly impact the design process. Additionally, de-

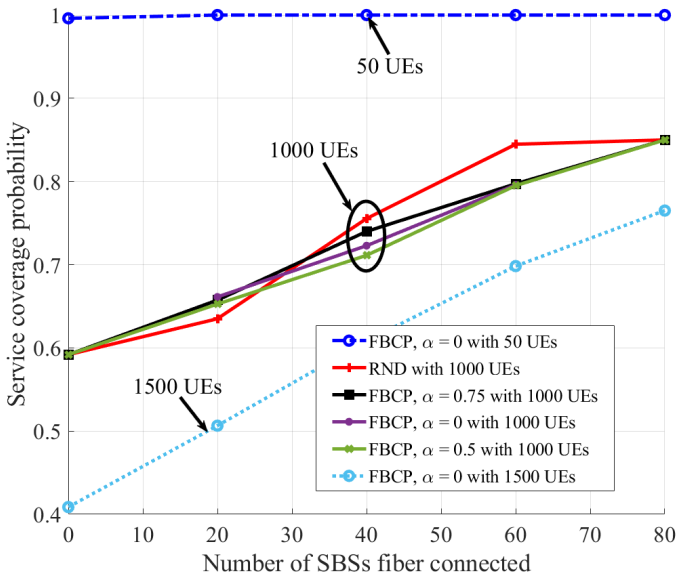

Figure 5: Service coverage probability as a function of the number of SBSs connected with fiber, $P_{\text{MBS}} = 40$ dBm, $P_{\text{SBS}} = 24$ dBm

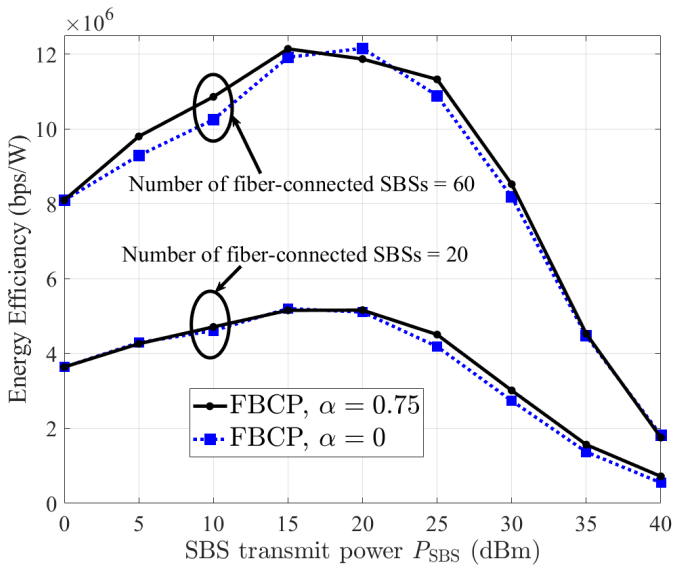

Figure 6: Energy efficiency as a function of the SBS transmit power with $P_{\text{MBS}} = 40$ dBm, power loss in fiber at 1W/km, and the power consumption of a fiber transceiver at 8W.

signers may need to account for planned infrastructure modifications, regional cost considerations, and seasonal fluctuations.

Acknowledgment

This work was supported by the ECO-eNET project with funding from the Smart Networks and Services Joint Undertaking (SNS JU) under grant agreement No. 10113933. The JU receives support from the European Union's Horizon Europe research and innovation.

Reference

[1] M. Alsabah et al., "6G wireless communications networks: A comprehensive survey," *IEEE Access*, vol. 9, pp. 148 191–148 243, 2021, ISSN: 21693536.

[2] A. V. Parambath, J. Flordelis, C. Madapatha, F. Rusek, E. Bengtsson, and T. Svensson, "Integrating reconfigurable intelligent surfaces (RISs) into indoor D-MIMO networks for 6G," in *IEEE 100th Vehicular Technology Conference*, 2024, pp. 1–6.

[3] M. Jaber, M. A. Imran, R. Tafazolli, and A. Tukmanov, "5G backhaul challenges and emerging research directions: A survey," *IEEE Access*, vol. 4, pp. 1743–1766, 2016, ISSN: 21693536.

[4] S. B. A. Anas, F. H. Hamat, S. Hitam, and R. K. Sahbudin, "Hybrid fiber-to-the-x and free space optics for high bandwidth access networks," *Photon. Netw. Commun.*, vol. 23, pp. 33–39, 1 Feb. 2012, ISSN: 1387974X.

[5] K. Hassan, M. Masarra, M. Zwingelstein, and I. Dayoub, "Channel estimation techniques for millimeter-wave communication systems: Achievements and challenges," *IEEE Open Journal of the Communications Society*, vol. 1, pp. 1336–1363, 2020, ISSN: 2644125X.

[6] C. Madapatha et al., "On integrated access and backhaul networks: Current status and potentials," *IEEE OJ-COMS*, vol. 1, pp. 1374–1389, Sep. 2020.

[7] S. A. H. Mohsan, M. A. Khan, and H. Amjad, "Hybrid FSO/RF networks: A review of practical constraints, applications and challenges," *Opt. Switch. Netw.*, vol. 47, Feb. 2023, ISSN: 15734277.

[8] H. Yin, S. Roy, and L. Cao, "Routing and resource allocation for IAB multi-hop network in 5G advanced," *IEEE Trans. Commun.*, vol. 70, no. 10, pp. 6704–6717, 2022.

[9] C. Madapatha, B. Makki, H. Guo, and T. Svensson, "Constrained deployment optimization in integrated access and backhaul networks," in *2023 IEEE Wireless Communications and Networking Conference (WCNC)*, 2023, pp. 1–6.

[10] S. Singh, M. N. Kulkarni, A. Ghosh, and J. G. Andrews, "Tractable model for rate in self-backhauled millimeter wave cellular networks," *IEEE J. Sel. Areas Commun.*, vol. 33, no. 10, pp. 2196–2211, May 2015.

[11] C. Saha and H. S. Dhillon, "Millimeter wave integrated access and backhaul in 5G: Performance analysis and design insights," *IEEE J. Sel. Areas Commun.*, vol. 37, no. 12, pp. 2669–2684, 2019.

[12] O. P. Adare, H. Babbili, C. Madapatha, B. Makki, and T. Svensson, "Uplink power control in integrated access and backhaul networks," in *Proc. DySPAN'2021*, Virtual, 2021, pp. 163–168.

[13] 3rd Generation Partnership Project (3GPP), "Study on channel model for frequencies from 0.5 to 100 GHz," 3rd Generation Partnership Project (3GPP), Technical Report TR 38.901 V14.1.1, Aug. 2017, Release 14.

[14] T. S. Rappaport, Y. Xing, G. R. MacCartney, A. F. Molisch, E. Mellios, and J. Zhang, "Overview of Millimeter Wave Communications for Fifth-Generation (5G) Wireless Networks—With a Focus on Propagation Models," *IEEE Trans. Antennas Propag.*, vol. 65, no. 12, pp. 6213–6230, Dec. 2017.

[15] S. M. Azimi-Abarghouyi, B. Makki, M. Nasiri-Kenari, and T. Svensson, "Stochastic Geometry Modeling and Analysis of Finite Millimeter Wave Wireless Networks," *IEEE Trans. Veh. Technol.*, vol. 68, no. 2, pp. 1378–1393, Feb. 2019.

[16] R. Matzner, D. Semrau, R. Luo, G. Zervas, and P. Bayvel, "Making intelligent topology design choices: Understanding structural and physical property performance implications in optical networks [invited]," *J. Opt. Commun. Netw.*, vol. 13, pp. D53–D67, 8 Aug. 2021, ISSN: 19430639.

[17] A. Udalcovs et al., "Total cost of ownership of digital vs. analog radio-over-fiber architectures for 5G fronthauling," *IEEE Access*, vol. 8, pp. 223 562–223 573, 2020.